

INFORMATION TO USERS

This manuscript has been reproduced from the microfilm master. UMI films the text directly from the original or copy submitted. Thus, some thesis and dissertation copies are in typewriter face, while others may be from any type of computer printer.

The quality of this reproduction is dependent upon the quality of the copy submitted. Broken or indistinct print, colored or poor quality illustrations and photographs, print bleedthrough, substandard margins, and improper alignment can adversely affect reproduction..

In the unlikely event that the author did not send UMI a complete manuscript and there are missing pages, these will be noted. Also, if unauthorized copyright material had to be removed, a note will indicate the deletion.

Oversize materials (e.g., maps, drawings, charts) are reproduced by sectioning the original, beginning at the upper left-hand corner and continuing from left to right in equal sections with small overlaps.

Photographs included in the original manuscript have been reproduced xerographically in this copy. Higher quality 6" x 9" black and white photographic prints are available for any photographs or illustrations appearing in this copy for an additional charge. Contact UMI directly to order.

ProQuest Information and Learning
300 North Zeeb Road, Ann Arbor, MI 48106-1346 USA
800-521-0600

UMI[®]

University of Alberta

Flow Control Reduction of Smokestack Downwash

by

John Khai Quang Diep



A thesis submitted to the Faculty of Graduate Studies and Research in
partial fulfillment of the requirements for the degree of Master of Science.

Department of Mechanical Engineering

Edmonton, Alberta
Spring 2001



National Library
of Canada

Acquisitions and
Bibliographic Services

395 Wellington Street
Ottawa ON K1A 0N4
Canada

Bibliothèque nationale
du Canada

Acquisitions et
services bibliographiques

395, rue Wellington
Ottawa ON K1A 0N4
Canada

Your file Votre référence

Our file Notre référence

The author has granted a non-exclusive licence allowing the National Library of Canada to reproduce, loan, distribute or sell copies of this thesis in microform, paper or electronic formats.

The author retains ownership of the copyright in this thesis. Neither the thesis nor substantial extracts from it may be printed or otherwise reproduced without the author's permission.

L'auteur a accordé une licence non exclusive permettant à la Bibliothèque nationale du Canada de reproduire, prêter, distribuer ou vendre des copies de cette thèse sous la forme de microfiche/film, de reproduction sur papier ou sur format électronique.

L'auteur conserve la propriété du droit d'auteur qui protège cette thèse. Ni la thèse ni des extraits substantiels de celle-ci ne doivent être imprimés ou autrement reproduits sans son autorisation.

0-612-60421-7

Canada

University of Alberta

Library Release Form

Name of Author: John Khai Quang Diep


Title of Thesis: Flow Control Reduction of Smokestack Downwash

Degree: Master of Science

Year this Degree Granted: 2001

Permission is hereby granted to the University of Alberta to reproduce single copies of this thesis and to lend or sell such copies for private, scholarly, or scientific research purposes only.

The author reserves all other publication and other rights in association with the copyright in the thesis, and except as hereinbefore provided, neither the thesis nor any substantial portion thereof may be printed or otherwise reproduced in any material form whatever without the author's prior written permission.



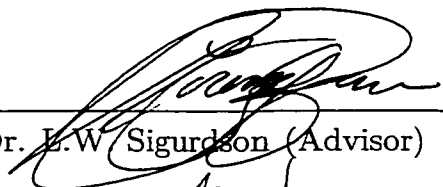
John Khai Quang Diep
13347-110 ave.
Edmonton, Alberta,
Canada. T5M 2M1

April 11, 2001

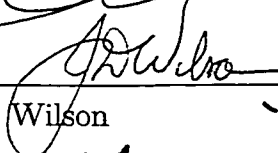
University of Alberta

Faculty of Graduate Studies and Research


The undersigned certify that they have read, and recommend to the Faculty of Graduate Studies and Research for acceptance, a thesis entitled Flow Control Reduction of Smokestack Downwash submitted by John Khai Quang Diep in partial fulfillment of the requirements for the degree of Master of Science.



Dr. E.W. Sigurdson (Advisor)



Dr. J.D. Wilson



Dr. D.J. Wilson

Date April 10, 2001

To my mother

ABSTRACT

The objective of this work was to discover and evaluate a method of smokestack downwash reduction using unsteady forcing. The final wind-tunnel model applied an annular synthetic jet coaxially to a plume with turbulent or laminar pipe flow at the stack exit. Primary diagnostics were hot-wire measurements and image processing of smoke flow visualization photographs of the plume gas. Downwash was measured using a downwash index as well as plume height measured at a fixed location downstream, giving an inverse indication of downwash. Plume height increases by as much as 1.8 stack diameters for a turbulent pipe flow. This data is collapsed using a simple model based on the idea that synthetic jet momentum dominates the plume at high forcing amplitudes. Plume height increases up to 100% more than when using steady annular blowing of similar velocity, and this is explained. At a lower Reynolds number the turbulent plume relaminarizes for select forcing parameters.

ACKNOWLEDGEMENTS

I would like to thank Dr. Lorenz Sigurdson for sharing with me his ideas, experience, and advice for the past few years. His patience and persistence has allowed me a fascinating glimpse into the world of science and research.

Thanks also to the faculty and staff of the Mechanical Engineering Department for their assistance over the course of this project. In particular: Dave Pape for building the rig, Terry Nord for his help with the electronics, Albert Yuen, Don Fuhr, and Bernie Faulkner for their advice and assistance, and of course, all of the wonderful people working in the office. I would also like to thank the members of my defence committee: Dr. David Wilson, Dr. John Wilson, and Dr. Larry Kostiuik.

I especially thank Andrew Coward for contributing his ideas and considerable expertise in seemingly all areas of practicality. Thanks also to Chris Apps for lending a hand whenever it was needed, and for our many enjoyable discussions regarding fluid dynamics and other forces in life and in nature. Thanks as well to Dallas Chapple for his help in getting started.

Support from my family was crucial throughout this degree. For this I thank every one of them. I also thank Jennifer and her family for their support and encouragement.

Financial support from the Natural Sciences and Engineering Research Council, Luscar Ltd., and the University of Alberta was also greatly appreciated.

CONTENTS

1	Introduction	1
1.1	Motivation	1
1.2	Background	2
1.2.1	Downwash Review	2
1.2.2	Synthetic Jet Review	5
1.2.3	Applications to Downwash	8
1.3	Objective	10
1.4	Thesis Outline	10
2	Experimental Apparatus	12
2.1	Introduction	12
2.2	Preliminary Apparatus	13
2.2.1	Background	13
2.2.2	Objective of Preliminary Apparatus	14
2.2.3	Design and Discussion	15
2.2.4	Results	21
2.3	Final Apparatus	36
2.3.1	Design	36
2.3.2	Construction and Instrumentation	42
2.3.3	Performance	56
2.4	Summary	62
3	Results and Discussion	67
3.1	Introduction	67
3.2	Introduction to Photographic Plume Measurements and Data	68
3.2.1	Experimental Data Cases	68
3.2.2	Plume Measurements	70
3.3	Results of Plume Measurements	74

3.4	Plume Forced with Synthetic Jet	76
3.4.1	Plume Measurements with Synthetic Jet Forcing	76
3.4.2	Qualitative Plume Behaviour	83
3.4.3	Plume Rise Equations	88
3.4.4	Application to Plume Rise Predictions	94
3.4.5	Induced Plume Flow	104
3.4.6	Observations of a Plume with Laminar Pipe Flow . . .	109
3.5	Plume Forced with Steady Annular Blowing	118
3.6	Entrainment Due to Steady Blowing or Synthetic Jetting . . .	121
3.7	Downwash Index	130
4	Conclusions and Future Work	136
4.1	Summary and Conclusions	136
4.2	Future Work	145
	Bibliography	147
A	LabVIEW® Programs	153
A.1	Description of <i>towerII-3.vi</i>	154
A.2	Description of <i>average waveform.vi</i>	157
A.3	Description of <i>integrate waveform.vi</i>	160
A.4	Description of <i>popup-tow-6c.vi</i>	162
B	Sample Photographs	164

LIST OF TABLES

3.1 Experimental Operating Points 69

3.2 Operating Points for Figure 3.14 106

3.3 Downwash Grading Criteria 133

LIST OF FIGURES

2.1	Wind Tunnel Schematic	16
2.2	Preliminary Apparatus Installation in Test Section	18
2.3	Preliminary Apparatus Smoke-Wire and Photography Setup	20
2.4	Synthetic Jet Measurements	23
2.5	Reference Photograph Showing Smoke-Wire Flow Visualization (no forcing)	26
2.6	1 m/s Synthetic Jet Visualized using Smoke-Wire	27
2.7	Various Synthetic Jet Configurations Explored	28
2.8	Vertical Synthetic Jet Applied in a Crossflow	30
2.9	Upstream Synthetic Jet Applied in a Crossflow	32
2.10	Downstream Synthetic Jet Applied in a Crossflow	34
2.11	Cross-stream Synthetic Jet Applied in a Crossflow	35
2.12	Potential Model Stack Tip Configurations	39
2.13	Schematic of Final Apparatus	41
2.14	Installation of the Final Apparatus	43
2.15	Plume Velocity Profile Near the Exit Plane	47
2.16	Calibration of Plume Exit Jet Centerline Velocity	49
2.17	Frequency Map of the Final Apparatus	59
2.18	Slit Velocity versus Forcing Pressure Data For Final Apparatus Compared to Equation 2.4	60
2.19	Calibration of Mean Centerline Synthetic Jet Velocity 3 mm From Orifice of Final Apparatus	63
2.20	Collapsed Mean Centerline Synthetic Jet Velocity 3 mm From Orifice of Final Apparatus	64
3.1	Sample Plume Measurements from Reference Case 21	75
3.2	Comparison of Reference Cases	77
3.3	Plume Heights of Cases 4-6, Varying Synthetic Jet Frequency	79
3.4	Plume Heights of Cases 13-15, Varying Synthetic Jet Frequency	80

3.5	Plume Heights of Synthetic Jet-Forced Plumes	82
3.6	Plume Heights of Reference Plumes	84
3.7	Plume Heights of Synthetic Jet-Forced and Reference Plumes .	85
3.8	Reference Photograph of Unforced Plume; Case 22: $R = 1.75, Z_p \approx 1D$	87
3.9	Photograph Showing Plume Forced with 40 Hz Synthetic Jet; Case 1: $R = 0.7, Z_p \approx 1D, W_{SJ}/U_\infty = 1.3$	87
3.10	Photograph of Plume Forced with High Amplitude 40 Hz Synthetic Jet, Case 1: $R = 0.70, W_{SJ}/U_\infty = 2.1$	89
3.11	Smoke-wire Photograph of Preliminary Apparatus Forced With Upwards-Directed 10 Hz Synthetic Jet: $U_\infty \approx 1 \text{ m/s}$	90
3.12	Synthetic Jet-Forced Plume height vs. Momentum Ratio M_t .	99
3.13	Plume height under Synthetic Jet Forcing vs. Momentum Ratio M_M	102
3.14	Normalized Plume Pressure Head vs. Synthetic Jet Velocity .	106
3.15	Normalized Plume Pressure Head vs. Synthetic Jet Velocity Normalized by Plume Velocity	107
3.16	Normalized Plume Pressure Head vs. Synthetic Jet Velocity Normalized by Plume Velocity (all available cases)	108
3.17	Change in Structure of Laminar Plume Under Synthetic Jet Forcing	112
3.18	Photograph of Plume Forced with Steady Annular Blowing, $R = 0.73, \frac{W_h}{U_\infty} \approx 0.88$	119
3.19	Photograph of Plume Forced with 40 Hz Annular Synthetic Jet, $R = 0.73, \frac{W_{SJ}}{U_\infty} \approx 0.88$	119
3.20	Comparison of Plume Heights Between Synthetic Jetting and Steady Annular Blowing	122
3.21	Plume Heights of Plumes Forced with Steady Annular Blowing and Reference Unforced Plumes	123
3.22	Plume Height With Steady Annular Blowing vs. Momentum Ratio M_M	124
3.23	Idealization of Forced Flow Near Exit Plane	127
3.24	Downwash Grading versus Forcing Velocity	134
3.25	Downwash Grading versus Velocity Momentum Ratio M_M . .	135
A.1	Main Control Panel of <i>towerII-3.vi</i>	156
A.2	Control Panel of Program to Approximate Phase-Average: <i>average waveform.vi</i>	159

A.3	Hot-Wire De-Rectification and Integration Program Control Panel <i>integrate waveform.vi</i>	161
A.4	Data Aquisition and Sensor Configuration Panel of <i>popup-tow-6c.vi</i>	163
B.1	Photographs from Case 21	166
B.2	Photographs from Case 1	167
B.3	Photographs from Case 16	168

NOMENCLATURE

A_p	cross-sectional area of plume
$A_{p,s}$	plume exit area from stack
A_f	exit area of annular forcing
A_M	momentum-weighted exit area
A_t	total exit area of plume and forcing
D	diameter of outside stack profile
d	width of rectangular slit in preliminary apparatus
d_a	width of annular slit in final apparatus
$F_{p,s}$	momentum flux of plume close to stack exit
F_{SJ}	estimated momentum flux of synthetic jet
F_b	estimated momentum flux of annular blowing
F_t	estimated total momentum flux above stack tip of plume and forcing
f	synthetic jet forcing frequency, Hz

M_M	momentum ratio considering the plume and forcing, using the momentum-weighted exit area
M_p	momentum ratio considering only the plume
M_t	momentum ratio considering only the plume, using the total exit area
P_c	pressure across plume flow contraction
P_p	dynamic pressure derived from plume velocity
P'_f	RMS forcing pressure in chamber
Q_p	plume volume flux
Q_s	stack volume flux near exit
R	plume velocity ratio
Re_p	Reynolds Number of plume, using plume diameter
Re_∞	Reynolds Number of cross-flow, using outer stack diameter
r_s	radius of plume exit
St	Strouhal Number
U_∞	crosswind velocity
U_{SJ}	synthetic jet velocity of preliminary apparatus
u'_{slit}	RMS average of slit velocity of preliminary apparatus
v_e	entrainment velocity

W_p	average vertical velocity of developed plume
w_s	spatially-varying vertical velocity above stack tip, including both plume and forcing exit areas
W_t	average velocity of plume and forcing above stack tip
$W_{p,s}$	average velocity of plume flow at stack tip
W_{SJ}	mean centerline synthetic jet velocity of final apparatus measured at 3 orifice diameters
W_b	steady annular blowing velocity
W_f	forcing velocity
$w_{p,s}$	velocity of plume flow at stack tip
w'_{slit}	RMS average of slit velocity of final apparatus
Z_p	height of plume centerline at $x = 7.5D$
Z	height of plume centerline
β	entrainment coefficient
ρ_s	density of stack gases
ρ_a	density of ambient air
ν	kinematic viscosity
g	gravitational constant
α_M	momentum correction factor using momentum weighted area

α_t momentum correction factor using
total exit area

γ fraction of synthetic jet mass flux
entrained from plume

subscripts:

b blowing

f forcing

p plume

M using momentum-weighted area

s stack

SJ synthetic jet

t total (plume and forcing)

CHAPTER 1

INTRODUCTION

1.1 Motivation

The purpose of this study was to experimentally study the effectiveness of using synthetic jets or other unsteady forcing techniques as some form of turbulence control to reduce smokestack downwash. Downwash occurs in stronger cross-winds when portions of an effluent plume move closer to ground level instead of rising away from the stack to be dispersed. While the problem could be solved in most cases by either raising the stack height or increasing the flow velocity through the stack, this is not always practical. Either solution has consequences in terms of both capital and operational costs. Furthermore, none of these solutions may be viable for an existing facility that has a set operating point resulting in downwash.

The goal of this thesis work was not to attempt an understanding of the downwashing phenomena itself. Instead, the goal was to find an active means of downwash reduction using either synthetic jets, a phenomena that

has recently received increasing attention in the field of flow control, or other unsteady turbulence control techniques. Synthetic jets have previously been shown to be able to affect shear flows with length scales up to two orders of magnitude greater than those of the jets themselves (Smith and Glezer, 1998). Then, having found a suitable method of flow control, its effectiveness would need to be evaluated. Achieving this would aid in future efforts in scaling this to a full-sized smokestack, as well as evaluating the same method for other practical applications. These include sewage or outfall drains discharging into a cross-current close to shore, or from vehicles such as city buses and trucks, which tend to entrain exhaust smoke into their strong wakes. The bulk of the literature presents models and empirical fits to predict downwash, but only contributes to methods of downwash reduction insofar as to allow design modifications based on these predictions. Results from these experiments are expected to have some relevance to oil-field flaring efficiency and mixing of un-premixed cross-jets for combustion.

1.2 Background

1.2.1 Downwash Review

1.2.1.1 Causes of Downwash

It has been well known for some time that, aside from larger-scale flow factors in the immediate environment, it is the effect of the wake behind the stack that causes downwashing. It was Sherlock and Stalker (1941) who first sug-

gested that the vortical structure behind the smokestack was responsible for downwash downwind of the immediate stack wake. They conjectured that a counter-rotating vortex pair embedded in the plume swept gases downward from the main plume into the open ends of the von Karman vortex street being shed off of the main stack section. Once entrained in the vortices of the vortex street the gases would then be transported further downward. Their suggestion of a vortex pair being imbedded in the plume resulted from time-averaged velocity measurements taken of streamwise cross-sections of a simple-ended cylinder in a crossflow. Through the course of their experiments it was concluded that significant downwash only occurred when the ratio of average plume vertical exit velocity to cross-wind velocity ($R = W_p/U_\infty$) fell below 1.5. This critical velocity ratio is still generally used as a rule of thumb in predicting the onset of downwash.

Scorer (1958) explains that with low stack exit velocity, plume gases enter the standing recirculation eddies in the immediate wake of the stack. These gases are transported downwards within these eddies before being convected away horizontally by the crosswind.

Briggs (1969) suggested it was the low-pressure region in the immediate wake of the stack that tended to entrain plumes lacking adequate vertical momentum or buoyancy force to escape it. Using a similar assumption, Tatom (1986) performed a force balance between the buoyancy, centrifugal, and pressure forces in the near-field of the bending-over plume. This simple analytical model was favourably compared to downwash data for momentum-

dominated as well as highly buoyant plumes.

Overcamp and Hoult (1971) compared plume rise to the vertical growth of the stack wake in order to obtain a critical speed at which interactions between the plume and the wake would begin to occur. More recently Snyder and Lawson (1991) performed experiments investigating the effect of having sub-critical versus super-critical cross-flow Reynolds numbers on downwash. At cross-flow Reynolds numbers greater than a critical value of approximately 3×10^5 (Fox and McDonald, 1992), the boundary layer along the stack surface becomes turbulent, delaying separation and thus reducing the size of the wake. They found reduced downwash for super-critical cross-flows and provided an explanation that relied upon changes in the low-pressure wake due to changes in separation characteristics. This is the idea behind Concept 3 on page 9.

Johnston (1994) developed a trailing vortex downwash model that expanded the ideas of Sherlock and Stalker (1941). This downwash model incorporated a continuous induced downward velocity from a pair of counter-rotating line vortices imbedded in the plume and trailing from the stack tip. Based on his water-tunnel flow-visualization experiments, Johnston (1994) showed that this vortex pair did not exist instantaneously, but only as a result of time-averaging. He proposed a vortex model where the staggered vortices in the von Karman vortex street were linked to each other through the plume. By using the model of a time-averaged vortex pair imbedded in the plume he was able to make accurate predictions of downwash for their

neutrally buoyant plume. In the same thesis he also synthesized an initial entrainment model that modelled downwash as being aided by the dilution of vertical momentum through the entrainment of ambient air near the stack exit.

1.2.1.2 Attempts at Reducing Downwash

To date there has been little done regarding active suppression of downwash. Solutions to existing downwash cases usually include increasing the plume exit velocity (Scorer, 1958). Sherlock and Stalker (1941), following their analysis, suggested adding an extra nozzle section to the end of a stack in order to eliminate downwashing. In the same paper they alluded to the success of active as well as passive devices in reducing cases of severe downwash on their wind tunnel models, but did not elaborate. Scorer (1958) suggests ornate protrusions at the top of stacks contributed to downwash, and also states that downwash can be averted by placing an annular disk around the stack at the exit plane in order to shield the plume from the wake suction region.

1.2.2 Synthetic Jet Review

Smith and Glezer (1997) describe synthetic jets as being formed through the breakdown of a train of vortices. These vortices are formed at the sharp edge of an orifice which has an oscillating flow of zero average mass flux passing through it. The resulting mean flow a few orifice diameters downstream of

the orifice qualitatively resembles a momentum jet, but consists only of entrained fluid (Smith and Glezer, 1997). The definition of “entrained” fluid that will be used here with respect to synthetic jets differs from the traditional use of the term in describing conventional jets. A conventional jet is typically described as consisting of source jet fluid (emanating from the jetting orifice) as well as additional fluid which is “entrained” into the jet from its surroundings via the jet shear layer downstream of the orifice. A synthetic jet, however, lacks any significant source jet fluid other than what was originally in the small cavity. It thus consists primarily of fluid originating from the external vicinity of the orifice. Conceptual observation within the course of one ejection and suction cycle would see a jet-flow emanating from the orifice in the ejection cycle, and a sink flow into the orifice during the suction cycle. This sink flow draws ambient fluid into the orifice from the external vicinity of the orifice exit which is then ejected at the beginning of the next cycle. It is through a time-averaged view of this process that the entirety of the synthetic jet fluid can be seen to come from ambient fluid entrained from near the orifice exit, and explains the distinction of the term “entrained” fluid used in describing the composition of synthetic jets.

Earlier experimenters referred to this phenomena as acoustic streaming (Ingard and Labate, 1950; Mednikov and Novitskii, 1975; Lebedeva, 1980). The more recent term of synthetic jet will be used throughout this dissertation due to its more common use in current literature. As described in Smith and Glezer (1998), Ingard and Labate (1950) placed an orifice plate

at a pressure node of an acoustically excited resonance tube. They observed a series of vortex rings forming synthetic jets along both axial directions. Mednikov and Novitskii (1975) later induced synthetic jetting velocities of up to 13 m/s using a piston-driven apparatus. Lebedeva (1980) placed an orifice plate at the end of an acoustic resonance tube and observed synthetic jetting.

Other experimenters using oscillatory forcing to influence the external flows around bodies were likely to have been producing and applying synthetic jets at some point, including Sigurdson (1995), Hsiao et al. (1988), and Hsiao et al. (1990). Sigurdson (1995) changed the shedding and drag characteristics of the blunt-faced end of a circular cylinder aligned with the approach flow. Acoustic forcing was applied to a circumferential gap along the leading edge of the cylinder. Hsiao et al. (1988) used acoustical forcing to excite the air in a longitudinal slit on the outer surface of a cylinder in a cross flow, changing the lift and drag characteristics of the cylinder. Amitay et al. (1997) later performed experiments with a similar forcing geometry, but using discrete synthetic jet actuators.

More recently, work has been on better understanding the synthetic jet formation and evolution itself, as well as developing and studying applications for these jets. Smith and Glezer (1998) conducted a comprehensive study regarding synthetic jet formation and development, including qualitative observations as well as measurements of synthetic jet properties. In the same paper they demonstrate the ability of synthetic jets in vectoring

a conventional jet around an order of magnitude larger than the synthetic jet. Direct numerical simulation of a synthetic jet approximating the geometry used by Smith and Glezer (1998) was done by Rizzetta et al. (1999). Numerical results generally agreed with experiment, and revealed details of the vortex breakdown and resultant synthetic jet development. Micromachined synthetic jet mechanisms are being made and used to influence flows on macroscopic scales (Coe et al., 1995).

A continuing application of synthetic jetting is for aerodynamic flow control over airfoils, where lift, drag, and stall characteristics of the airfoil are affected. Hsiao et al. (1990), using an apparatus related to that used by Hsiao et al. (1988), applied forcing to the flow around an airfoil. Other forcing on airfoil flows was later done using discrete synthetic jetting mechanisms (Amitay et al., 1998; Bryant et al., 1999) as well as slits directly excited by acoustic elements (Siller and Fernholz, 2000).

1.2.3 Applications to Downwash

Whether downwash results from purely a deficit in plume momentum, vortical structures in the stack wake, mean properties in the stack wake, or a combination of these, it is reasonable to expect that an alteration of these components should have an effect on downwash. Synthetic jets offer one potential means of influencing these downwash mechanisms. Given the complexities of the flow field around a plume in a cross-flow, analytical or numerical simulation approaches are not viable methods of evaluating plume

response. Thus, experiments were performed in order to establish the most suitable means of flow control. Originally there were three main forcing concepts that were to be evaluated during the course of this study. These are listed below along with corresponding forcing configurations, which are described in further detail in Section 2.2.4.3 and illustrated in Figure 2.7:

1. Apply forcing to augment vertical plume momentum upon leaving the stack exit.
 - Jetting axially along the plume to both augment the vertical momentum of the plume, helping it escape the entrainment area, and also perhaps influencing the vortex structure resulting from the plume/stack interaction.
2. Provide a perturbation to be amplified by naturally occurring instabilities of the plume or stack-wake shear layers.
 - Jetting perpendicular to the cross-flow to either displace or destroy the vortices contributing to the downward transport of plume materials.
3. Reduce wake suction pressure by affecting separation and wake characteristics.
 - Jetting directly downstream into the stack wake in order to add momentum into the wake fluid and reduce the mean pressure deficit.

- Jetting directly upstream from the stack in order to influence the effective aerodynamic profile of the stack (Amitay et al., 1997).

1.3 Objective

Primarily, the goal of this experimental wind-tunnel study is to establish whether synthetic jetting or other unsteady forcing can be used to reduce or eliminate downwash from smokestack plumes. Knowledge gained from this exploratory study has the potential to aid in the understanding of this complicated flow, as well as paving the way for potential work to follow. If this is accomplished successfully, it is important to determine the extent of this effect, and understand the basic principles of its operation. This is important for optimization of the effect and when considering the scaling up of the technique for various other practical uses.

1.4 Thesis Outline

This dissertation is written in a traditional format, with all bibliographic entries at the end. Chapter 1 contains an introduction to the problem being studied and its relevance, along with a brief literature review. Chapter 2 describes the preliminary apparatus and experimental results used to steer the design of the final apparatus. A more detailed description of the design and construction of the final apparatus is given along with the experimental procedures used when taking data. Chapter 3 contains a discussion of results

from the final apparatus, along with relevant equations. Chapter 4 presents a summary of this thesis work and provides recommendations for work to follow.

CHAPTER 2

EXPERIMENTAL APPARATUS

2.1 Introduction

This chapter discusses the development and final design of an apparatus built for a wind-tunnel study of the effectiveness of using synthetic jets in reducing or eliminating smokestack downwash. While experiments on related flows have been previously performed, there are special considerations relating to the current geometry that required new techniques and equipment to be developed. The final apparatus allows visualization of a neutrally buoyant plume in a cross-flow with and without forcing from either an annular synthetic or conventional jet concentric with the stack.

In Section 2.2 the preliminary apparatus that was used in order to steer the development of the final apparatus is briefly discussed. A number of forcing configurations were tried before selecting the most effective configuration. Measurements of synthetic jets made with this preliminary apparatus provided some insight into the frequency and amplitude dependency of these

jets. In Section 2.3, details are given regarding the design and construction of the final apparatus. A summary of the apparatus development and testing is given in Section 2.4.

2.2 Preliminary Apparatus

2.2.1 Background

This is not the first experiment to have been built where discrete sources of time-harmonic forcing have been used to influence the characteristics of unbounded flows around bodies. Speakers have been used to acoustically excite cavities with gaps along their walls (Sigurdson, 1995; Seifert et al., 1993; Hsiao et al., 1988; Hsiao et al., 1990). It is through these gaps that the forcing is transmitted to the flow. More recently, millimeter and micrometer-scale devices using piezoelectric forcing have been used to produce synthetic jets for the purposes of study of the jets themselves as well as new methods of producing them (Coe et al., 1995; Smith and Glezer, 1998). These millimeter-scale acoustic and piezoelectric forcing mechanisms have been used for modifying the flow around the blunt face of a cylinder aligned coaxial with the freestream (Sigurdson, 1995), cylinders in a crossflow (Hsiao et al., 1988; Amitay et al., 1997), as well as separation characteristics of airfoils (Hsiao et al., 1990; Seifert et al., 1993; Smith et al., 1998). Also related to modification of the stack flow, in that the plume is essentially a jet at the stack exit, is work done where steady mass jets as well as synthetic jets

have been modified by using non-steady excitation (Wiltse and Glezer, 1993; Smith and Glezer, 1997; Freund and Moin, 2000).

2.2.2 Objective of Preliminary Apparatus

References using an apparatus similar to the final apparatus, where synthetic jetting was applied at the circumference of a conventional jet, with or without a cross-wind, have not been found by the author. Smith and Glezer (1997) forced a nominally two dimensional conventional jet in ambient air with a pair of synthetic jet operating either separately or together but in different phases. There was no mention of experiments performed with both synthetic jets operating in-phase. Because for the current experiments the aerodynamic stack profile must be preserved, the synthetic jetting mechanism used on the final model had to be very well integrated. Thus, it was desirable to have some indication beforehand as to which synthetic jet configuration built into the model would give the best results. That is one of the reasons why a preliminary apparatus was built. In all, the purposes behind building the preliminary apparatus were threefold:

1. Give an initial indication as to the optimum synthetic jet configuration to use in designing the final experiment.
2. Allow experience to be gained in producing synthetic jets that were of the appropriate strength and length scale for our application.
3. Finally, to allow measurements to be performed on the synthetic jets

produced in order to try and gain insight into their response and optimization. Formation parameters such as amplitude and frequency were expected to have an effect on synthetic jet performance.

2.2.3 Design and Discussion

As an exploratory investigation preceding the main experiments, many different jetting arrangements were to be tried on the preliminary apparatus. The preliminary experiments were done with no plume, which relaxed the design constraints and allowed greater versatility in changing the synthetic jet configuration in the preliminary apparatus. Sherlock and Stalker (1941) and Johnston (1994) did experiments with no plume flow in order to isolate specific components in the wake that they believed contributed to downwash. Similarly, observing the effects of synthetic jetting on the flow around this simplified geometry would suggest corresponding effects on a plume flow.

The resulting flow-field to be modified using synthetic jets is that of a finite cylinder in a cross-flow. It is known that this flow has both a recirculation bubble downstream of the tip and von Karman vortex shedding off of the cylinder. Both of these phenomena are elements in the plume flow that are believed to cause downwash. By observing the effects on these structures as well as the flowfield near the cylinder, the corresponding effects on a plume flow could be conjectured.

The wind tunnel used for these as well as for later experiments was a variable speed open return tunnel with a 30.5 cm by 30.5 cm (12" by 12")

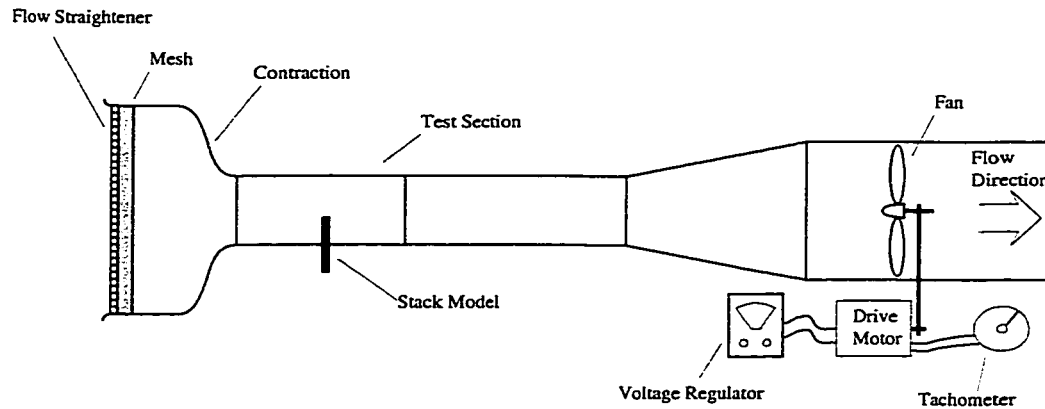


Figure 2.1: Wind Tunnel Schematic

test section located in the Mechanical Engineering Building at the University of Alberta. Figure 2.1 is a schematic of the wind tunnel showing the test section and tunnel layout. Further details about the wind tunnel can be found in Section 2.3.2.5 on page 50.

The design of the preliminary apparatus is illustrated in Figure 2.2, showing a schematic of the apparatus as well as the tunnel test section in which it is installed. The preliminary apparatus used a speaker to excite the air in a closed-ended acrylic resonance tube with slits cut into the walls. A sinusoidal acoustic wave sent through the tube excited the air in these slits, producing the synthetic jets. The closed end (hereafter referred to as the “end”) containing these slits was placed into the test section of an open-return suction-type wind tunnel, and was meant to represent the stack profile in a cross flow. By making the end replaceable, different jetting configurations could be tried

by substituting different ends with different slits cut into them. These different slit configurations are discussed later in Section 2.2.4.3 on page 25. This easy change in configuration is an advantage of a resonance tube based system over one where the general forcing geometry is built into the model near the synthetic jet orifice. Hsaio et al. (1988) and Sigurdson (1995) have used apparatus with somewhat similar forcing arrangements.

The rest of the tube was further divided into a section containing pressure sensors and a section connecting to the expansion leading to the speaker. Signals from the pressure sensors were used to estimate the resonant acoustical pressure and velocity distribution throughout the length of the tube. This was calculated from pressure amplitude and phase information, so the sensors were specifically chosen based on their matched phase response. Phase response matching was done by comparing the phase measurements from two different sensors making identical measurements of a sinusoidal pressure source. These three sections were joined with snug-fitting couplers machined out of Teflon to fit around their outer circumference. The overall tube length, from the tip to the expansion was 1200mm with a 25.4mm (1 inch) outer diameter and approximately 1.6mm (1/16") wall thickness. Unless otherwise stated, the end was inserted 152mm (6") into the 30.5cm X 30.5cm (12" X 12") wind tunnel test section.

Flow visualization was done using the smoke-wire technique (Corke et al. (1977) cited by Chapple (1998)). In Figure 2.2 the relative placement of the smoke-wire components is shown. A more detailed illustration of the system

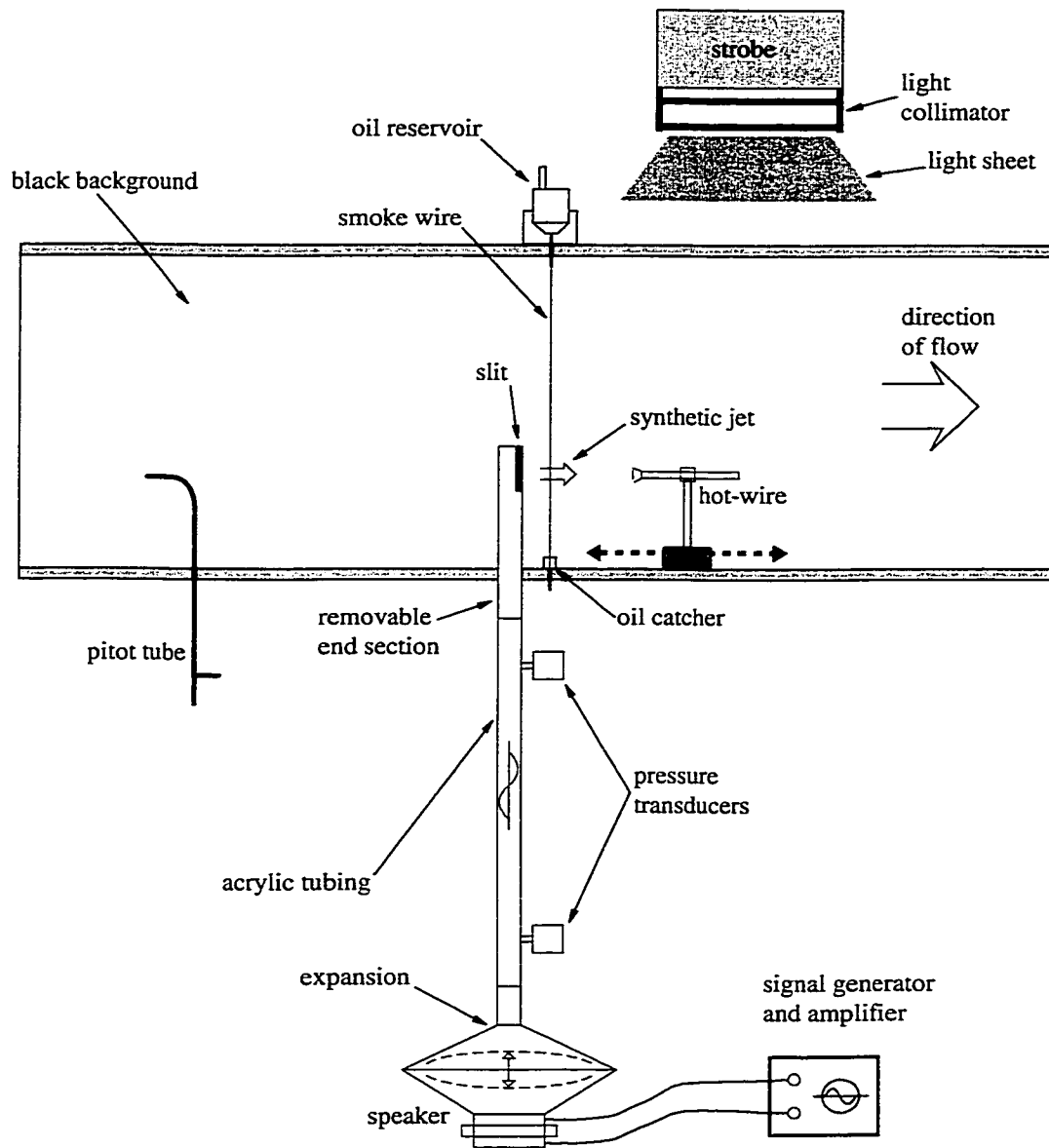


Figure 2.2: Preliminary Apparatus Installation in Test Section

is shown in the cross-sectional view of the test section of Figure 2.3. The smoke-wire technique is where a drop of oil (mineral oil) is allowed to run down a thin (0.005") vertical wire, depositing a series of droplets along the way. When a 60 Hz electric current from a Variac W5MT3A power supply is passed through the wire, the wire and oil heats up, atomizing the oil into an aerosol resembling smoke. Because of the alternating heating and cooling of the wire, timelines appear in the smokesheet as vertical striations of denser and lighter smoke. These striations have a frequency of 120 Hz due to the rectification property of resistive heating. The wire was placed approximately 0.5 stack diameters away from the downstream side of the stack, along the centerline. Placing the wire at this location allowed visualization of the vortex structures shed off the tip of the stack as well as the recirculation bubble and backflow region in the immediate stack wake. This also allowed observation of downwashed streaklines occurring downstream of the tip in order to help elucidate the overall effect of forcing.

When reviewing smoke-wire results it is important to keep in mind buoyancy effects due to the slightly heated smoke. It was estimated from visual observations that the smoke on it own rises at approximately 0.4 m/s. This is when the smoke wire is activated with no cross flow, so the smoke is always enveloped in the rising thermal plume surrounding the wire. When a cross flow is present, the smoke is not surrounded by a concentrated buoyant plume. Thus, there was not a problem with smoke buoyancy when the visualized flow phenomenon was on the order of 1 m/s and above, where the

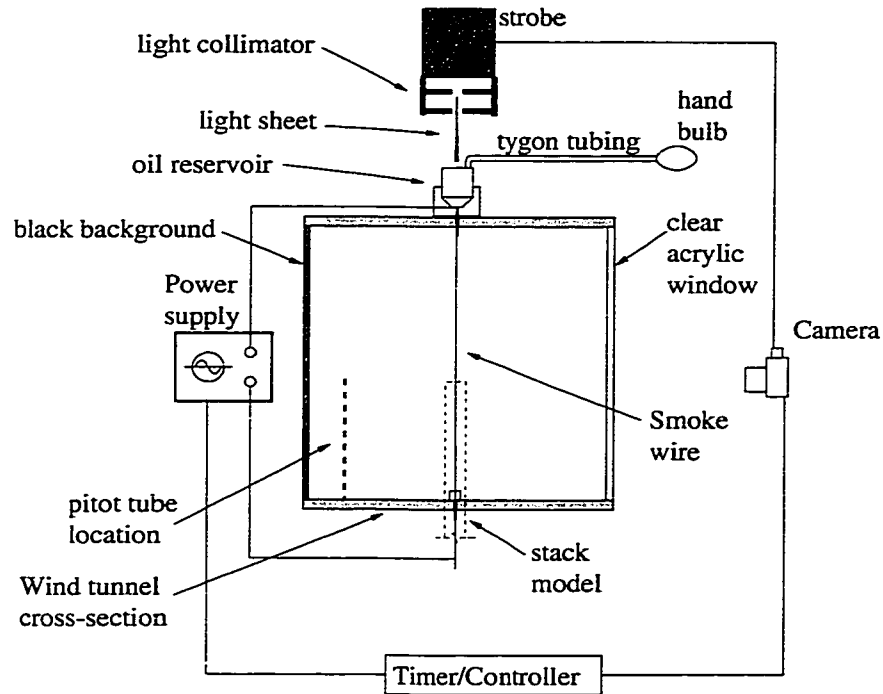


Figure 2.3: Preliminary Apparatus Smoke-Wire and Photography Setup Looking Downstream

rise angle was negligible.

Photographs for both this preliminary experiment as well as the final experiment were taken from side-view with the flow going from left to right (the same point of view as Figure 2.2). The camera used was a Nikon F3 35mm camera using Kodak 3600ASA TMAX black and white film. A General Radio Type 1540 Strobolume was used as a flash. This light was then collimated by passing it through 2 parallel slits before illuminating the plane of the smoke. A piece of black cardboard was used to cover the inside of the

opposite tunnel wall for better contrast against the white smoke. Figure 2.3 shows the orientation of this equipment. A timing box was used to coordinate the activation of the smoke wire with the picture taking apparatus.

2.2.4 Results

2.2.4.1 Synthetic Jet Results¹

Noticeably lacking in the current literature is discussion regarding the response of synthetic jets to formation frequency. If the design of the final apparatus was to be optimized it was important to have knowledge of any such behaviour. As explained in previous sections this was one of the goals in building and testing the preliminary apparatus. Hot-wire measurements were made for synthetic jets produced at several frequencies and amplitudes, and Figure 2.4 shows the results of these measurements. The jetting configuration used for these measurements was the vertical side-slit with two different slit widths, d . On the vertical axis is the mean centerline jet velocity U_{SJ} normalized by u'_{slit} , the RMS average of the oscillating flow just inside the orifice at its centerline. This normalized velocity is plotted against the number of slit widths downstream of the orifice. These plots show clearly the rise and then decay of mean centerline velocity, which is consistent with the measurements of Smith and Glezer (1998). There are two sets of mea-

¹Part of these results were presented by the first author in a talk entitled "Production of Synthetic Jets Using Slots in an Acoustic Resonance Tube", by Diep, J. and Sigurdson, L., at the Annual Meeting of the Fluid Dynamics Division of the American Physical Society, New Orleans, LA., Nov. 1999. Abstract published in Bulletin of the APS, Nov., 1999.

measurements shown on this graph, one set with frequency held constant and varying forcing amplitude, and one at a fixed forcing amplitude but with changing excitation frequency.

It can be seen by the constant-frequency series of Figure 2.4 that more than doubling the forcing amplitude of u'_{slit} from 3.5 to 9.0 m/s has little change in the normalized synthetic jet velocity throughout the measurement range. This suggests that U_{SJ} is approximately linear with forcing amplitude measured by u'_{slit} , for a fixed forcing frequency. Also, the same series shows that the location of the peak in centerline velocity does not shift significantly with jets of fixed frequency. The streamwise location of this peak was found to coincide with transition to turbulence of the vortex pairs in the experiments of Smith and Glezer (1998).

The other set of curves taken with constant $u'_{slit} = 3.5$ m/s shows the effect of changing frequency while keeping excitation amplitude constant. In contrast to the fixed-frequency curves, this set shows a relatively large change in normalized synthetic jet velocity depending on excitation frequency. The maximum normalized velocity at 150 Hz is almost double that at 400 Hz. The resultant normalized velocity of U_{SJ}/u'_{slit} depends on formation frequency, with higher relative jetting amplitudes resulting from lower forcing frequencies. Attempts were made to learn how to properly scale this frequency effect via various Strouhal numbers, but were inconclusive.

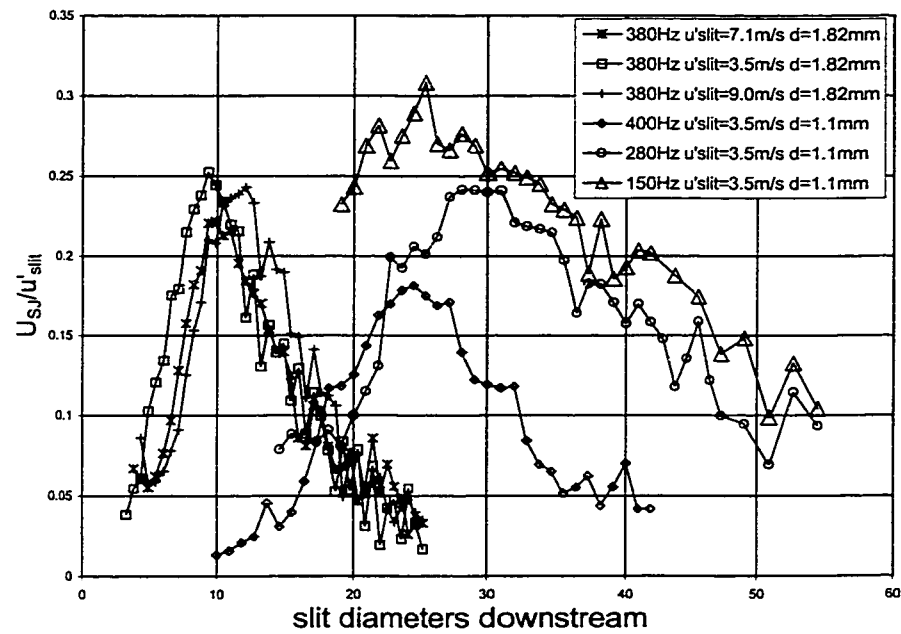


Figure 2.4: Synthetic Jet Measurements on Preliminary Apparatus

2.2.4.2 Flow Visualization

Figure 2.5 shows a reference photograph of the test section showing the tip in a cross flow and the resultant smoke streaklines. The stack extends 152mm (6 stack diameters) from the tunnel floor, and cross flow velocity is approximately 1 m/s, measured by the pitot tube and a Setra pressure transducer². This velocity measurement was later checked by calculating an estimated velocity based on the wavelength of the 120 Hz vertical striations in the smoke, which agreed to within 15%. There is no forcing in Figure 2.5, and the downwashed streaklines immediately downstream of the end of the stack are clearly shown. Other features suspected of contributing to downwash are also visualized by the smoke-wire. The periodic vortices shed off the tip are made visible as they are advected past the smoke-wire. This shedding frequency can be estimated to be approximately 20 Hz by counting the number of striations between vortices. These vortices descend gradually with downstream distance, by approximately 0.7 stack diameters at 11 diameters downstream of the stack. This gradual descent of the vortical structures is suggestive of the continual distributed downwash shown by Johnston and Wilson (1997). The recirculation region immediately downstream of the stack is also made visible through entrainment of smoke into the stack wake. While these structures are visualized with no plume present, the flow field can be thought of as simply having a very weak plume, which is precisely the condition for which downwash occurs. The changes to this flow field effected by different

²This measurement is further discussed in Section 2.3.2.6

synthetic jet forcing configurations should be observed with this in mind.

A 170 Hz synthetic jet produced by this apparatus with no cross-wind is visualized in Figure 2.6 using the smoke-wire. The slit used to produce this jet is 1.6mm wide by 40mm long ($AR=25$), and is oriented along the axis of the tube, starting from the closed end. In this photo, mean centerline jet velocity is ~ 1 m/s measured at 3mm from the orifice exit plane, and the strong entrainment towards the jet orifice mentioned by Smith and Glezer (1998) is indicated by the smoke just above the jetting region. Even though most of the smoke is moving up due to buoyancy, smoke just above the orifice is being drawn downwards towards the orifice, against the buoyancy force.

2.2.4.3 Forcing Configurations

Figure 2.7 shows a series of schematics illustrating the various synthetic jetting configurations used in this experiment. As indicated in this Figure, the jets are in general categorized as:

- (a) Jetting downstream
- (b) Jetting upstream
- (c) Jetting cross-stream
- (d) Jetting vertically

One other possibility is jetting vertically with azimuthally varying strength, either steadily or with time-dependence. This was not attempted here.

Using results from wind tunnel experiments on this preliminary apparatus, it was decided that the final apparatus would be designed with the



Figure 2.5: Reference Photograph Showing Smoke-Wire Flow Visualization (no forcing, $U_\infty \sim 1 \text{ m/s}$)

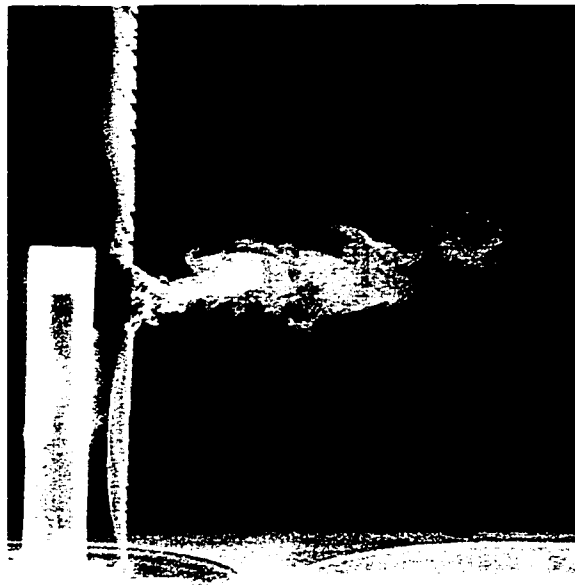


Figure 2.6: 1 m/s Synthetic Jet Visualized using Smoke-Wire, Jet Configuration Similar to Figure 2.7a, $f=170\text{ Hz}$, $V_{exc} = 2.43V_{rms}$

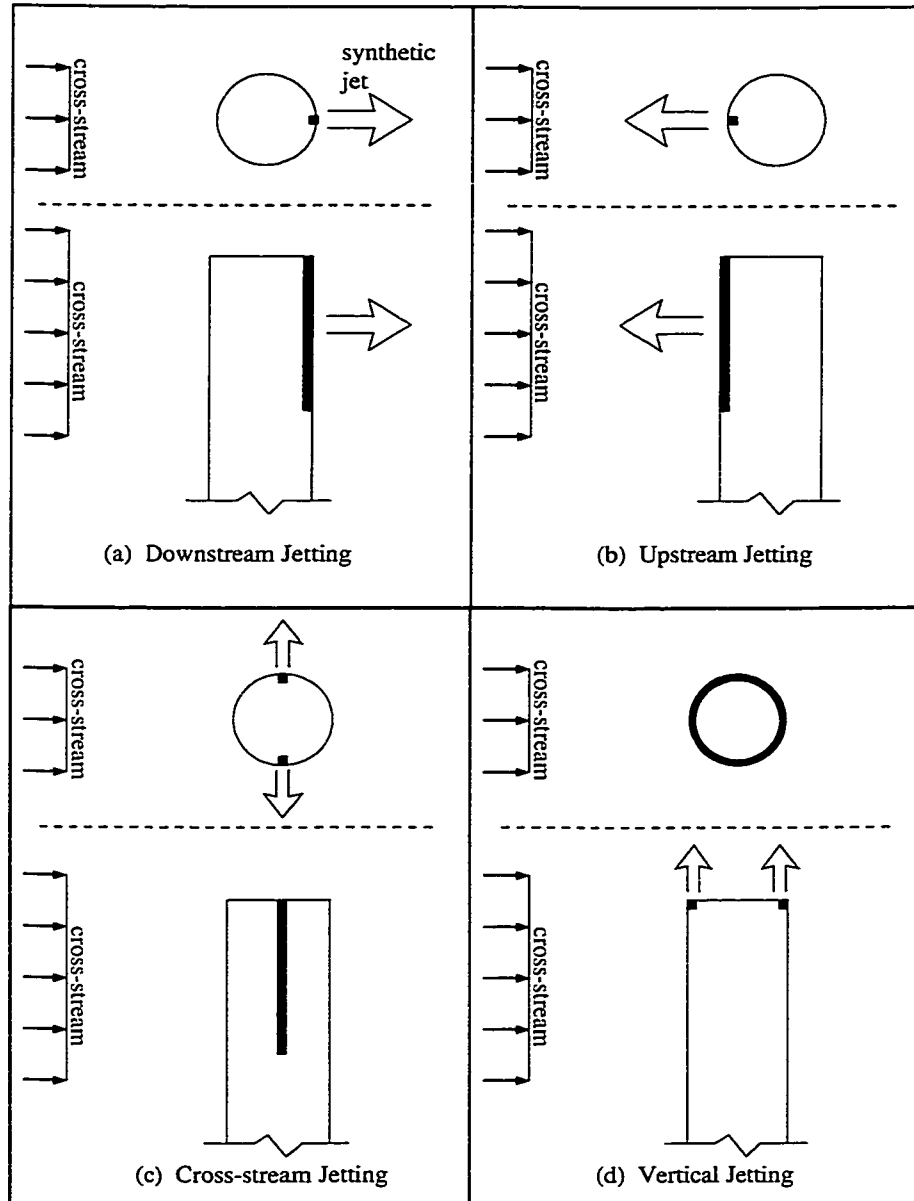


Figure 2.7: Various Synthetic Jet Configurations Explored. The synthetic jet is represented by the open arrow, and a dark heavy line indicates the synthetic jet orifice(s).

configuration (d) shown in Figure 2.7d, a vertically oriented annular synthetic jet co-axial with the plume flow. Figure 2.8 is a photograph showing the effect of this forcing. Speaker excitation is the same frequency (170 Hz) and amplitude as for Figure 2.6, although it is a horizontal synthetic jet orifice. Without forcing, vortices shed naturally off the tip at approximately 20 Hz. This configuration has the most dramatic influence on downwashed streaklines in the preliminary experiment, and shows evidence of reducing or destroying coherent structures shed off of the tip which may be related to similar structures suspected to cause downwash in a plume flow. This may serve to reduce downwash normally effected by these components. When applied to a plume, this forcing also adds momentum to the plume. This is the dominant mechanism in reducing downwash, because it helps plume gases escape the immediate near-wake entrainment zone. One practical advantage to the annular vertical forcing is its symmetry with respect to the approaching flow, which means that the approach direction of the cross-wind will not influence the effect of forcing.

Jetting upstream provides the second best results. Figure 2.9 shows a photograph of this, with a 1 m/s synthetic jet pointing upstream, as illustrated in Figure 2.7b. On average, originally downwashed streaklines are displaced upwards somewhat, although the effect is far less prominent than with the vertical jetting. Also, the smoke in the turbulent region of the stack wake does not reach as close to the wind tunnel floor as is does in the reference case. Even though these are indications that this configuration has

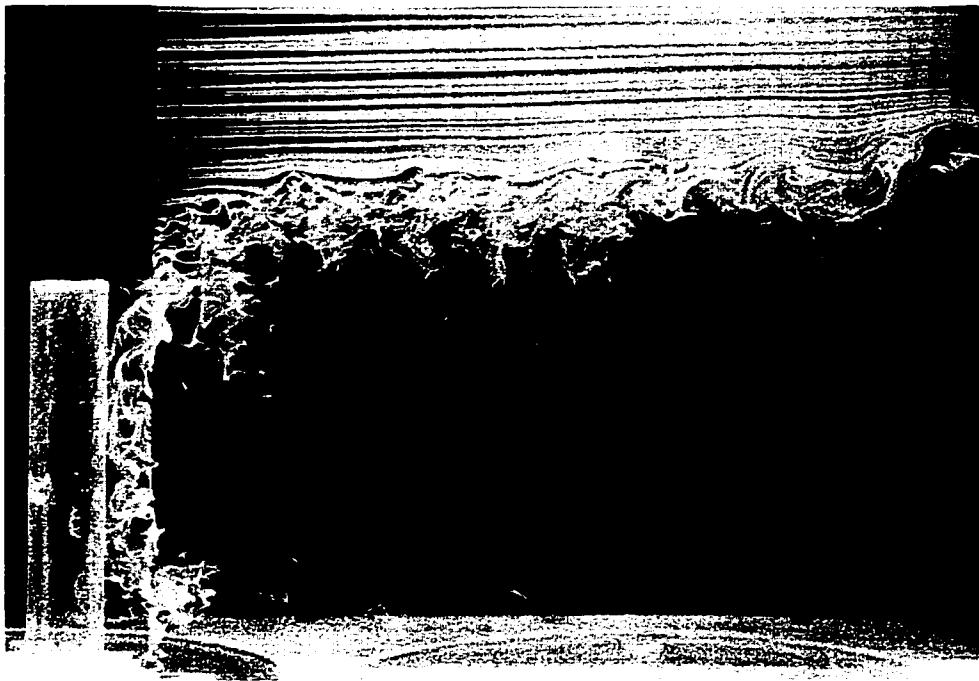


Figure 2.8: Vertical Synthetic Jet Applied in a Crossflow, Jet Configuration Similar to Figure 2.7d. $U_{\infty} \sim 1 \text{ m/s}$, $f = 170 \text{ Hz}$, $V_{exc} = 2.43V_{rms}$

the potential to alleviate downwash, the vertical jetting was chosen because it will have a more direct interaction with the plume, and has the benefit of insensitivity to flow direction due to its axis-symmetry. Light and dark regions in the smoke at and above the level of the stack wake are the result of deformations of the smoke sheet in and out of the plane of light running down the centerline. This asymmetry in the wake was not present in the reference photo.

Directing synthetic jets in the wake of the stack as illustrated in Figure 2.7a does not improve the downwash of streaklines, but in fact makes them downwash more strongly, as shown in Figure 2.10. Experiments with similar configurations have been done on infinite cylinders. Duke et al. (1993) did one such experiment using conventional jets, and noticed a reattachment of streamlines that made the flow resemble the potential flow solution around a cylinder. A numerical experiment by Mo and Duke (1993) with a similar geometry showed the same result. Amitay et al. (1997) performed the same experiment with a synthetic jet substituted for the conventional jet, and achieved similar results only with jetting velocities around an order of magnitude lower. Flow visualization from these experiments show normally separated stream-wise streamlines turning sharply towards the downstream stagnation point of the cylinder. This turning of near-field streamlines towards the orifice leads to resemblance to the potential flow solution with no separation for a cylinder in a cross-wind. Ostensibly this turning occurs due to the strong entrainment towards the jet orifice that was observed by Smith



Figure 2.9: Upstream Synthetic Jet Applied in a Crossflow, Jet Configuration Similar to Figure 2.7b. $U_{\infty} \sim 1 \text{ m/s}$, $f = 170 \text{ Hz}$, $V_{exc} = 2.43V_{rms}$

and Glezer (1998) in their synthetic jet study. However, far from resulting in zero form drag, as the potential solution would predict, the drag actually stays the same or increases. This is due to the reduction in pressure distribution over the lee side of the cylinder (Amitay et al., 1997). In the present case of the finite cylinder, this lower pressure region in the wake of the tip is what draws the streamlines towards the wake and thus increases their downwash in the near-field.

It is unknown if the effects of cross-stream jetting, illustrated in Figure 2.7c, can be adequately captured using the existing techniques. Figure 2.11 contains a photo with cross-stream forcing at the same frequency and speaker voltage as in Figures 2.6 through 2.10. It can be seen that there are no drastic changes in the downwashed streaklines. While it can be surmised that modifications to the vortex shedding and wake structures might be present when using this forcing due to the out of plane distortions evident in the smoke sheet, that is the best that can be done using this technique. Future investigations into this effect should take into account the visualization of flow-phenomena away from the centerline, in order to gain a better idea of the effect of this forcing.

Through the course of experiments, it was found that the advantages of having a resonance tube-type synthetic jetting apparatus are its relative simplicity as well as having the amplification effects of a resonance tube, requiring a smaller input to the speaker. As a result the acoustic total harmonic distortion is kept low, typically less than 5% as measured by the pressure sen-

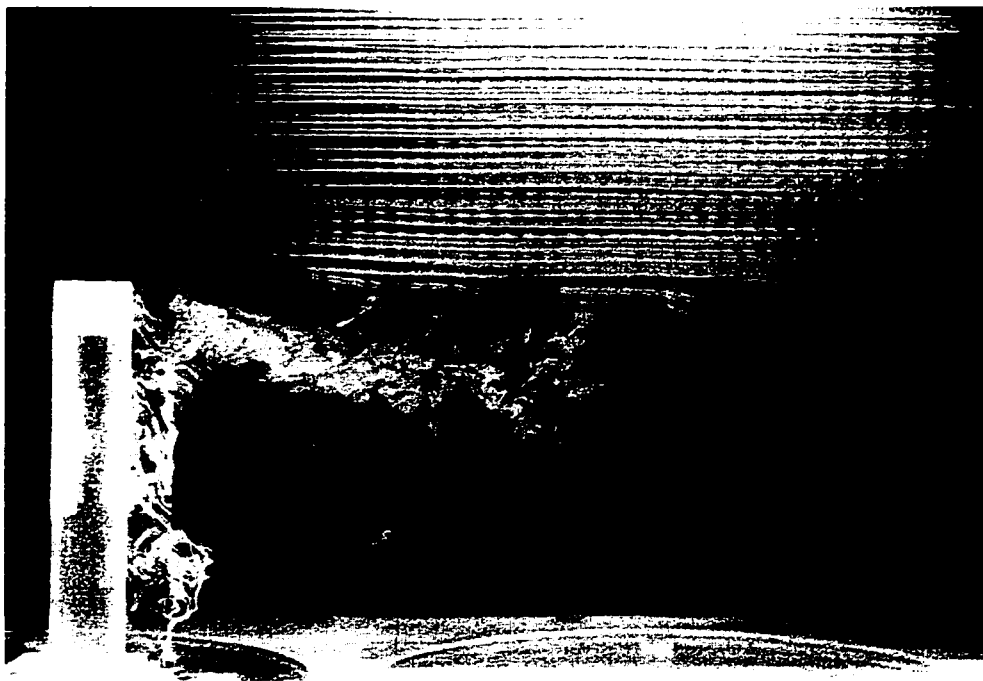


Figure 2.10: Downstream Synthetic Jet Applied in a Crossflow, Jet Configuration Similar to Figure 2.7a. $U_{\infty} \sim 1 \text{ m/s}$, $f=170 \text{ Hz}$, $V_{exc} = 2.43V_{rms}$

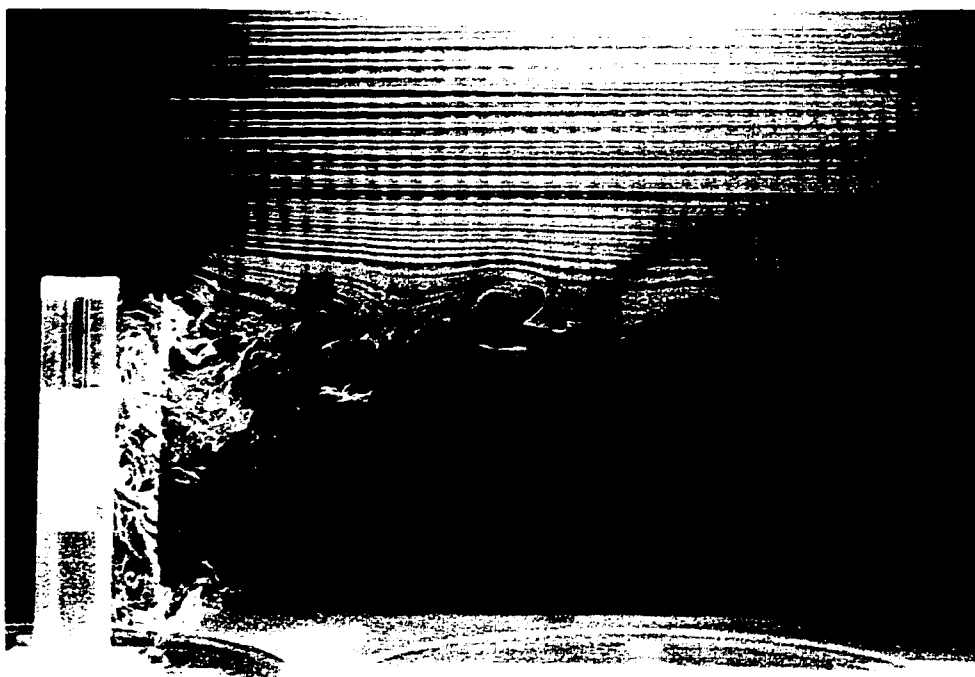


Figure 2.11: Cross-stream Synthetic Jet Applied in a Crossflow, Jet Configuration Similar to Figure 2.7c. $U_{\infty} \sim 1 \text{ m/s}$, $f=170 \text{ Hz}$, $V_{exc} = 2.43V_{rms}$

sors. The main disadvantage is an offshoot of this, being that the jet forcing frequency is confined to ranges close enough to the tube resonances to provide high enough forcing amplitude along with low harmonic distortion. This would not be a problem, however, if it was known beforehand what jetting frequencies were desired and the apparatus designed accordingly.

A problem encountered with using this resonance-tube technique for producing synthetic jets was with non-uniform jetting along the length of a slit running along the axial direction of the tube. Photos showing visualization of only the synthetic jet, with no background flow, shows this happening, possibly due to local pressure loss through the slit. In this case the problem was solved by shortening the slit.

2.3 Final Apparatus

2.3.1 Design

Based on results from the preliminary experiments, the final apparatus was designed with a neutrally buoyant plume flow forced by an annular synthetic jet. While experiments in other laboratories have looked at the behaviour of two dimensional conventional jets in response to the application of a single synthetic jet on one side (Smith and Glezer, 1998), to the author's knowledge this is the first time an annular synthetic jet has been created and used in this manner. A summary of the design constraints for this apparatus goes as follows:

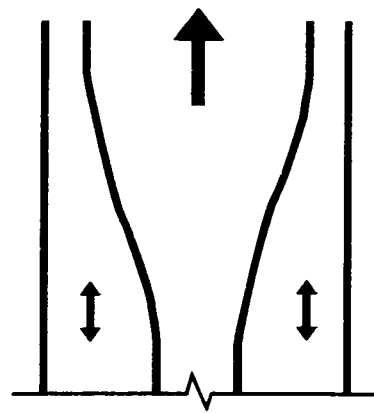
1. The initial plume flow is turbulent and fully developed.
2. The cross-sectional area of the stack tip that contains the plume flow is maximized relative to the total area of the stack tip.
3. An annular synthetic jet is oriented co-axially to the plume and directed along the initial direction of the plume.
4. Synthetic jet velocity is at least comparable to plume flow velocity.
5. The aerodynamic profile of the apparatus seen by the flow resembles a simple-ended cylinder.

The first design constraint meant that the plume flow had to be considered carefully. The original concept, as shown in Figure 2.12a, was to have a stack tip where the plume is carried along a small-diameter tube housed within a larger tube. At the exit plane of the stack, the stack-tube diverges into a final diameter that is closer to the diameter of the larger tube, to maximize the resultant cross-sectional area of the plume. This design leaves a cavity running along the length of the two sets of tubes which is meant to carry the acoustic waves to the opening at the end, producing synthetic jets the same way as the preliminary experiment did. However, having a well-behaved fully developed plume flow at the exit means that the tubing containing the plume requires a section of straight pipe upstream of the plume flow. This precludes the use of any expansions close to the exit plane. Thus the idea of Figure 2.12b was adopted, which is essentially two co-axial thin-walled tubes

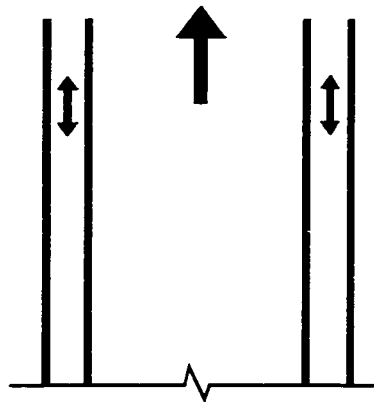
with a small annular space between them. This tip is discussed further in Section 2.3.2.1, and the plume flow in Section 2.3.2.3.

Accounting for the plume flow unfortunately makes it impossible to use the same technique for producing synthetic jets as was used for the preliminary apparatus. Cursory experiments showed that with the narrow width of the resultant annulus between the two tubes, viscous losses were too high to produce significant synthetic jetting at the orifice. This was concluded following a proof of concept experiment where a length of circular tubing was connected to a chamber excited sinusoidally by a shaker table, similar to the forcing of a speaker only at much higher amplitudes. Originally the tubing diameter was chosen to give the same quasi-steady viscous pressure loss as the annulus, and had a similar length as the resonance tube of the preliminary experiment. When this resulted in no discernable jetting at the orifice, shorter sections were used until appreciable synthetic jetting was noticed. This occurred when using approximately 6 inches of tubing, forced at between 40 Hz to 80 Hz. This more direct forcing method was used in the design of the final apparatus.

Applying the results of the proof of concept experiments by shortening the length of the annulus and employing a more direct excitation of the fluid in the annulus, the problem of viscous losses in the annulus is overcome. The resulting design concept was proposed by Coward (2000), and has a resonance chamber connected to the small volume of the annulus, as is shown in Figure 2.13. This design appears to more closely resemble a Helmholtz



(a) Diverging plume flow



(b) Non-diverging plume flow

Figure 2.12: Potential Model Stack Tip Configurations

resonator than the resonance tube. However, it differs from a Helmholtz resonator due to the long length and high aspect ratio of the slit, and the movable piston that comprises one of the chamber walls. This piston is connected to a B&K Vibration Exciter Type 4809, and excited by an in-house built power oscillator. This shaker table-piston arrangement is used instead of a speaker for the larger forces it is capable of applying. Sinusoidal movement of the piston creates a similarly varying pressure in the chamber, and thus across the annulus (between the chamber and ambient air outside the device), which produces an oscillating flow within the slit, and resultantly, jetting at the stack tip.

At the expected experimental forcing frequencies of 40 Hz to 200 Hz, the idea of theoretically treating the fluid in the short tube as a resonating air column is not appropriate, and a quasi-steady approach is more realistic. This is where the pressure gradient along the slit, between the chamber and ambient air, is assumed to reach steady-state within the time-frame of the forcing. This quasi-steady approach is only valid if the forcing frequency is much lower than the resonance frequencies of components in the system (Doebelin, 1972)³. This is the case here, as forcing is in the range of 40 Hz to 200 Hz, while component resonances are in the thousands of Hz, neglecting any viscosity effects. What this also means is the pressure distribution throughout the chamber should be relatively uniform within the timescale of the forcing frequency, and relatively insensitive to the gross geometry of

³This concept is termed a “lumped parameter” approach in this reference.

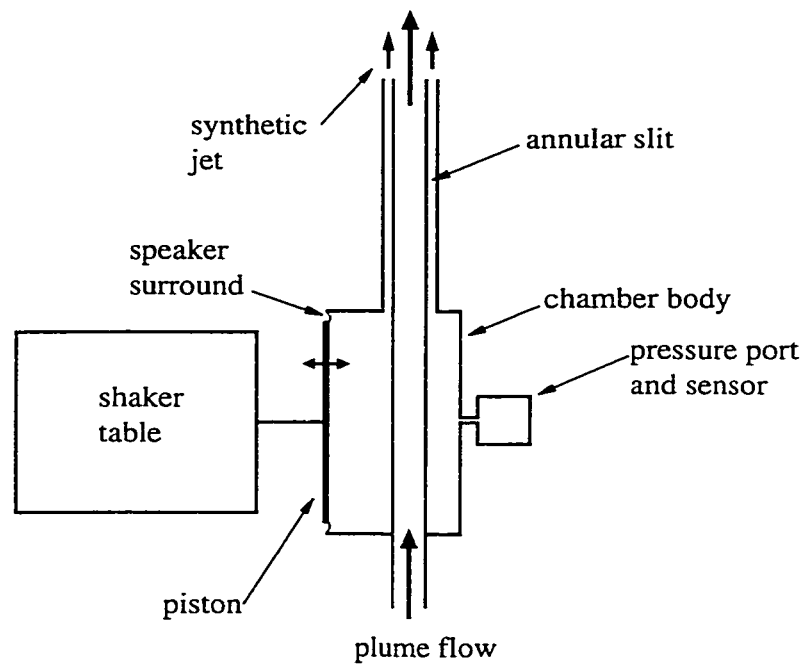


Figure 2.13: Schematic of Final Apparatus

the chamber. This allows a pressure reading taken from anywhere within the chamber to represent the overall pressure everywhere in the chamber. More importantly, this also means that an azimuthally uniform pressure field is expected within the annular slit. This should result in axisymmetric jetting about the orifice.

2.3.2 Construction and Instrumentation

A schematic illustrating the installation of the final apparatus in the wind tunnel test section as well as indicating pressure measurements is shown in Figure 2.14. Components shown in this Figure will be referred to in the following discussion.

2.3.2.1 Stack Tip

The stack tip, which enters the test section of the tunnel, is constructed of two concentric thin-walled brass tubes. The wall thickness of both tubes is 0.74mm (0.029"), with 25.4mm (1") and 20.6mm (13/16") outer diameters for the inner and outer tube, respectively. This sizing results in a plume area of 57% of the total stack cross section, with a 1.64 mm gap between the tubes. This gap is 200mm long, and forms the annulus through across which the oscillating pressure field is applied, creating a synthetic jet at the open end. The inner tube is positioned within the outer tube through 4 screws set in the outer tube. The screw threads are sealed with Teflon® plumbing tape to prevent air leakage out of the gap. These screws do not significantly

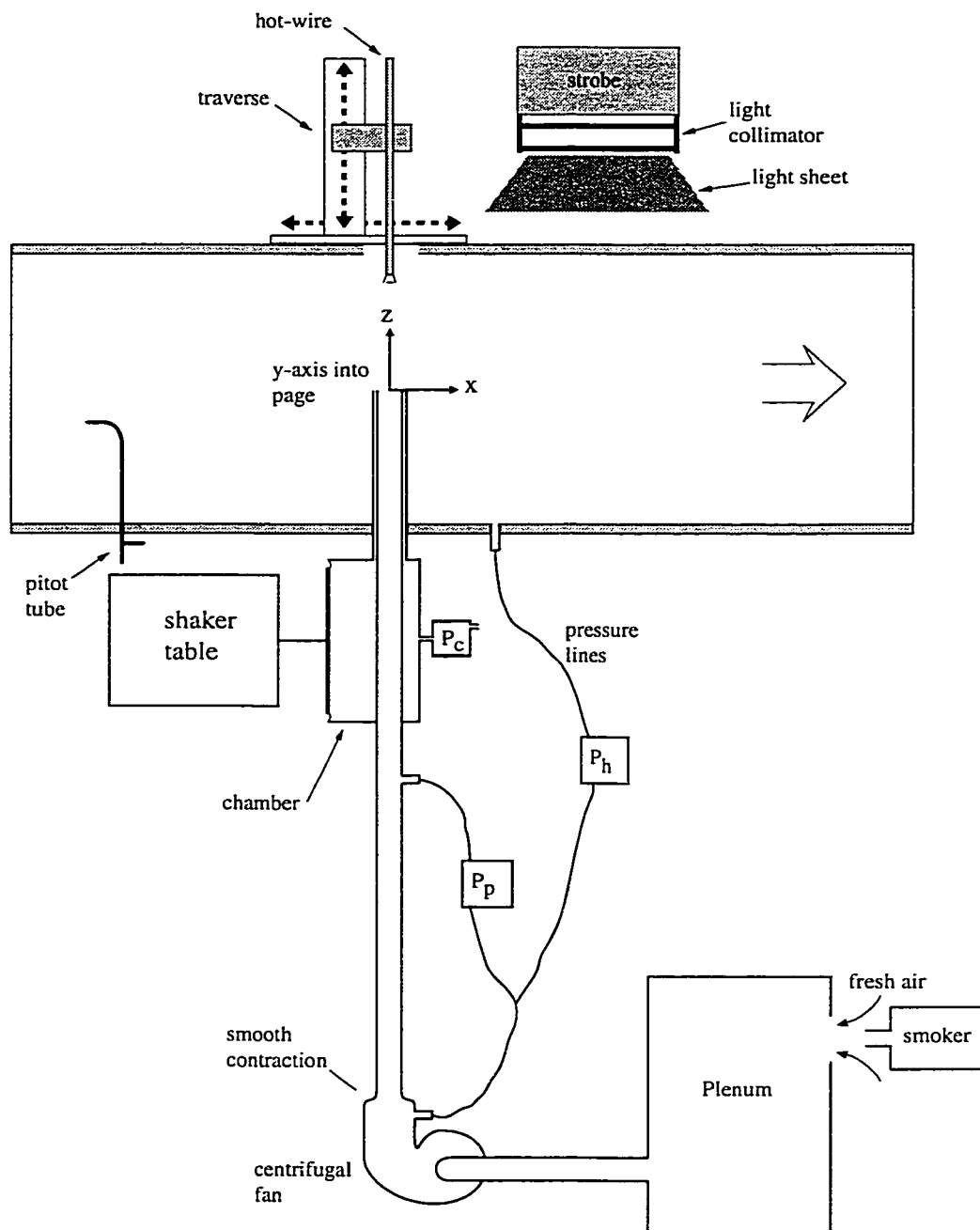


Figure 2.14: Installation of the Final Apparatus in the Test Section

affect the flow in the slit due to their small diameter compared with the wavelength of forcing. Any characteristic frequencies of shedding from the screws are around an order of magnitude higher than the forcing frequencies, meaning that they should be of little consequence. Also, they are placed far enough away from the end of the stack tip so that they can reside outside of the test section, and not affect either the synthetic jetting that occurs at the tip, or the cross flow around the stack.

2.3.2.2 Chamber

The chamber body is constructed of a 51 mm long steel pipe section machined to 154 mm inner diameter and 6.4 mm wall thickness. Final chamber volume after final assembly is approximately $3.3(10^{-3}) \text{ m}^3$, including the volume lost to the tube passed through it. The inner brass tube containing the plume flow passes through the entire chamber body, while the outer tube only passes through 1 wall and ends flush with the inner diameter. One end of the chamber is capped with an acrylic plug that is bolted into place.

Chamber dimensions are based around an available 8" diameter speaker surround used to seal around the piston. Previously experience (Chapple, 1998) has shown that the speaker surround is essential in preventing air leakage, while still presenting minimal resistance to piston movement. The design of the foam surround allows it to withstand at least up to 2 kPa of chamber pressure without buckling, which means that the energy transferred to the fluid is maximized. The piston is an approximately 140 mm diameter

piece of 2.4mm (3/32") thick pexiglass which is epoxied to the inner portion of the surround. A hole in the center of the piston accepts a threaded drive rod from the shaker table. Grease is spread around this connection to prevent air leaks. An air-seal around the piston and surround is made by sandwiching the outer flange of the surround between an acrylic ring and a corresponding flange on the chamber body which are bolted together. The copper tubes running through the chamber body are snug-fit and further sealed with grease. All threaded holes are sealed with silicon plumbing tape. The acrylic cap on one end of the chamber is sealed with an o-ring.

Pressure inside the chamber is measured using a Validyne DP15 differential pressure transducer with a 2200 Pa (#3-24) diaphragm. This transducer is connected directly to the chamber cavity through a swagelock fitting attached to the acrylic end cap. The pressure measured by this sensor should very closely follow the bulk pressure in the entire cavity, due to the relatively low frequencies of excitation when compared to the acoustic resonance frequencies of the chamber geometry. In later experiments this pressure port was installed with a tapered nipple to allow compressed air to be sent into the chamber.

2.3.2.3 Plume Flow

The final apparatus is designed to operate with an axisymmetric fully developed turbulent plume flow which is seeded with an aerosol for flow visualization. This aerosol is provided by a Radio Shack chemical fog machine. The

plume is driven by an small DC centrifugal fan powered by a Harrison 855b variable DC power supply providing a maximum of 18 volts. The fog machine fills a plenum with fog that is then allowed to mix with ambient air and cool, as the fog is slightly warm upon leaving the fog machine. This aerosol is then drawn out of the plenum past a valve before entering the fan inlet. This valve is in place in the case that there is a need to restrict the plume flow that is induced by the suction inside the wind tunnel when it is operating. Immediately downstream of the pump the plume flow passes through a smooth contraction with a 2.35:1 area contraction ratio before entering the flow development section. To ensure that the plume is fully developed there are approximately 50 pipe diameters of length between this contraction and the exit plane of the plume. From White (1999), this should be sufficient for fully developed flow even with the highest pipe Reynolds number of 13000 used in these experiments. Figure 2.15 shows a typical velocity profile with $Re = 5400$ near the exit plane of the plume. This profile is symmetrical and shows the characteristic flattened profile of a turbulent pipe flow. The centerline to mean velocity ratio of 0.76 calculated from this profile is comparable to that reported in Schlichting (1979). Using only the fan the plume can be driven at up to 8 m/s centerline velocity. The pipe Reynolds numbers of all of the forced cases are between 3500 and 5400.

Plume flow rate was calculated by using a calibration of the plume centerline velocity, W_{CL} , against the measured pressure drop across the contraction and approximately 30 diameters of straight pipe, P_c . Figure 2.16 shows the

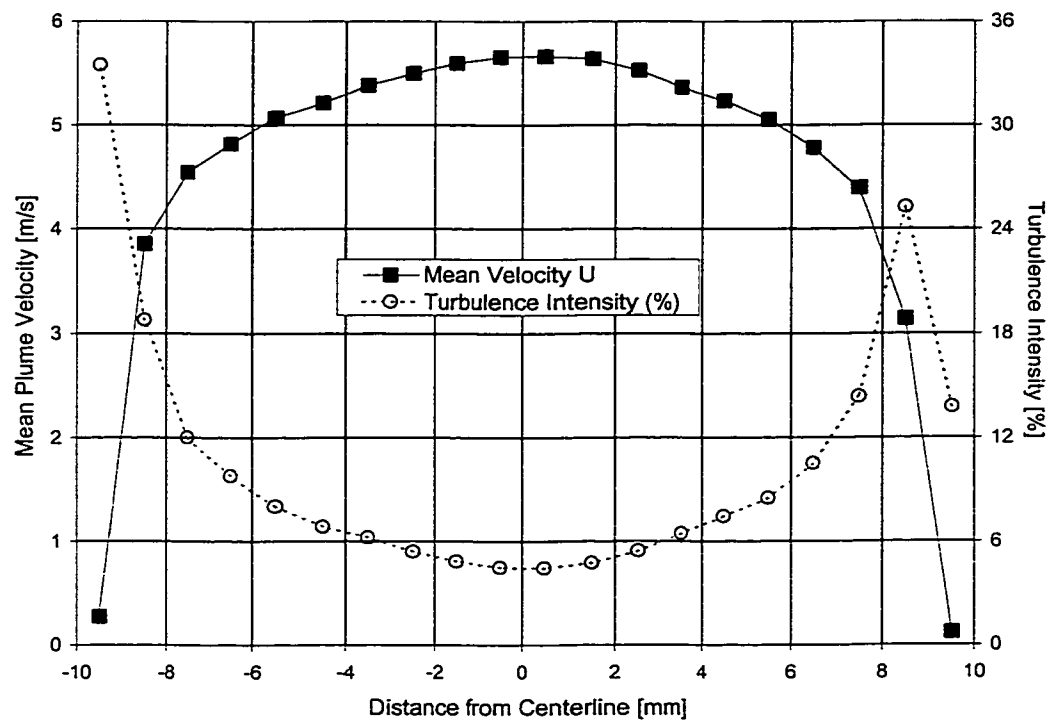


Figure 2.15: Plume Velocity Profile Near the Exit Plane, $Re_p=5400$

results of this calibration. In this graph the transition from laminar to turbulent flow is indicated by the “knee” in the velocity curve near 0.4 Pa, reflecting the different velocity to pressure loss functions for laminar and turbulent flow. In the turbulent region the centerline turbulence intensity stays relatively constant at approximately 4.4%. This is on the order of values cited by Hinze (1975) of around 2.8, measured at a Reynolds number two orders of magnitude higher. This turbulent portion of the velocity versus pressure drop curve is fitted with the functional form for minor losses in turbulent pipe flow shown in Equation 2.1 (Fox and McDonald, 1992):

$$W_{CL} = \sqrt{\frac{P_c - A}{B}} \quad (2.1)$$

where A and B are constants of fit. On subsequent days, this calibration was tested and estimated velocity using the pressure readings fell within 4% of direct hot wire centerline velocity measurements.

In Equation 2.1, W_{CL} is used in the place of mean velocity W_p , with the assumption that the ratio between the two stay relatively constant throughout the turbulent regime. The assumption used in Equation 2.1 is justified both by the relatively good fit of the curve, as well as results taken from direct plume velocity profile measurements where the W_p/W_{CL} ratio was calculated for several operating points. This ratio ranged from 0.725 to 0.750 for W_p of 2.77 m/s to 4.24 m/s, respectively. This change in W_p/W_{CL} is about 3%. For better accuracy, a linear interpolation was applied between these two points

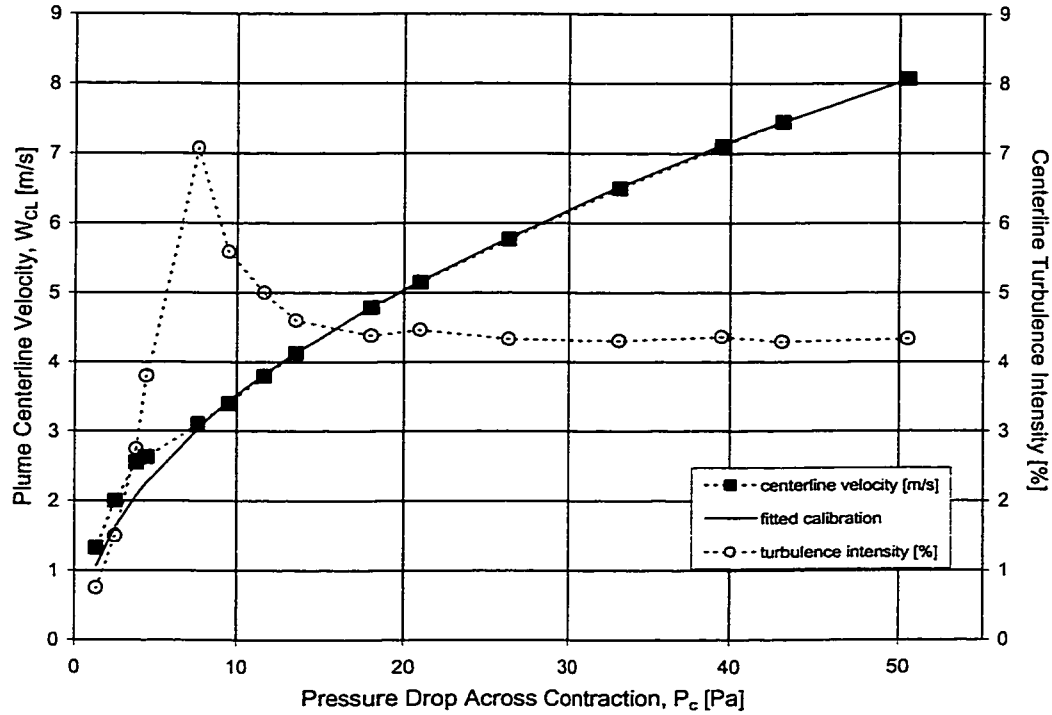


Figure 2.16: Calibration of Plume Exit Jet Centerline Velocity vs. Pressure Drop Measured Across Contraction

and this was used to estimate mean plume velocity for the turbulent portion of the plume centerline velocity calibration.

It was assumed that the addition of the aerosol (“smoke”) into the plume flow did not change the flow rate significantly. To try and verify this, hot-wire velocity readings of the centerline plume velocity were taken with and without smoke with the same pressure drop across the contraction, P_c . Velocity measurements were typically 4%-5% higher with smoke in the plume. This is

possibly due to evaporative cooling of the aerosol depressing the temperature of the plume gas, and therefore causing the erroneous hot-wire measurement. It was noticed that smoke released from the stack at very low velocity into quiescent ambient air tended to sink slowly (< 0.05 m/s) toward the floor of the wind tunnel. This slight density difference is neglected in experiments, but supports the explanation for the differences in measured plume velocity being caused by a temperature difference. Hence, this discrepancy in velocity measurement was ignored in these experiments, and the original calibration shown in Figure 2.16 is used.

2.3.2.4 Support

Due to the strong cyclic forcing being imparted on the apparatus by the shaker table when the synthetic jets were activated, there was concern that vibrations occurring in the chamber structure would be amplified over the length of the stack tip. Vibration of the stack can impart its own influence on the flow around it, possibly giving misleading results. To reduce vibrations in the apparatus as a whole, the support mating the chamber to the shaker table was made very stiff to resist the axial forces of the shaker table. As a result the vibration of the stack even at high forcing amplitudes is negligible.

2.3.2.5 Wind Tunnel

The suction-type open-circuit wind tunnel used for the final experiments is the same as was used for the preliminary experiments. Figure 2.14 shows the

final apparatus installed in the tunnel test section, and a diagram of the tunnel itself was introduced earlier as Figure 2.1 on page 16. The variable-speed drive motor is capable of running the tunnel at velocities up to 8 m/s. No attempt was made to account for the planetary boundary layer. A tachometer on the drive motor allows rough adjustment of wind tunnel velocity given that the flow rate through the tunnel is proportional to the rotational speed of the fan. Turbulence intensities were measured at 0.6% at a flow velocity of 1 m/s, the lowest background velocity used for the test runs, and 0.5% at 4 m/s, the highest velocity used in tests. The test section has a cross section of 30.5cm by 30.5cm (12" by 12"). One side of the test section is constructed of clear acrylic for taking pictures, and the inside wall of the other side is covered in matte black art paper to provide a dark backdrop for better contrast against the white smoke in the photos. Due to the thinness of this paper, it is assumed to have no effect on the flow through the test section.

2.3.2.6 Measurements and Data Acquisition

Operation of the apparatus and wind tunnel are monitored primarily with 4 pressure sensors and 1 hot-wire anemometer. All pressure sensor calibrations were performed with an adjustable water column pressure source and a Dwyer micropoint manometer with a resolution of 0.002 inches of water, or about 0.5 Pa. The following is a description of each of these measurements and their respective uncertainties.

A Validyne DP45 pressure transducer is used to measure P_c , the pressure drop of the plume flow across the smooth contraction and about 35 diameters of straight pipe. The uncertainty in this measurement is about ± 1.2 Pa from its calibration.

A Validyne DP15 pressure transducer is used to measure P'_f , which is the RMS chamber pressure compared to atmospheric pressure. Since the static pressure inside the chamber decreases when the tunnel is operating, the RMS is taken with respect to the mean pressure in order to take into account this offset. The uncertainty of this sensor is estimated to be ± 1 Pa from its calibration curve.

In tests using a conventional annular jet, the fitting usually housing the chamber pressure sensor is changed to a tapered nipple to allow compressed air from the building supply to be run into the chamber and through the slit. When this is done a fourth sensor is used to measure the pressure drop caused by the flow of this compressed air through a laminar flow element. For some synthetic jet test runs, when the laminar flow element is not needed, this same pressure sensor is used to measure the static pressure differential between the inside of the wind tunnel and in the plume flow just upstream of the smooth contraction. Calibration of this sensor gave an uncertainty of ± 5 Pa over a range of 400 Pa. This calibration range is much smaller than the operational range of this sensor (up to 3 kPa), but since this reading is calibrated to the velocity read by the hot-wire at the slit exit, this is not a problem. A few points of this slit velocity calibration was repeated and

agreed to within 4%.

Cross-flow velocity during experiments is measured using a Setra model 264 differential pressure transducer connected to a pitot tube installed 22 cm upstream and 7.5 cm offset from the centerline of the stack. The Setra typically has an uncertainty of ± 0.7 Pa. For typical experimental cross-flow velocities of 3 to 4 m/s this translates to measurement uncertainties of 7% to 4%, respectively.

Hot-wire calibrations were done in the center of the empty wind tunnel test section against velocity measured by the pitot-tube and Setra pressure transducer. The calibration range was between 0.8 to 8 m/s. Hot-wire calibration results show an uncertainty in the calibration of $\pm 5\%$ for velocities above 0.8 m/s. Uncertainty in velocity reading calculated from the Setra pressure transducer at 0.8 m/s is around $\pm 98\%$. However, suitably linearized calibration data points show little deviation from a similarly linearized calibration curve both in the higher velocity ranges, where reference velocity uncertainty is below $\pm 2\%$, as well as in the lower range where this uncertainty is higher. From this it can be estimated that the overall uncertainty in the hot-wire velocity reading is $\pm 5\%$ from the hot-wire calibration curve itself, in the range of 0.8 to 8 m/s.

On the roof of the wind tunnel test section is an x - z traverse to which the hot-wire probe is mounted to measure positive z -components of the plume and forcing velocities. Due to physical limitations the furthest inside the slit the hot-wire can reach is 3mm, or about 1.8 slit diameters. Movement in

the x direction is screw-adjusted with a resolution of 0.5mm. Adjustments in the z -direction are made by hand-moving a slider that has adjustable stops for repeatable placement, with a resolution of 1.0mm. There is limited adjustment in the y -direction, but this was used only to align the hot-wire with the smokestack.

The acquisition and processing of all pressure and hot-wire sensor data is done using an 800 MHz Pentium equipped with a 12-bit AT-MIO-16-E National Instruments data acquisition board and running LabVIEW® 4.1.1⁴. The signal rate is approximately 16 kHz and the scan interval is 4 seconds. These 4-second intervals of data are stored and can be later retrieved using the same LabVIEW® program. Measurements of steady voltage signals from the board have been compared to readings using a Fluke 8062A digital multimeter, and agree to $\pm 1\%$. The dynamic data acquisition of this system has also been verified using a sine function generator and oscilloscope. DC and AC voltage readings from the plume flow fan and shaker table input, respectively, are read using Fluke 8050A digital multimeters, and manually typed into LabVIEW® to be recorded along with the data signals.

2.3.2.7 Photographs and Procedure

The camera and light source is the same as was used for the preliminary experiments. Because there is no smoke-wire used for these photos, the timing box was not necessary. Instead, the camera was hand-triggered and

⁴For the preliminary experiments a 166 MHz Pentium was used with the same hardware and software.

the built-in flash port activated the strobe through a specially built signal conditioner. Once the the background flow velocity is set by reading the pitot-tube velocity from LabVIEW®, the procedure for setting each operating point and then for taking photographs and data is as follows:

1. Adjust the plume fan voltage until the plume reaches it set point. This is monitored using a multimeter reading the P_c pressure transducer voltage output, which has been calibrated against the plume flow.
2. Fill the plenum up with smoke from the chemical fogger. This takes between 1 to 2 seconds of smoking.
3. Wait approximately 4-10 seconds for the smoke to mix with air in the plenum and for the plume flow to stabilize. The plume is checked visually for a steady flow of consistent smoke density.
4. Turn off the light and take a photograph using the push-button on the camera power winder.
5. Take a 4-second data sample using LabVIEW®.
6. Record shaker table and plume fan Voltages.

Photographs are taken of a series of operating points corresponding to “strips”. These strips consist of 11 to 12 photographs where the first one is at the operating point without excitation, and then single photographs are taken at different levels of excitation for a fixed frequency. Because it

is the trend of the downwashing effect that is of interest, it is not critical to precisely quantify the effect at any one operating point. Thus multiple photographs or multiple-exposure photographs are not necessary. Between strips, the apparatus is inspected and cleaned if necessary. This cleaning is required as over time the fog solution collects into droplets on the lower section of the pipe, inside the fan casing, and around the synthetic jet orifice where strong section entrains plume fluid into the slit.

2.3.3 Performance

2.3.3.1 Slit Flow

An analytical solution of the momentum equation for oscillating flow in a a two-dimensional channel, which the author refers to as a slot, is given in Panton (1996). The oscillating flow velocity measurement in the final experiment, given by w'_{slit} , is taken near the exit of such a channel which is actually annular but approximated as being flat. In this solution, a constant pressure differential is applied along the length of the channel along with a superimposed sinusoidal pressure variation. It is assumed that the solution is dependent on time and channel diameter d_a , but not streamwise channel length l . These equations are linear along the length of the channel so the full solution is separated into one considering the constant pressure differential, and one considering the oscillating pressure component. Only the solution to the oscillating portion will be considered here. There are two different solutions depending on the value of the parameter Λ , which compares channel

diameter to the viscous diffusion length.

$$\Lambda = \frac{d_a}{2\sqrt{\nu/(\pi f)}} \quad (2.2)$$

In this equation forcing frequency is f , and kinematic viscosity is ν . The solution as $\Lambda \rightarrow 0$ is a quasi-steady-state result for f approaching zero. The velocity profile across the channel is parabolic and is able to follow the changing pressure gradient because viscous diffusion length is great compared to the channel diameter. The channel centerline velocity of this solution is evaluated as Equation 2.3:

$$w'_{slit} = \frac{d_a^2}{8\mu l} P'_f \quad (2.3)$$

where μ is absolute viscosity, w'_{slit} is the RMS value of the axial velocity fluctuations inside the channel, and P'_f is the RMS value of the fluctuating pressure inside the chamber due to forcing by the piston. P'_f creates the pressure differential across the length of the channel. Equation 2.3 is identical to that for steady laminar channel flow.

Values of Λ for the final experiment are 0.95 with 40 Hz forcing, and 1.5 with 100 Hz forcing. Neither of these values are close to zero. Looking at the other solution for $\Lambda \rightarrow \infty$, and evaluating it for centerline velocity, yields the unsteady solution:

$$w'_{slit} = \frac{1}{2\pi l \rho_s} \frac{P'_f}{f} \quad (2.4)$$

In this equation ρ_s is the air density. Air density, forcing frequency, or

channel length did not appear in the quasi-steady-state solution given by Equation 2.3. This is because inertia effects of the fluid mass inside the slit are taken into account in the unsteady solution. With greater density, channel length, or excitation frequency, the inertial loading of the channel fluid increases giving a reduced w'_{slit} for a fixed forcing pressure. The absence of the variable d_a is due to the relatively short viscous length causing the fluid in the channel center to not be affected by the walls. It is as if the walls are not even there. What this solution shows is that the oscillating velocity in the channel should depend on the amplitude of the forcing pressure divided by the forcing frequency.

Figure 2.17 shows a graph of the w'_{slit} frequency-response of the final apparatus with no background flow. Hot-wire measurements of w'_{slit} were made approximately 2 slit diameters into the slit. The excitation frequency to the shaker table was increased in approximately 5 Hz increments while adjusting the voltage at every step to keep a constant input voltage of 3 V_{rms} . It can be seen from this response curve that even though there is a fairly constant response in chamber pressure, there is a strong frequency dependence in the w'_{slit} response, as predicted by Equation 2.4. There is a slight peak at 230 Hz in the pressure response, possibly around the system resonance of the shaker table exciter-rod mass and the air-spring in the chamber, but running the tower at this frequency would offer no advantages due to the low w'_{slit} near this frequency.

The w'_{slit} data from Figure 2.17 is shown in Figure 2.18 using the lineariza-

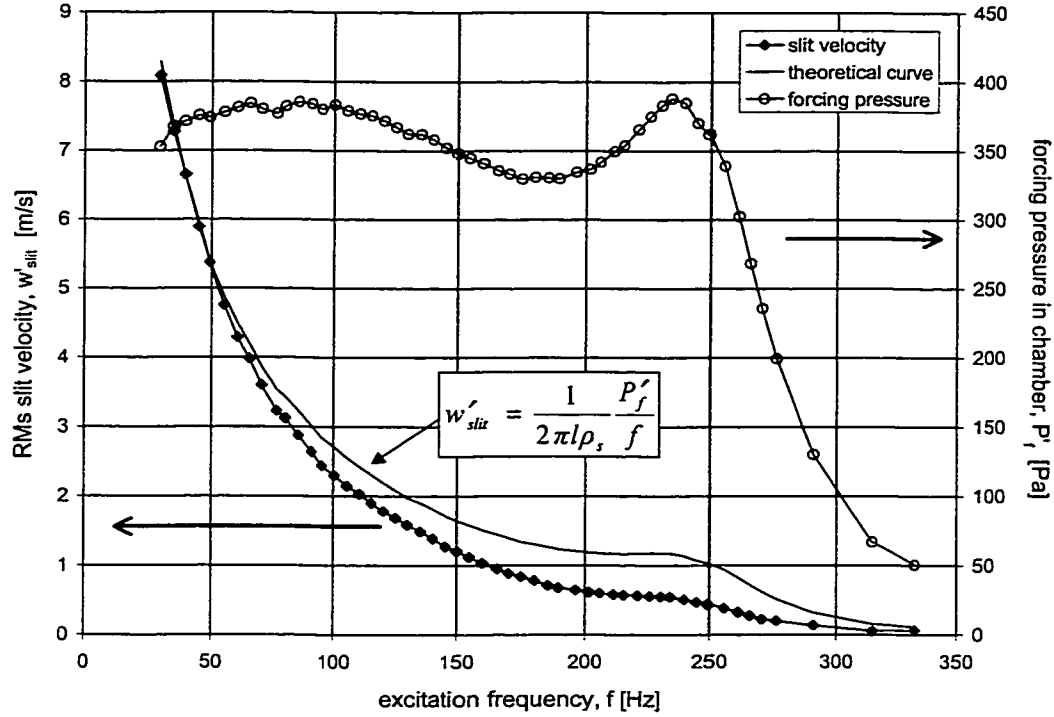


Figure 2.17: Frequency Map of the Final Apparatus

tion suggested by Equation 2.4. Calibration curves of w'_{slit} vs. P'_f made for the fixed frequencies of 40 Hz, 70 Hz, and 100 Hz, are also shown in this Figure. A fitted line is shown on this plot, and the slope of this line differs from the calculated slope from Equation 2.4 by less than +2%. Total harmonic distortion of the pressure reading throughout these measurements is typically less than 5%, and the largest deviation of the individual calibration curves to the predicted slopes is +8%. This agreement seems reasonable, bearing in mind the following two points: 1) The geometry here is an annulus with

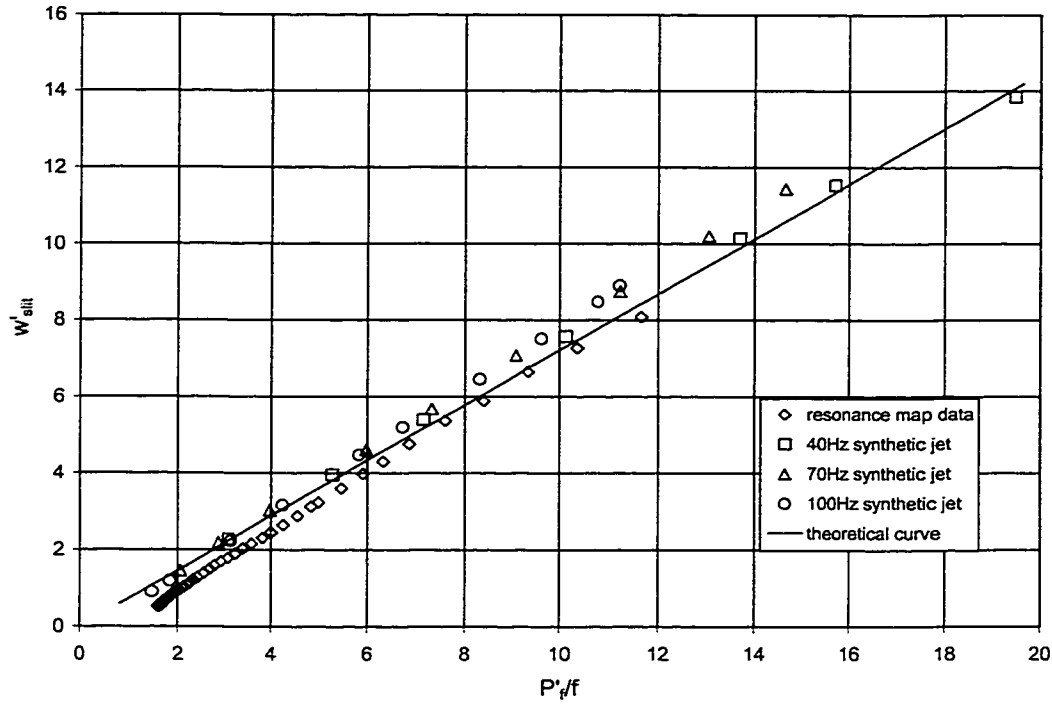


Figure 2.18: Slit Velocity versus Forcing Pressure Data For Final Apparatus Compared to Equation 2.4

relatively high curvature while the original equations were solved for a thin slit with no curvature, and 2) Λ is on the order of 1, while the equations are solved for the limit of $\Lambda \rightarrow \infty$.

The actual measured slopes of the fixed-frequency curves shown in Figure 2.18 are used to estimate w'_{slit} from P'_f measurements during experiments using those same frequencies. This avoids having to directly measure w'_{slit} . It was found that when measured at the furthest upstream location of the an-

nulus, the w'_{slit} vs. P'_f slope increases up to 16% when $U_{inf} = 3.0$ m/s. This is likely a local effect due to the small pressure differential that exists between 3 mm inside the slit and the ambient air. Regardless, it seems likely that the averaged w'_{slit} further into the slit still follows the original calibration, due to the relatively small dynamic pressure of the background flow compared to the larger pressure differential across the length of the slit ($< 1\%$). For this reason the original calibration done with no background flow was used for estimating w'_{slit} during experiments.

2.3.3.2 Synthetic Jet Measurements

Synthetic jet velocity W_{SJ} is characterized by a centerline mean hot-wire reading taken 3 mm ($z/d_a = 2$) from the orifice exit plane. This location is used as a compromise between being too close to the jet orifice where flow reversal takes place, and too far downstream of the jet to measure the jet speed that is affecting the emerging plume close to the exit plane. Flow reversal results from entrainment of air into the orifice during the suction phase. Flow reversal inside the orifice is equal to the outflow in the ejection phase, by conservation of mass. As centerline measurements are made away from the orifice, a hot-wire trace shows a dominant peak, corresponding to the ejection phase, and a smaller peak corresponding to flow reversal in the suction phase. These peaks are of course rectified as the hot-wire cannot differentiate by velocity direction. Smith and Glezer (1998) found this flow reversal to end at $z/d = 3$ for their experiments. Similarly, for the

final apparatus, this flow reversal ends between $z/d_a=2$ to $z/d_a=3$ for the test frequencies used⁵. At $z/d_a=2$ phase-averaged hot-wire measurements show this flow reversal to be either minimal or nonexistent. Amitay et al. (1997), using a synthetic jetting mechanism similar to those used by Smith and Glezer (1998), characterized synthetic jet velocity using average cross-jet mean velocity measurements taken at $z/d=2$.

Synthetic jet velocity is linear with excitation amplitude, as measured by the chamber RMS pressure. Furthermore, they scale with P'_f/f similar to the slit flow. Figure 2.19 shows the response curves of the 3 frequencies used, and Figure 2.20 shows the same data but reparameterized to show the collapse of the three curves onto one. The identical linear scaling of W_{SJ} and w'_{slit} means there is a constant ratio of $W_{SJ}/w'_{slit} = 0.46$. The measured slopes of Figure 2.19 were used to provide an estimation of jetting velocity from the chamber pressure recorded during experiments. The slope of Figure 2.20 was used to estimate jetting velocity when either un-calibrated frequencies were used for experiments, the jetting amplitude was too low to be reliably measured using the hot wire, or both of these problems were present.

2.4 Summary

The design and performance of a wind-tunnel model smokestack with a plume forced by a synthetic jet has been discussed. A preliminary model without a

⁵Flow reversal was observed using a LabVIEW[®] routine to approximate phase-averaged data from time-series measurements. In this case the data was phase-averaged over the period of synthetic jet forcing frequency.

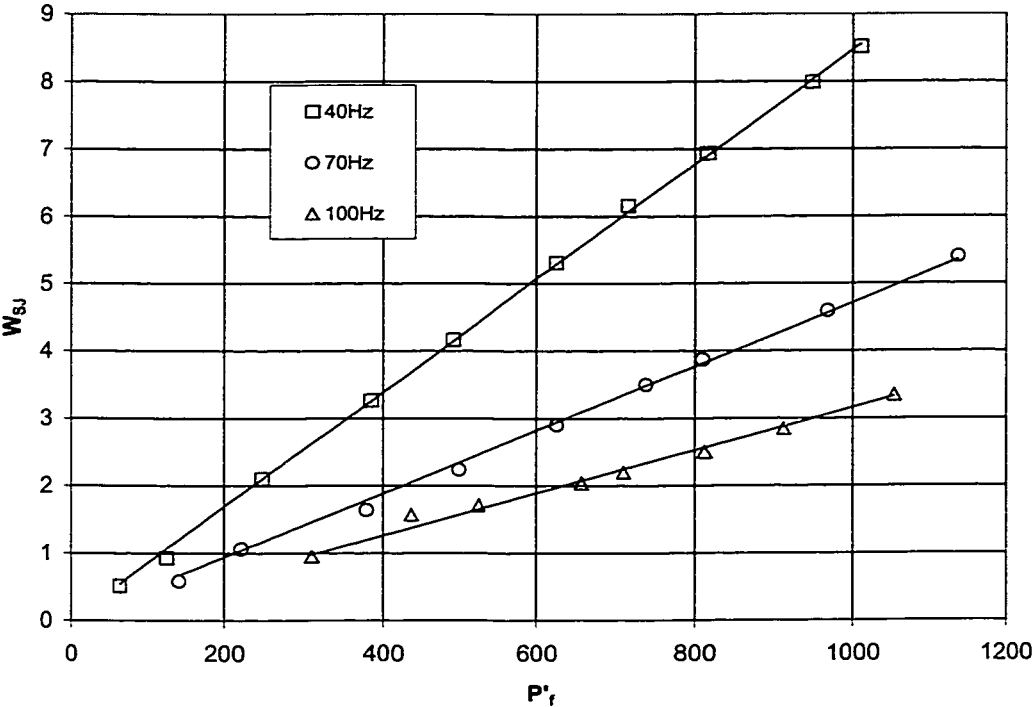


Figure 2.19: Calibration of Mean Centerline Synthetic Jet Velocity 3 mm From Orifice vs. Forcing Pressure of Final Apparatus for 3 Forcing Velocities

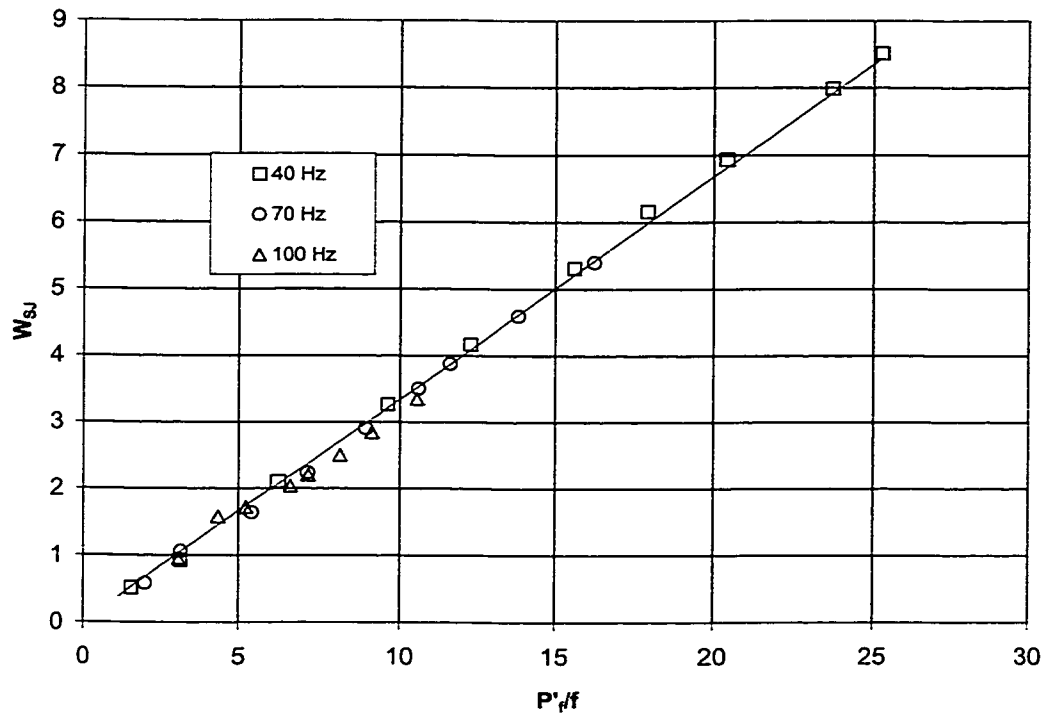


Figure 2.20: Collapsed Mean Centerline Synthetic Jet Velocity 3 mm From Orifice of Final Apparatus, For 3 Different Forcing Frequencies

plume was built and tested in order to find the most effective and practical synthetic jetting configuration to use in the final model. The most effective configuration, with annular synthetic jet is directed upwards coaxial with the initial plume direction, is used in the final apparatus. This forcing configuration has the advantage of having the most direct influence upon the plume, and no dependence upon the approach direction of the crossflow. The design is based around 2 thin-walled concentric tubes, with the inner one containing the plume flow, the outer one providing the aerodynamic profile to the background flow, and a thin slit between the two to contain the oscillating pressure field creating the synthetic jet. Due to viscous losses in the thin slit, the same acoustic forcing technique as the preliminary experiment could not be used. Instead, the slit length was shortened, and the fluid therein was more forcefully excited using a shaker table and piston arrangement.

Synthetic jet measurements from the preliminary experiments suggest that jetting velocity is approximately linear with forcing amplitude and decreases with forcing frequency. This is verified by a calibration of the final apparatus showing that the oscillating slit flow scales linearly with forcing pressure amplitude divided by the frequency. This result is consistent with an analytical solution of the Navier-Stokes equations. The mean centerline synthetic jet velocity 2 slit diameters outside of the orifice also scaled linearly with forcing pressure amplitude divided by the frequency, which means there is a constant ratio of synthetic jet velocity to oscillating slit flow velocity. Appropriately scaled calibration values of synthetic jet velocity are used to

approximate jetting velocity during experiments, and a fit of the collapsed calibrations are used to estimate jetting velocities when either uncalibrated frequencies or very low jetting amplitudes are used.

CHAPTER 3

RESULTS AND DISCUSSION

3.1 Introduction

Experiments were performed using the procedures and apparatus described in the previous chapter. Results from these experiments are presented and discussed in the current chapter. In Section 3.2 details of these operating points are explained along with how plume measurements were performed. An example of these plume measurements is presented in Section 3.3, and reference data is compared with results from other studies. In Section 3.4, results are presented from experiments where the plume is forced with a synthetic jet. Measured and photographic data is discussed, and equations for plume rise are presented. This leads to a suggested model for predicting the behaviour of a plume forced by synthetic jets. Other observations regarding the forced turbulent and laminar plumes are also discussed later in this section.

For comparison, some experiments were performed with a steady annular

jet used in place of the synthetic jet. These results are discussed in Section 3.5 and compared to results using synthetic jetting. Differences in these results are discussed in Section 3.6, and a suggestion is made as to why they are different. Finally, in Section 3.7 the effect of forcing on plume downwash is discussed.

3.2 Introduction to Photographic Plume Measurements and Data

3.2.1 Experimental Data Cases

Operating points for the plume and background velocities were chosen to provide a range of plume velocity ratio $R = W_p/U_\infty$. These points consist of 3 crossflow velocities and 2 plume velocities, and the plume is forced by either steady blowing or synthetic jets of different frequencies. In Table 3.1 these operating points are summarized along with their forcing, and assigned case numbers. From here on, these photographic data runs will be referred to by their case numbers unless otherwise noted.

The operating points of the cases shown in Table 3.1 were chosen in order to allow comparison between different cases sharing common parameters. This is useful when trying to determine if there are Reynolds Number effects, either of the plume (Re_p) or the cross-flow (Re_∞). Cases 10 through 12 are included to provide comparison data for runs 7 through 9 at close to the same velocity ratio, but with an increase in Re . Cases 21 and 22 are unforced plumes included for reference. Aside from the comparison cases 10 through

Table 3.1: Experimental Operating Points

Case	U_∞ [m/s]	W_p [m/s]	Re_∞	Re_p	R	Forcing
1	4.0	2.8	6770	3510	0.70	40 Hz synthetic jet
2	4.0	2.8	6770	3510	0.70	70 Hz synthetic jet
3	4.0	2.8	6770	3510	0.70	100 Hz synthetic jet
4	3.0	2.8	5080	3510	0.93	40 Hz synthetic jet
5	3.0	2.8	5080	3510	0.93	70 Hz synthetic jet
6	3.0	2.8	5080	3510	0.93	100 Hz synthetic jet
7	4.0	4.2	6770	5370	1.05	40 Hz synthetic jet
8	4.0	4.2	6770	5370	1.05	70 Hz synthetic jet
9	4.0	4.2	6770	5370	1.05	100 Hz synthetic jet
10	2.5	2.8	4230	3510	1.12	40 Hz synthetic jet
11	2.5	2.8	4230	3510	1.12	70 Hz synthetic jet
12	2.5	2.8	4230	3510	1.12	100 Hz synthetic jet
13	3.0	4.2	5080	5370	1.40	40 Hz synthetic jet
14	3.0	4.2	5080	5370	1.40	70 Hz synthetic jet
15	3.0	4.2	5080	5370	1.40	100 Hz synthetic jet
16	4.0	2.8	6770	3510	0.70	Steady annular blowing
18	3.0	2.8	5080	3510	0.93	Steady annular blowing
19	4.0	4.2	6770	5370	1.05	Steady annular blowing
20	3.0	4.2	5080	5370	1.40	Steady annular blowing
21	2.5	1.6–8.3	4230	2030–10510	0.9–3.4	Unforced plume
22	3.0	1.3–10.4	5080	1650–13170	0.6–3.6	Unforced Plume

(Note: there is no case 17)

12 and the reference cases 21 and 22, the rest of the cases have four plume velocity ratios forced by steady blowing as well as 40 Hz, 70 Hz, and 100 Hz synthetic jets. In all of the cases, the forcing amplitude attainable by the apparatus is sufficient to provide a measurable response.

Each case of photographic data began with a reference photo with the plume and background flow set to their operating points and no forcing applied. For subsequent photographs, forcing was applied with approximately evenly-spaced levels of amplitude throughout the range of the apparatus. There were generally 12 photographs taken for every photo, although only 11 were taken if forcing amplitude reached the limits of the apparatus.

3.2.2 Plume Measurements

Plume measurements were performed on digital scans of contact sheets printed with images of photographic negatives. These photographs were taken through the method described in Section 2.3.2.7 on page 54. The contact sheet scans were made at 600 dpi (dots per inch), resulting in a pixel resolution of around 0.02 stack diameters. Measurements of these scanned images were done with Matrox Inspector[®], an image analysis program.

Four plume measurements centered at 7.5 stack diameters downstream were made for each photo. This location is the furthest downstream where the plume smoke is clearly visible in all of the photographs, and also corresponds to the locations of plume height data points published by other authors. Two measurements were made at the top of the plume: $Z_{up,l}$ and $Z_{up,e}$.

$Z_{up,l}$ represents the upper limit where smoke is visible in the region, and $Z_{up,e}$ approximates the upper mean edge. Similarly, for the bottom of the plume, $Z_{lo,l}$ represents the lower limit where smoke is visible in the photos, and $Z_{lo,e}$ approximates the lower mean edge of the plume. The upper mean edge is determined by a horizontal line placed by inspection so that there are approximately equal portions of white smoke above the line as there are portions of black background visible below the line within the vicinity of $x = 7.5D$. The opposite is done for the lower mean edge of the plume. From these measurements the plume centerline can be represented as either the average of the upper and lower limits, $Z_{p,l}$, or the average of the upper and lower mean plume edges, Z_p . It was noticed that plume centerlines calculated from the limits of the plume show more scatter, presumably due to intermittent structures extending from the plume. The effect of these intermittent structures are more averaged out when measuring the plume edge.

In some cases plume centerlines calculated from the plume limits are lower than plume centerlines calculated from the plume edges. This is a reflection of downwash in the stack wake drawing tendrils of smoke downwards, which influences the measurement of the lower limit a great deal but has less of an effect on the mean lower edge. In these experiments the plume height is represented by Z_p , the plume centerline taken as the mean of the upper and

lower plume edges, and defined formally in Equation 3.1.

$$Z_p = \frac{Z_{up,e} + Z_{lo,e}}{2} \quad (3.1)$$

For the remainder of this thesis, the term “plume height” will refer to the plume centerline at $x = 7.5D$ and defined by Equation 3.1 unless otherwise stated. This plume height will be taken as an inverse indication of downwash, in that a higher measurement of plume height implies a greater distance between the bulk of the plume material and the ground.

A few of these scanned images were analyzed using software called Matrox Inspector[®] to see how well the method of measuring the plume edges was working. Using this software, a profile was drawn representing a series of horizontal integrations of pixel values (approximating light intensity) performed over a rectangular area surrounding the measurement area. This amounts to a vertical smoke intensity profile of the plume. It was found that the horizontal lines representing plume edges, placed by inspection, are generally located at the half-heights of the integrated intensity distributions. It was also observed that the averages of these lines fall close to the centroids suggested by these distributions.

At least several other researchers have used photographs to make experimental plume height measurements, including Vadot (1967), Fan (1967), Overcamp and Hoult (1971), and Hoult and Weil (1972). Vadot (1967) and Hoult and Weil (1972) measured the plume trajectory as the midpoint be-

tween traced outlines of the plume edges. In a series of towing tank experiments, Fan (1967) compared the locations of peak salt concentrations of a seeded plume with traced plume outlines. Plume heights indicated by the peak concentration measurements are slightly higher than those suggested by the traced outline. A similar observation is made by Briggs (1984) when comparing the measurements of Vadot (1967) to “observed” plume trajectories from other researchers. The term “observed” ostensibly refers to data collected through visual inspection, applying a criteria similar to those of Vadot (1967) and Hoult and Weil (1972), as well as to the current study. The equation for a neutrally-buoyant plume in a cross-flow used by Briggs (1984) compares well with other observed plume data, and will be presented and used in later sections.

In the current plume photographs, the plume is illuminated by a 1.0 cm to 1.5 cm wide light sheet along its centerline. Data collected from these photographs is meant to be representative of the whole plume. The basis for doing this is provided by Johnston (1994). By performing concentration measurements using laser-induced fluorescence techniques in a water channel, he showed that concentration centroids calculated from the x - z plane along the plume centerline matched those calculated from cross sections of the plume over the y - z plane. This suggests that measurements made of the plume centerline can sufficiently represent the whole plume.

3.3 Results of Plume Measurements

Figure 3.1 shows an example of the plume height measurements described in Section 3.2.2 plotted against increasing velocity ratio W_p/U_∞ for case 21. It can be seen from this Figure that plume height Z_p increases with increased plume velocity ratio until reaching 3 stack diameters above the tip, after which it levels off. It is surmised that this leveling off is a result of the plume being influenced by the roof of the wind tunnel. This is supported by the $Z_{up,l}$ series, representing the upper edge of the plume, reaching over five stack diameters above the tip. This location is only 5cm away from the roof of the 30.5cm square test section. However, given that case 21 contains one of the the highest plume edge measurements (other than case 4), and the majority of the experimental data is well below this level (more than 1 diameter less), the effect of the wind tunnel roof will be neglected for the purposes of these experiments.

Figure 3.2 shows plume height data at $x = 7.5D$ from the present experiments as well as from other researchers. Data points represented by triangles are measurements from cases 1 through 20 where forcing amplitude was zero. These data points were taken over the course of several days and as such, give an indication as to the repeatability of the experiment. One half of the the largest deviation between these data points is $0.15D$. This is a larger uncertainty than from either pixel resolution ($0.03D$), or measurement repeatability uncertainty ($0.09D$). This measurement uncertainty

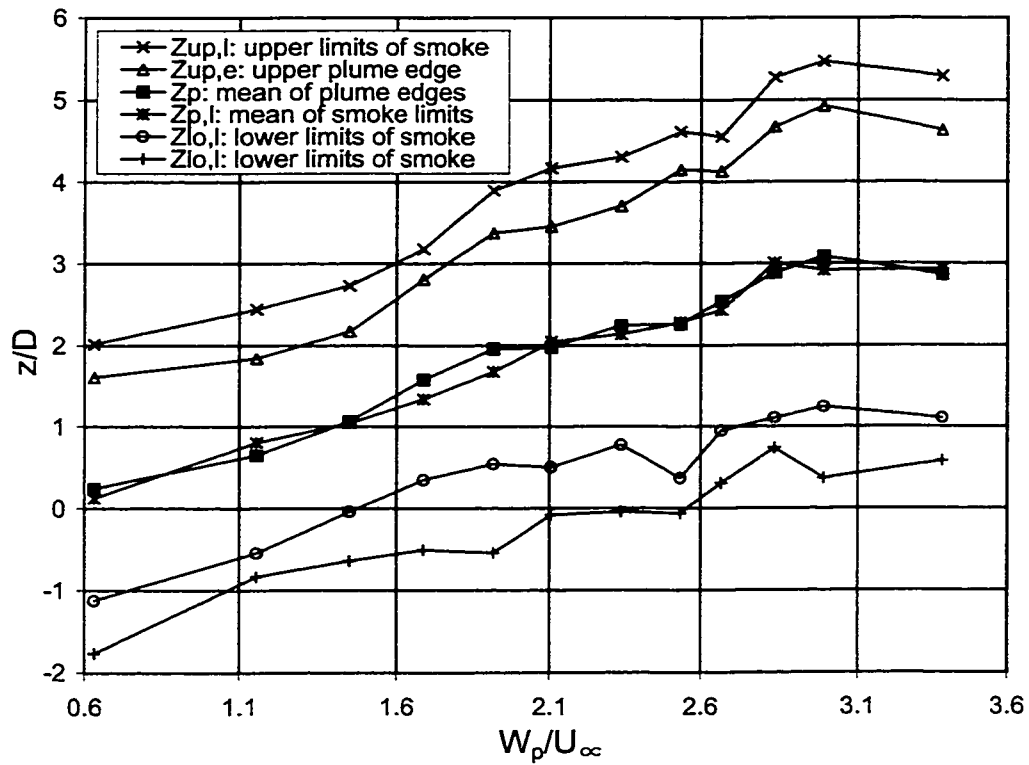


Figure 3.1: Sample Plume Measurements Taken From Case 21, a Reference Unforced Case

was determined by measuring the same photograph ten times. Current data points are observed to agree well with data from Snyder and Lawson (1991), matching qualitatively both in slope and in value. Their wind tunnel measurements represent centroids of stack gas concentration profiles along the vertical plume centerline. Data from Johnston and Wilson (1997) does not agree as well, although the general characteristics of the data is very similar. Similarly, a dashed line on Figure 3.2 representing a semi-empirical model from Briggs (1975), shows a match with the general trend of the data.

3.4 Plume Forced with Synthetic Jet

3.4.1 Plume Measurements with Synthetic Jet Forcing

3.4.1.1 Frequency Response

A potential consideration when studying the plume forced by synthetic jets is whether the forcing frequency plays a role in affecting the behaviour of the plume. Crow and Champagne (1971) found that by applying a periodic axial perturbation to a conventional round jet they were able to amplify naturally occurring instabilities within the jet. This occurred when Strouhal Number reached a “preferred mode” of $St = 0.3$, where

$$St = \frac{(\text{surging freq.})(\text{jet diam.})}{(\text{mean jet velocity})} \quad (3.2)$$

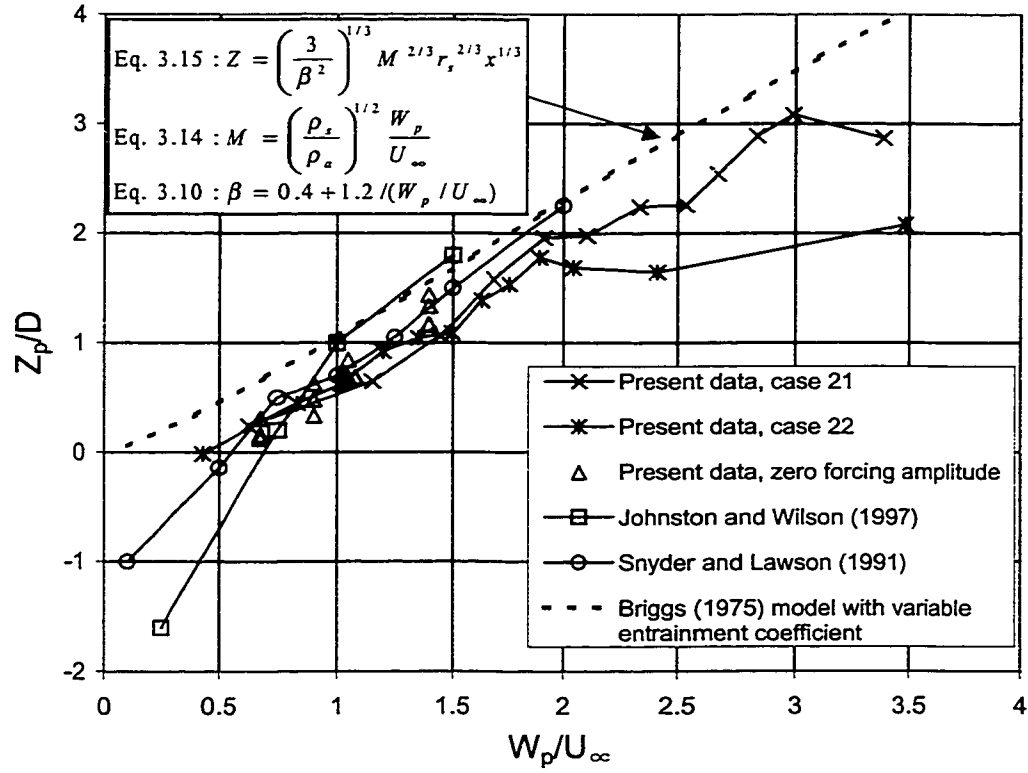


Figure 3.2: Comparison of Reference Cases With Theory and Other Data

Entrained flow volume increased 32% from the unforced case when this point was reached, forced with an amplitude of 2% of the mean jet flow. This has implications in modifying the plume trajectory upon leaving the stack, as an increase in entrainment into the plume diffuses vertical plume momentum, thereby reducing the effective plume velocity. While it is not known whether or not synthetic jetting applied in the current manner axially pulses the plume flow, it is possible that this could occur to some extent given the periodic synthetic jet vortex structure present at the immediate edge of the plume exit plane. An image of this structure interacting with the plume can be seen in Figure 3.17d on page 115.

In order to determine if there is any dependence of plume height to synthetic jet forcing frequency, plume height measurements were compared between cases with different synthetic jet frequencies but similar W_p and U_∞ . Figures 3.3 and 3.4 are examples of such a comparison for cases 4 through 6 and 13 through 15, respectively. In these graphs, Z_p is plotted against W_{SJ}/U_∞ for forcing frequencies of 40 Hz, 70 Hz, and 100 Hz. Both cases 4 and 14 have St close to 0.30, based on mean plume diameter and velocity, and synthetic jet frequency. It can be seen by these plots that based on plume height it is not possible to differentiate the cases operating closest to the preferred mode of the plume. Similarly the difference between $Z_{up,l}$ and $Z_{lo,l}$, roughly representing plume width in the vertical direction, was compared between different synthetic jetting forcing frequencies. Again, it was found that frequency did not have an observable effect on plume measurements within

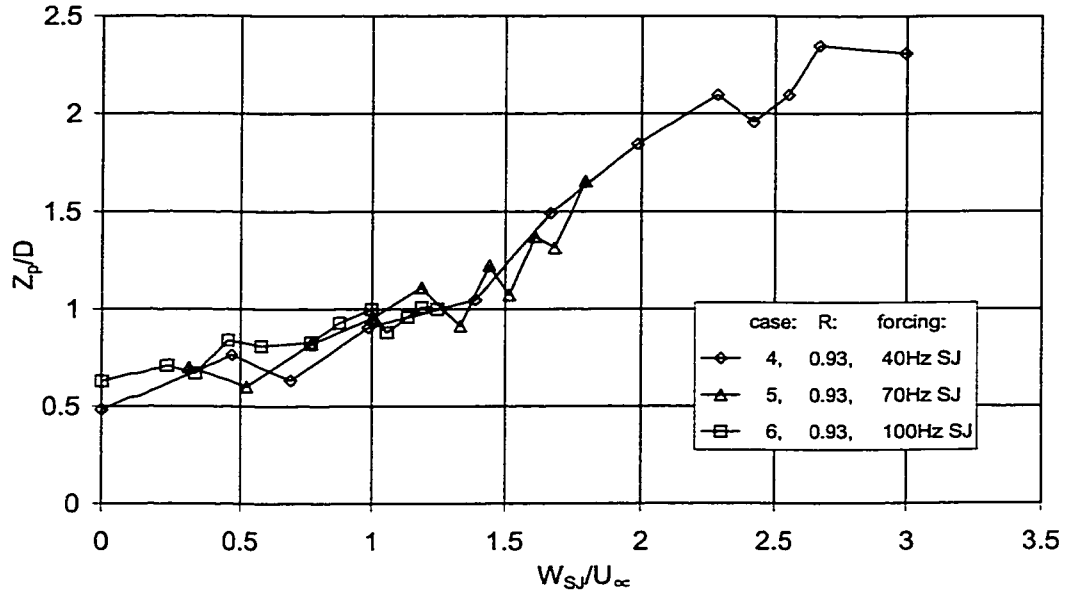


Figure 3.3: Plume Heights of Cases 4–6 vs. Forcing Amplitude: $R=0.93$, forced with synthetic jets of varying frequency

the limited range of forcing amplitude available using the highest synthetic jet frequency (100 Hz).

This apparent insensitivity of plume measurements to synthetic jet forcing frequency suggests that the natural instabilities originally present in the plume flow are either not being affected, or are not significant to plume height if they are. Overlaying of the plume height data in Figures 3.3 and 3.4 also support the use of W_{SJ} (from Section 2.3.3.2) in representing synthetic jet

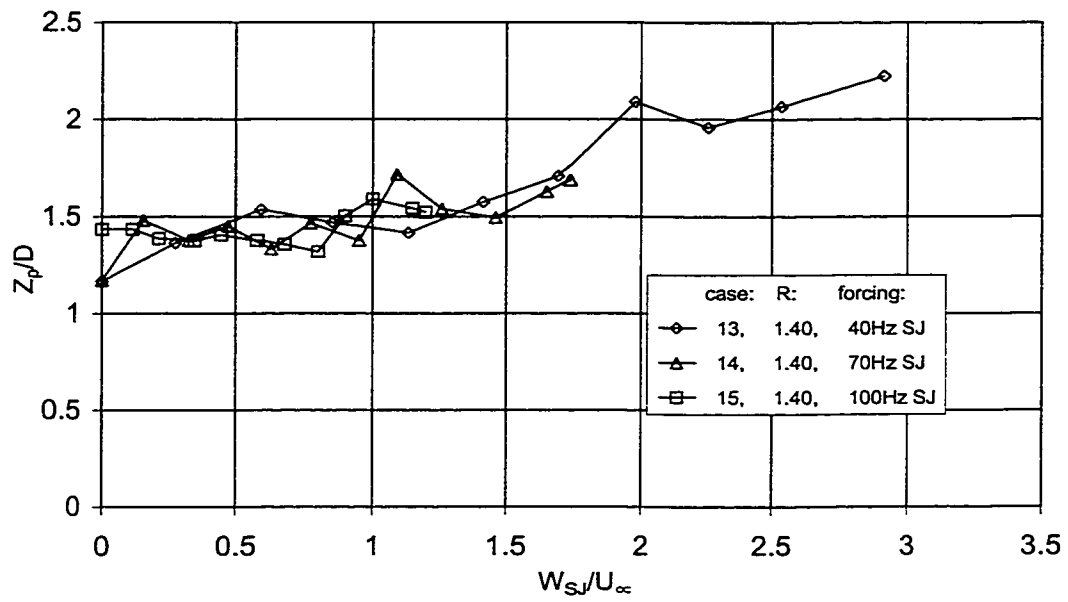


Figure 3.4: Plume Heights of Cases 13-15 vs. Forcing Amplitude: $R=1.40$, forced with synthetic jets of varying frequency

amplitude.

3.4.1.2 Increase in Plume Height With Synthetic Jet Forcing

Figures 3.3 and 3.4, introduced earlier, clearly show that plume height rises monotonically with increasing synthetic jetting amplitude when plume velocity ratio stays constant. To illustrate this further, Figure 3.5 contains a plot showing a selected number of cases using synthetic jet forcing (cases 1, 4, 7, 10, and 13). All of the synthetic jet cases were not included for clarity of the resulting plot. Instead, cases forced with the 40 Hz synthetic jet were used to represent the other two synthetic jet-forced cases with the same plume velocity ratio. For example, if looking at the data sets for cases 4, 5, and 6 as shown in Figure 3.3, case 4 would be used to represent the data in general for cases 4 through 6. The 40 Hz cases are used because they cover the greatest range of forcing amplitudes.

When looking at the data on Figure 3.5 it is important to emphasize that for these synthetic jet-forced cases the horizontal axis represents the non-dimensionalized velocity of the synthetic jet, and not the plume. Knowing this, it becomes clear that the data points lying on the y-axis, corresponding to no forcing, are simply the plume heights of the unforced plumes. As a result, the data is spread over a range of Z_p of about $\pm 1D$ with no forcing. Of course, this range would be larger with a greater range of tested velocity ratios. As forcing amplitude increases, the plume heights of all the forced cases increase and appear to converge in Z_p until beyond W_{SJ}/U_∞ of around

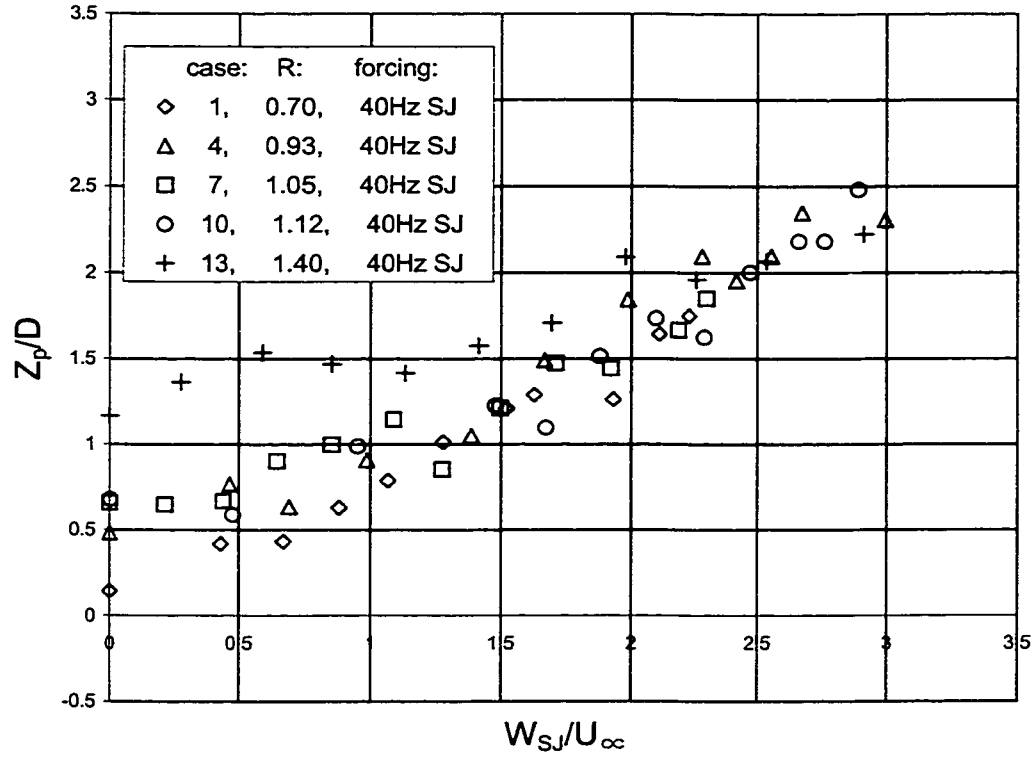


Figure 3.5: Plume Heights of Synthetic Jet-Forced Plumes. Plume height normalized by stack diameter is plotted against synthetic jet velocity normalized by cross-wind velocity, and shows convergence at higher forcing amplitudes.

2, the data has a maximum spread of approximately $\pm 0.3D$.

The plume height curves of Figure 3.5 appear to converge when forced with high amplitude synthetic jets regardless of their plume to crosswind velocity ratios. This convergence, independent of plume velocity, suggests that at high amplitudes of forcing, the synthetic jet velocity and not the plume velocity is controlling the plume height. Heuristically, the synthetic jet momentum can be seen as overwhelming the plume momentum as the main source of vertical momentum flux into the combined plume. In essence, the synthetic jetting is becoming the entire plume. If this was truly the case, a greatly idealized outlook would predict that at higher forcing amplitudes the forced plume heights should approach unforced plume heights. Figure 3.6 is a plot of normalized unforced plume heights plotted against normalized plume velocity. The data from both Figure 3.5 and Figure 3.6 are shown together in Figure 3.7. In this figure, it can be seen that to some extent, data points corresponding to plumes heights with high synthetic jet forcing velocity begin to lie within the region of the unforced plume data. This may or may not be coincidental because of course there are other factors that also have an effect on plume rise. There will be further discussion regarding this in the next section as well as in Section 3.6.

3.4.2 Qualitative Plume Behaviour

A photograph of an unforced plume from case 22 is shown in Figure 3.8. The plume velocity ratio R is 1.75, and Z_p is approximately $1D$. Figure 3.9 is

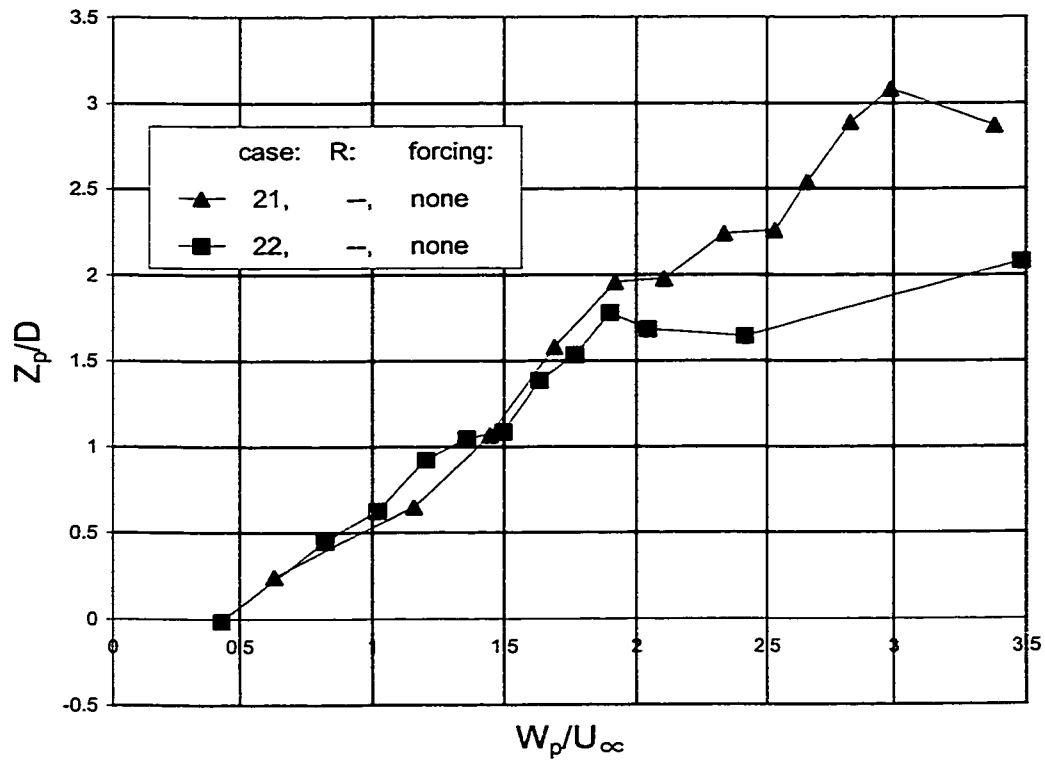


Figure 3.6: Plume Heights of Reference Plumes. Plume height normalized by stack diameter is plotted against average plume velocity normalized by cross-wind velocity.

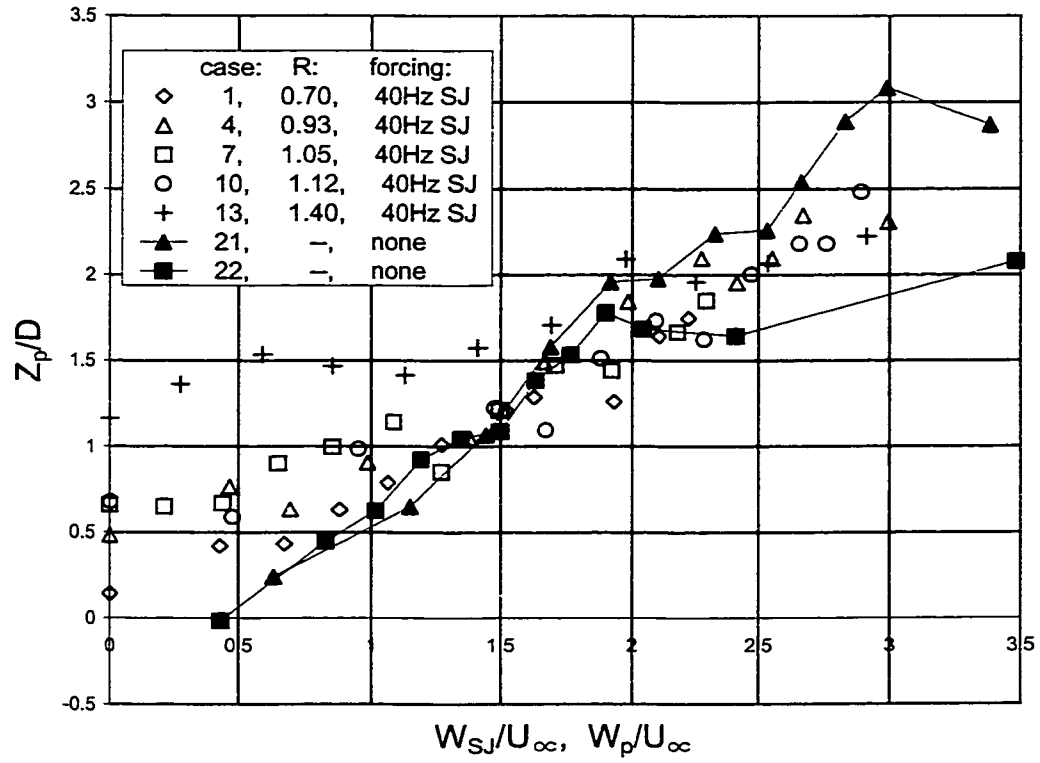


Figure 3.7: Plume Heights of Synthetic Jet-Forced and Reference Plumes. Forced data is plotted against synthetic jet velocity normalized by cross-wind velocity and unforced plume data is plotted against average plume velocity normalized by cross-wind velocity using the same axis.

a photograph from case 1 of a plume forced by a 40 Hz synthetic jet with an amplitude of $W_{SJ}/U_\infty = 1.3$. R is 0.70, and Z_p is also approximately $1D$. When these photographs are compared, it becomes obvious that there are differences between the forced and unforced plume that would be missed if referencing only plume height measurements or time-averaged instrument readings. The effect of pulsation from the low-frequency (40 Hz) synthetic jet can be seen in the “puffing” of the plume at the frequency of synthetic jetting. This is not surprising given that the peak value of the alternating velocity inside the slit is around 15.5 m/s, which is almost four times the plume velocity in case 1. Ostensibly this puffing is caused by the blowing and suction phases of the synthetic jet alternately adding and then taking momentum from the plume, although resulting in a net addition. Further evidence of this can be found in the overall structure of the forced plume. Both the tops and the bottoms of the puffs have dense smoke, indicating that they contain a significant portion of the plume mass. This means that the mass center must be alternately moving up and down with time with respect to the stack. In other words, the synthetic jetting is not just sending tufts of smoke above and below the main plume body, but it is actually raising and lowering the entire plume body as a whole.

A clearer example of this control that the synthetic jetting has over the plume trajectory can be made by examining photographs of an even stronger synthetic jetting case. Figure 3.10 is a photograph again from case 1, forced with a 40 Hz synthetic jet with an amplitude of $W_{SJ}/U_\infty = 2.1$. For com-



Figure 3.8: Reference Photograph of Unforced Plume; Case 22: $R = 1.75$, $Z_p \approx 1D$

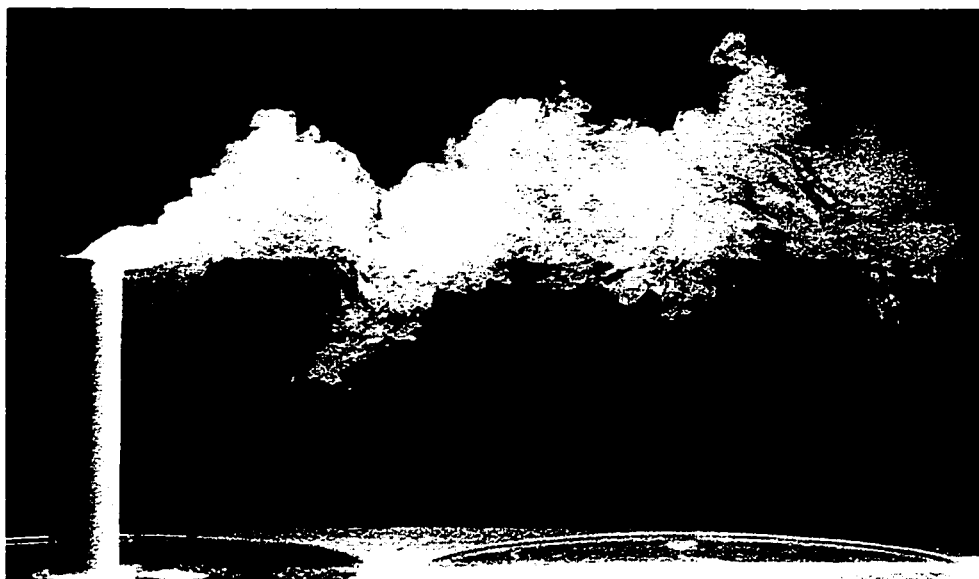


Figure 3.9: Photograph Showing Plume Forced with 40 Hz Synthetic Jet; Case 1: $R = 0.70$, $Z_p \approx 1D$, $W_{SJ}/U_\infty = 1.3$

parison, Figure 3.11 is a smoke-wire photograph taken of the preliminary apparatus with a crossflow velocity of around 1 m/s. From the tip is created a 10 Hz upwards-directed synthetic jet similar in configuration to the final apparatus. In Figure 3.11, the low frequency synthetic jetting is creating disturbances in the smoke-sheet that are very similar in structure to the puffing seen in the forced plume of Figure 3.10. The spatial wavelengths are approximately matched because even though the crosswind velocity is four times lower in the smoke-wire photograph, so is the jetting frequency. The tops of the disturbances are rising with downstream distance, as are the puffs. Even the tendrils of smoke extending upstream towards the stack from the bottom of the smoke-sheet have an equivalent structure in appearance in the forced plume. The similarities in structure between these photographs suggest that the synthetic jet-forced plume is behaving the same way as a synthetic jet of similar configuration with no plume. In other words, the plume is having little or no effect on the flow. This further supports the conjecture made earlier in Section 3.4.1.2 regarding the independence of plume trajectory to plume velocity when synthetic jet forcing is very high, as in this case.

3.4.3 Plume Rise Equations

A plume rise model is used which was presented by Briggs (1975). A more complete derivation can be found in this reference as well as in Johnston (1994). This section will only present important aspects of the model that will aid in the understanding of later sections.



Figure 3.10: Photograph of Plume Forced with High-Amplitude 40 Hz Synthetic Jet: Case 1, $R = 0.70$, $W_{SJ}/U_{\infty} = 2.1$



Figure 3.11: Smoke-wire Photograph of Preliminary Apparatus Forced With Upwards-Directed 10 Hz Synthetic Jet: Synthetic jet configuration shown in Figure 2.7, no plume, $U_\infty \approx 1 \text{ m/s}$

The basis of this plume rise model for an unforced stack lies in evaluating the mass, buoyancy, and momentum conservation equations for an ideal cylindrical plume. The general continuity equation is simplified using the Boussinesq approximation, where it is assumed that density differences between the plume and ambient air are negligible for inertial terms, and only apply to buoyancy forces. Integrating this simplified continuity equation over a section of the cylindrical plume results in an expression for the change in plume volume flux Q_p ,

$$\frac{dQ_p}{dz} = 2r_p v_e \quad (3.3)$$

where r_p is the plume radius, and the π is divided out to follow the convention of Morton et al. (1956). Here we introduce the entrainment velocity v_e , which represents the addition of entrained ambient air into the plume through turbulent mixing at the plume edges. This entrainment velocity is important because it is responsible for the dilution of vertical plume buoyancy and momentum, and thus reducing plume rise in the model. At the stack exit we write the buoyancy and momentum flux terms as follows:

$$\text{Buoyancy Flux: } F_b = \frac{g(\rho_a - \rho_s)}{\rho_a} W_{p,s} r_s^2 \quad (3.4)$$

$$\text{Momentum Flux: } F_{p,s} = \frac{\rho_s}{\rho_a} W_{p,s}^2 r_s^2 \quad (3.5)$$

Again, a π is missing from both terms in order to follow the convention of Morton et al. (1956), and both terms have been normalized by ρ_a , the ambient

air density. The density of the stack gases is given by ρ_s . The subscripts “ p,s ” indicate quantities at the stack exit. Thus $W_{p,s}$ is the average vertical plume velocity at the stack exit. By integrating over a control volume around the plume (Briggs, 1975; Johnston, 1994), the following expression can be determined for the change in buoyancy flux:

$$\frac{dF_b}{dx} = -S \frac{F_{p,s}}{U_\infty} \quad (3.6)$$

where S represents an atmospheric stability parameter. In the present experiments S is zero, corresponding to the neutrally stable crossflow of the wind tunnel. In neutrally stable conditions, the plume buoyancy flux is constant throughout its rise. This value S would otherwise be positive for stable conditions, and negative for unstable conditions.

Similar to the expression found for buoyancy flux, the following expression for the change in momentum flux can be found by integrating over a plume control volume:

$$\frac{dF_{p,s}}{dx} = \frac{F_b}{U_\infty} \quad (3.7)$$

For the present experiments using a neutrally buoyant plume, the buoyancy flux is always zero. Equation 3.7 shows that when this is the case, vertical momentum flux is conserved throughout the rise of the plume. For a general case the Boussinesq approximation is applied so that $\rho_s/\rho_a \approx 1$, and we can

write an expression for momentum flux at the source as

$$F_{p,s} = W_{p,s}Q_s = W_pQ_p \quad (3.8)$$

where $Q_s = W_{p,s}r_s$ is the plume volume flux near the stack exit, with a factor of π missing, and W_p is the average plume velocity along the plume trajectory.

In order to complete the equations, a closure assumption is required to account for the entrained flow v_e entering the plume through its circumference. The assumption of Morton et al. (1956) will be used as follows:

$$v_e = \beta W_p \quad (3.9)$$

where β is an empirical entrainment coefficient. Hoult and Weil (1972) found that a constant value of $\beta = 0.6$ fit their neutrally buoyant plume measurements well. However, there are arguments that support the use of a variable β . Briggs (1975), citing observations that β depends on the plume to cross-wind velocity ratio, suggests the expression:

$$\beta = 0.4 + \frac{1.2}{R} \quad (3.10)$$

to account for variation in entrainment with velocity ratio. Johnston (1994) argues that at higher plume velocity ratios, a greater portion of the plume is near vertical, and that this should have an effect on β . They provide an em-

pirical expression for β that compares well with the data of other researchers. The expression used by Briggs (1975) will be used here to estimate β .

If it is assumed that for a bent-over plume being convected at the cross-flow velocity, perturbation velocity in the streamwise direction will be small compared to the mean cross-flow, then the plume volume flux can be expressed as

$$Q_p = \tau_p^2 U_\infty \quad (3.11)$$

Again, the factor of π is deleted to follow the convention of Morton et al. (1956). If this is combined with the definition of entrainment velocity in Equation 3.9, then Equation 3.8 can be rewritten as

$$F_{p,s} = \beta^2 U_\infty Z^2 W_p \quad (3.12)$$

Substituting $W_p = dx/dt$ and integrating from the origin at the stack exit to the plume height and distance results in the so-called “1/3 Law” for neutrally buoyant plume rise in a neutrally stable cross-wind:

$$Z = \left(\frac{3}{\beta^2} \frac{F_{p,s}}{U_\infty^2} x \right)^{1/3} \quad (3.13)$$

3.4.4 Application to Plume Rise Predictions

As discussed in Sections 3.4.1.2 and 3.4.2, the plume height is controlled by either plume or synthetic jet velocity, depending on whether the synthetic jet has either zero amplitude or very high amplitude. It is a fair assumption

that under moderate forcing the plume height is controlled by a combination of both. This means that in an attempt to produce a general plume height response curve, it will be necessary to consider the effect of both the already present plume as well as the added effects of the forcing.

3.4.4.1 Momentum Flux Correction

At this point, it is appropriate to introduce the concept of the momentum velocity ratio M_v . Johnston (1994) defines this as

$$M_v = \left(\frac{\rho_s}{\rho_a} \right)^{1/2} \frac{W_{p,s}}{U_\infty} \quad (3.14)$$

Substituting Equation 3.5 and Equation 3.14 into Equation 3.13 for plume rise results in the following:

$$Z = \left(\frac{3}{\beta^2} \right)^{1/3} M_v^{2/3} r_s^{2/3} x^{1/3} \quad (3.15)$$

So far, the source momentum flux $F_{p,s}$ has been calculated by using the average velocity of an assumed top-hat velocity profile at the stack exit. If this is not the case then a momentum flux correction factor can be used so that the actual momentum flux is applied in the calculations (Briggs, 1975; Johnston, 1994). This corrected momentum ratio is defined as

$$M_t = \alpha_t^{1/2} \left(\frac{\rho_s}{\rho_a} \right)^{1/2} \frac{W_t}{U_\infty} \quad (3.16)$$

where α_t is the correction factor. Note that the subscript t is used to denote application over the total stack exit area of the plume and forcing, A_t . Hence, W_t represents the average velocity of the plume and forcing over A_t . The definition of α_t is

$$\alpha_t \rho_s A_t W_t^2 = \int_{A_t} \rho_s w_s^2 dA_t \quad (3.17)$$

Values of α_t range from 2.0 for a laminar parabolic profile to 1.0 for a top-hat profile. In the present study α_t ranges from 1.09 to 1.11 due to the relatively flat turbulent plume profile. This represents a 4%–5% increase in calculated M_t versus taking a simple velocity ratio.

The right hand side of Equation 3.17 can be expressed as

$$F_t = \int_{A_t} \rho_s w_s^2 dA_t \quad (3.18)$$

or in words it is the total vertical momentum flux coming from the stack. For the purposes of this chapter, it is useful to take a closer look at Equation 3.16 in order to more clearly define what it represents. By using Equation 3.18 we can re-write Equation 3.17 as

$$\alpha_t = \frac{F_t}{\rho_s A_t W_t^2} \quad (3.19)$$

and substituting this into Equation 3.16 we get

$$M_t = \left(\frac{F_t}{\rho_a A_t U_\infty^2} \right)^{1/2} \quad (3.20)$$

What Equation 3.20 shows is that M_t is effectively the square root of the ratio between the total vertical momentum coming from the stack, and a momentum term derived from the crossflow velocity and total stack exit area, A_t . While as just mentioned, the practical change in momentum velocity ratio over the simple velocity ratio R is small with these particular experiments due to the turbulent plume velocity profiles, what is important is the physical interpretation suggested by Equation 3.20. With this understanding, it is now possible to make some assumptions regarding the behaviour of the forced plume and the combination of the source plume and forcing momentum.

3.4.4.2 Applying Total Momentum Flux

The simplest approach is to try and approximate the forced plume as an unforced plume that contains the momentum flux of both the pre-existent plume plus its forcing. This means the total momentum flux is:

$$F_t = F_p + F_f \quad (3.21)$$

with the terms suitably normalized, where F_f in this case is the momentum flux induced by the synthetic jet, F_{SJ} . Figure 3.12 shows the results of applying this approximation. Plume height is plotted against M_t , the total momentum velocity ratio calculated over the total stack exit area. Several data points from the unforced cases are included for reference, and these are

plotted against M_p . The main difference to notice in Figure 3.12 compared to Figure 3.7 is that the large initial data spread in Z_p for small or no forcing is not shown. Instead, when looking at the data points corresponding to zero forcing amplitude, indicated by the over-sized open symbols, they can be joined with a smooth curve. Scatter in the vertical data is approximately $\pm 0.25D$, which is close to the lowest scatter of the converging data series in Figure 3.7.

By Equation 3.15, the unforced plume height at a fixed downstream location should go as $M_t^{2/3}$ for a constant β . The present data has too much scatter to be able to discern such a relationship. To illustrate this, the function $Z_p/D = C_1 M_t^{2/3} + C_2$ is shown in Figure 3.12 as a dashed line, where the constants have been adjusted by inspection to fit the reference unforced data points. When compared to the linear regression curve fit shown as a solid line, the low curvature is made more apparent.

3.4.4.3 Momentum Weighted Area

Although the data points of the forced plumes in Figure 3.12 are generally grouped together, this group tends to depart from the trend of the reference data points of the unforced cases. While this is more noticeable for the larger forcing amplitudes, this departure is also present to a lesser extent for lower and zero forcing amplitudes, and depends on plume and forcing geometry. This happens because the total stack exit area, A_t , was used to calculate the momentum velocity ratio M_t . Considering the case of an unforced stack

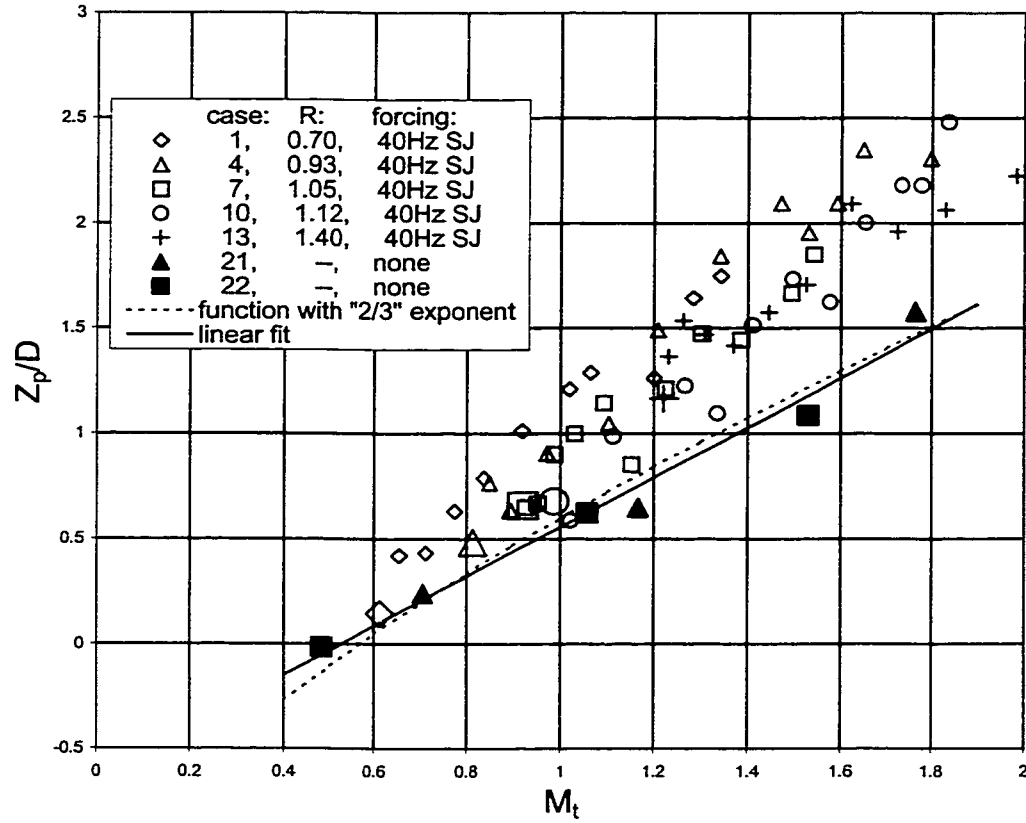


Figure 3.12: Plume Height vs. Momentum Ratio Calculated Using Total Area of Plume and Forcing, M_t : Enlarged symbols represent data points of zero forcing amplitude for each case. Shown for reference are solid symbols representing unforced plumes. The dashed line represent the function $Z_p/D = C_1 M_t^{2/3} + C_2$, where the constants have been adjusted by inspection to fit the reference unforced data points, and the solid line is a linear regression curve also fit to the reference unforced data points.

plume, A_t on the left hand side of Equation 3.17 should be substituted with plume area A_p , because that is the only surface having momentum flux. So in the case of using Equation 3.20 to evaluate M_t for the unforced stack plume, the area term A_t is too large by A_f/A_p , about 40% for this particular geometry. After taking the square root and inverting, the momentum velocity ratio M_t is resultantly about 15% too small. This relative error results in larger absolute errors with higher momentum velocity ratios, thus increasing the departure from the reference cases. A similar argument can be made for the limiting case as the synthetic jet momentum divided by the plume momentum approaches infinity. This is equivalent to having no plume flow, with all vertical momentum provided by the synthetic jet, and the correct area to use in Equation 3.20 is A_f . Therefore, this limiting case results in an error in area of A_p/A_f of about 250%, giving a momentum velocity ratio that is about 36% too small.

A suggested solution to resolve the error in calculated area is to use a corrected area that is weighted linearly to the relative momentum fluxes of the plume and forcing, F_p and F_f , respectively. A first guess for the empirical weighting is shown in Equation 3.22:

$$A_M = \frac{F_p A_p + F_f A_f}{F_t} \quad (3.22)$$

where F_t is defined by Equation 3.21. The area calculated using Equation 3.22 satisfies both the limits of no forcing as well as forcing approaching

infinite amplitude, in that it is equal to A_p when F_f equals zero, and approaches A_f when F_p/F_f approaches zero. Figure 3.13 shows the results of using this corrected area. The same data is used as in Figure 3.12 except it is plotted against M_M , the momentum velocity ratio using the momentum-weighted area, as defined by either Equation 3.23:

$$M_M = \alpha_M^{1/2} \frac{\rho_s}{\rho_a} \frac{W_t}{U_\infty} \quad (3.23)$$

where

$$\alpha_M \rho_s A_M W_t^2 = \int_{A_t} \rho_s w_s^2 dA_t \quad (3.24)$$

or in a more functional alternate form, by Equation 3.25:

$$M_M = \left(\frac{F_t}{\rho_a A_M U_\infty^2} \right)^{1/2} \quad (3.25)$$

where F_t is given by Equation 3.21.

The results of applying the momentum-weighted area are shown in Figure 3.13, where Z_p is plotted against M_M . A linear regression fit of all the forced data points shown in Figure 3.13 has a slope that is 19% lower than a similar fit for the reference unforced data points. As expected, the points corresponding to no forcing now lie on the same curve as the reference unforced cases also shown in the plot. Also expected was a shift of the strongly-forced data points towards larger values of the momentum velocity ratio. The forced series are still grouped closely, with a spread of $\pm 0.25D$ throughout most of

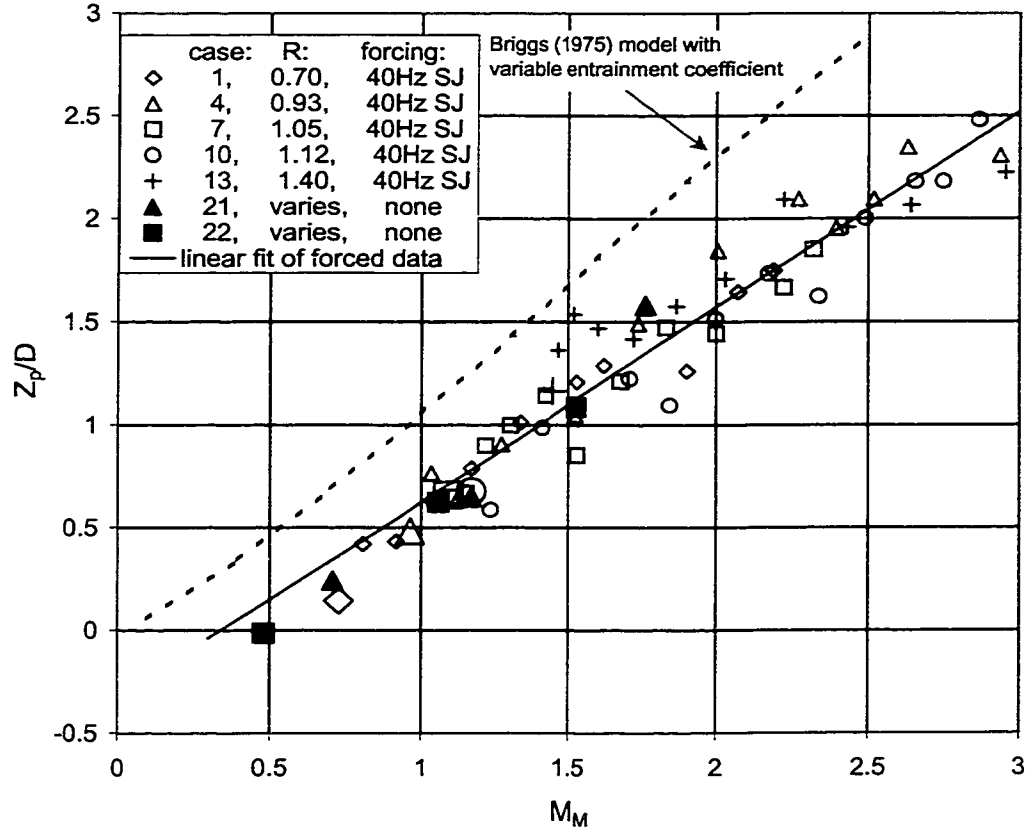


Figure 3.13: Plume height under Synthetic Jet Forcing vs. Momentum Ratio Calculated Using Momentum-Weighted Area, M_M : Enlarged symbols represent data points of zero forcing amplitude for each case. A linear regression of the forced data points is indicated by a solid line. Shown for reference are solid symbols representing unforced plumes.

their range. There is no evident Reynolds Number dependency, even through plume and cross-flow velocities change by over 50%. Aside from the grouping of the forced data points, there are two other important features of the data that support the model used to achieve this. First is the contiguity of the beginnings and ends of different data series. Secondly is the fact that even for high synthetic jetting amplitudes, the trend of plume height for the forced cases is close to the plume heights of the unforced reference cases. This is remarkable, given the photograph in Figure 3.10 showing the grossly distorted plume at high forcing amplitude. This reveals that even though an instantaneous view of the forced plume tells us the plume height may be either enhanced or retarded by the synthetic jetting at any given moment, what matters in terms of the *average* plume height is the *average* effect of the forcing. What this also suggests to us is that the simplified model that has been applied is appropriate for calculating plume height for a plume under synthetic jet forcing.

A downwash criteria using plume height measurements can be determined by looking at Figure 3.13 and applying the commonly-used downwash threshold of plume velocity ratio greater than or equal to 1.5. From this figure, it can be seen that the reference unforced plumes, shown by the solid symbols, have plume heights of around 1 stack diameter ($1D$) at this velocity ratio. Therefore, the downwash threshold using plume height measurements is $1D$ above the stack tip. When applying this criteria to establish whether a plume is downwashing, it is important to note whether or not there are plume gases

being entrained into the recirculation region in the immediate wake of the stack tip. Through examination of the experimental photographs, it was determined that every plume considered not in downwash using this criteria also did not show recirculation in the immediate stack tip wake.

3.4.5 Induced Plume Flow

When the model smokestack is operating in a cross-flow there is an induced plume flow caused by the negative static pressure inside the tunnel test section. In addition to this, it was found that there is also an induced flow from the application of synthetic jet forcing. It is conjectured that this induced flow is caused by the net suction pressure known to exist at the exit of the synthetic jet orifice (Smith and Glezer, 1998). This is similar to the operating principle of jet pumps, apart from the lack of an enclosed mixing chamber (Karassik et al., 1976).

Pressure measurements made while performing photographic data runs allow some quantification of this induced flow, which was first noticed during testing of the final apparatus. Because plume velocity is kept constant throughout each data run, the effect of this on the plume flow is measured by the reduction in pressure head required to drive the plume at any given velocity. This plume pressure head, P_h , is measured at the pressure port upstream of the contraction, and referenced to the static pressure inside the tunnel. Figure 2.14 on page 43 is a schematic where this measurement is illustrated. This differential pressure is then normalized by a dynamic pressure term P_p ,

derived from the mean plume velocity as:

$$P_p = 1/2\rho W_p^2 \quad (3.26)$$

In Figure 3.14, this normalized plume pressure head is shown plotted against synthetic jet velocity W_{SJ} for cases 1, 7, and 13. It can be seen from this figure that for $W_{SJ} > 2 \text{ m/s}$, P_h decreases with increasing synthetic jet amplitude, indicating increasing suction at the plume exit. It is also evident that in this range of W_{SJ} , cases 7 and 13 are grouping together while case 1 is not. The operating points of these three cases are shown in Table 3.2. This table shows that all these cases have varying velocity ratios, but cases 7 and 13 have similar plume velocities, which are different from that of case 1. This suggests a normalization based on plume velocity, and not velocity ratio or cross-stream velocity. Figure 3.15 shows such a normalization, where the same pressure head data is plotted against W_{SJ}/W_p . It can be seen from this plot that for values of $W_{SJ}/W_p > 0.6$, all three curves show a reasonable collapse. More cases are shown in Figure 3.16, plotted against the same parameters. These additional cases are at the same plume operating points as cases 1, 7, and 13, but have different synthetic jet frequencies. These additional cases also show a reasonable collapse, and show that the effect of this induced flow is relatively insensitive to synthetic jet frequency, depending only on synthetic jet amplitude.

Table 3.2: Operating Points for Figure 3.14

	R	W_p	U_∞
case 1	0.70	2.8	4.0
case 7	1.05	4.2	4.0
case 13	1.40	4.2	3.0

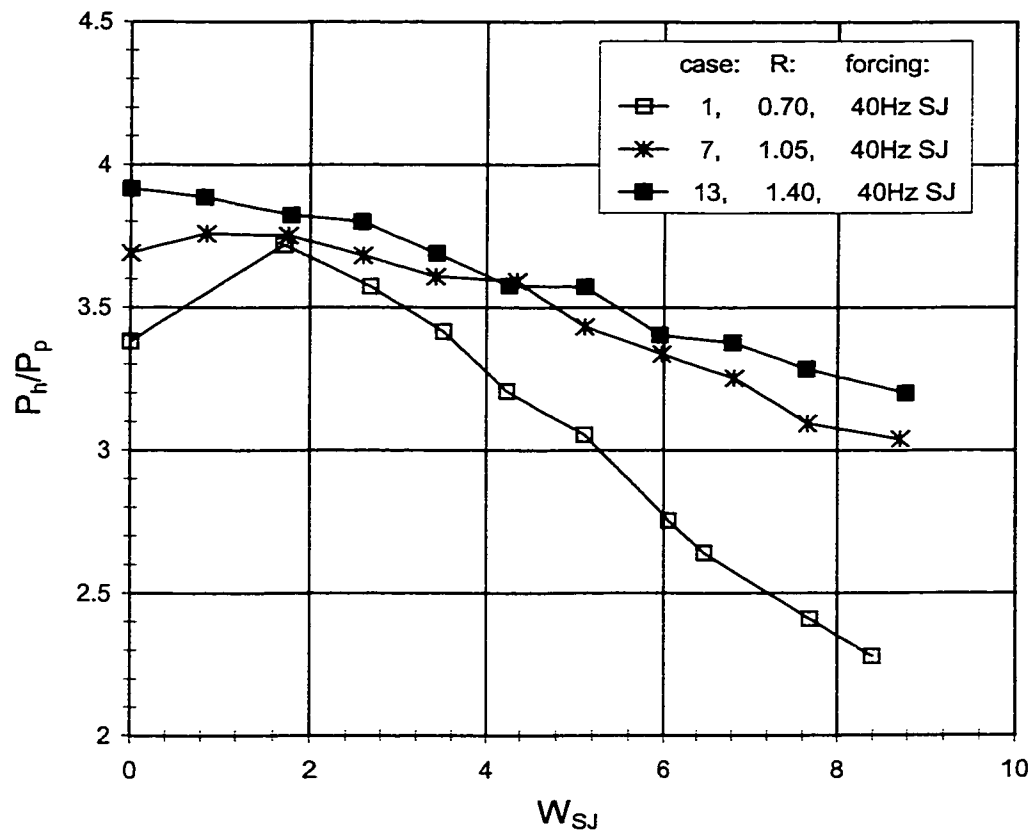


Figure 3.14: Normalized Plume Pressure Head vs. Synthetic Jet Velocity

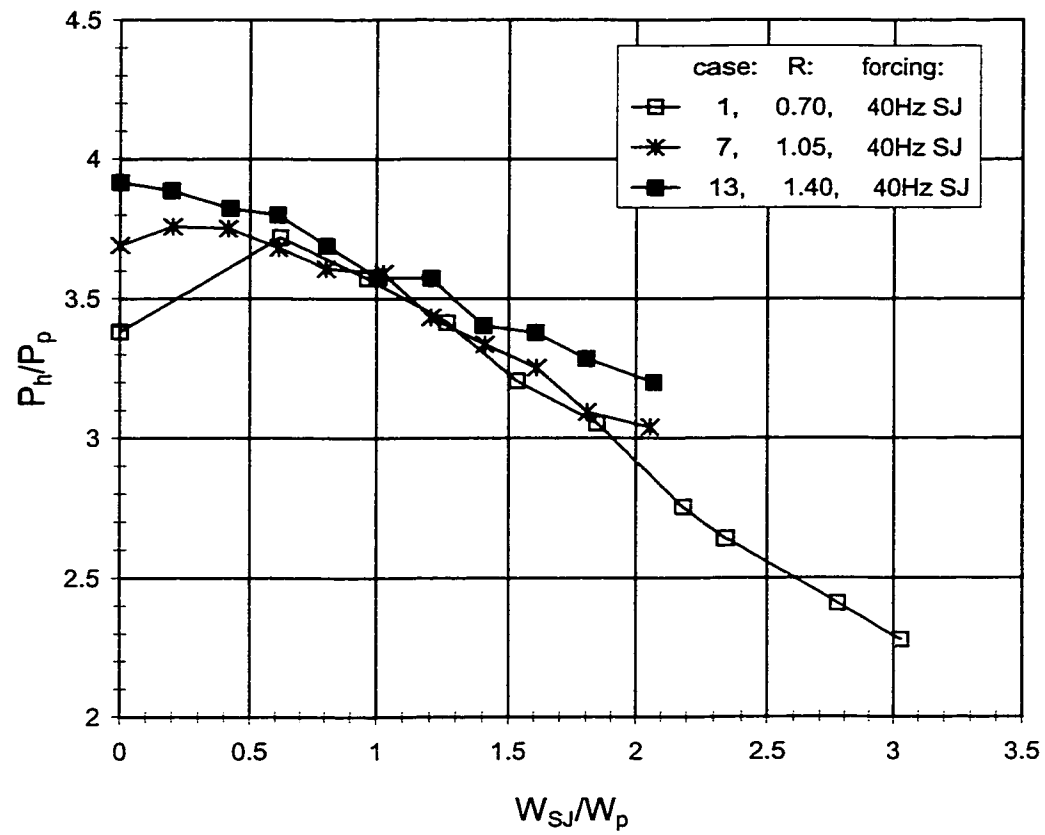


Figure 3.15: Normalized Plume Pressure Head vs. Synthetic Jet Velocity Normalized by Plume Velocity

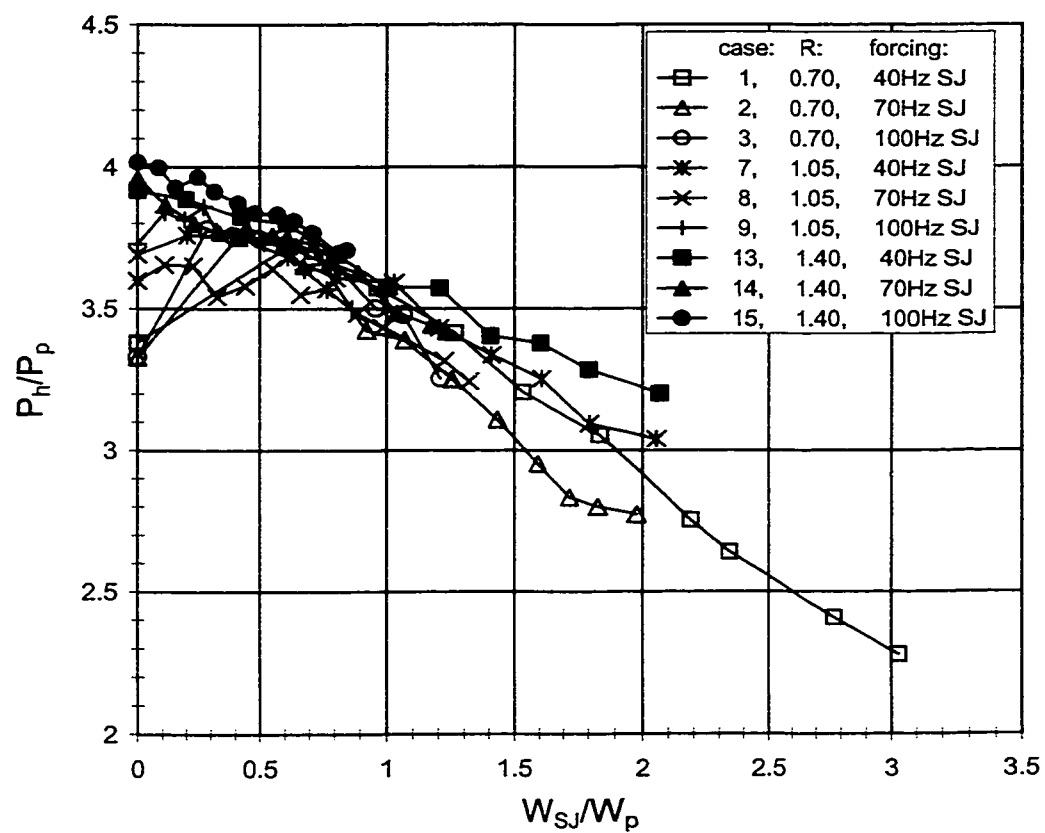


Figure 3.16: Normalized Plume Pressure Head vs. Synthetic Jet Velocity Normalized by Plume Velocity (all available cases)

3.4.6 Observations of a Plume with Laminar Pipe Flow¹

This section describes observations made of the special case of a plume from a laminar pipe flow in a cross-flow forced with a 60 Hz synthetic jet. During the course of these observations no effort was made to keep the plume flow constant while forcing was applied, but P_c only deviated a maximum of 15% from the average of readings taken over the course of observations. Cross-stream velocity was approximately 0.5 m/s and the unforced centerline velocity of the pipe flow was measured to be 0.9 m/s using the hot-wire. Assuming a parabolic laminar velocity profile within the pipe, the average plume velocity can be approximated to be 0.45 m/s, giving a plume flow Reynolds number of 570. Shown for reference, Figure 3.17a is a side-view of the unforced plume. From this view, the vortex structures within the plume are clearly visible. Vorticity in these structures originate from the boundary layer of the plume flow while inside the pipe. This vorticity is shed into the plume jet as vortex rings, which are then tilted and distorted by the velocity gradient between the cross-flow and the slower fluid in the wake of the plume and stack (Moussa et al., 1977). Some downwashing is evident in this Figure, as would be expected in the case of a plume from a turbulent pipe flow with

¹Part of these results were presented as a poster entitled "Cross-Jet Influenced by a Concentric Synthetic Jet", by Diep, J. and Sigurdson, L., at the Annual Meeting of the Fluid Dynamics Division of the American Physical Society, Washington, D.C., Nov. 2000. It was selected to be published as a one-page article in the Gallery of Fluid Motion, Physics of Fluids, Sept. 2001. A poster entitled "Mixing in a Cross-Jet Enhanced by a Coaxial Annular Synthetic Jet" by Sigurdson, L. and Diep, J. has been accepted by the IUTAM Conference on Turbulent Mixing and Combustion, Queen's University, Kingston, Ontario, June 2001.

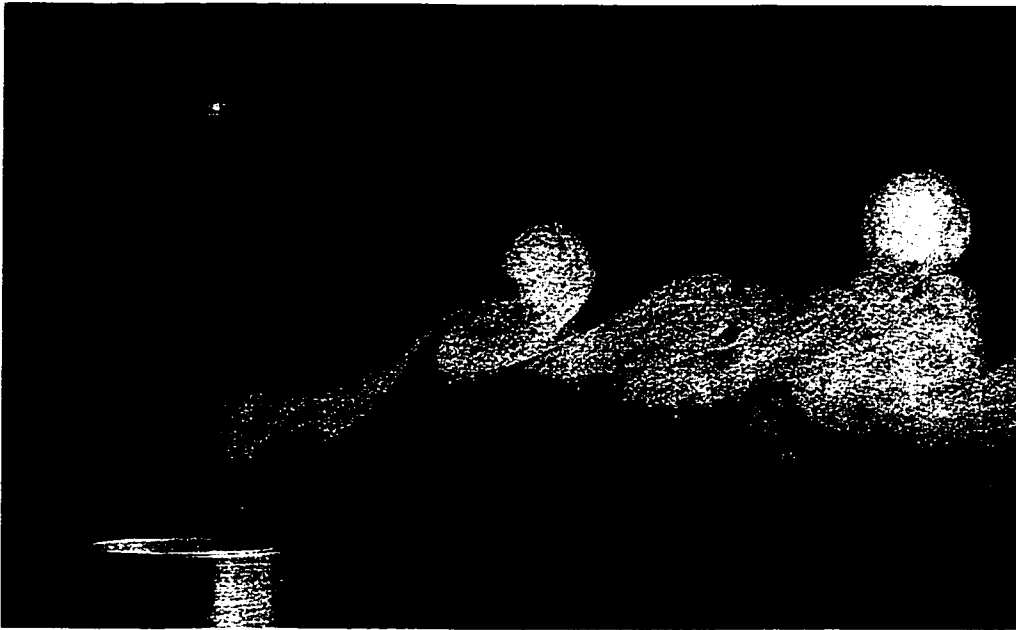
a similar velocity ratio of $R = 0.9$.

As low-amplitude synthetic jetting is applied ($U_{SJ} \approx 0.1 \text{ m/s}$), the three-dimensional vortex structure on the upstream side of the plume disappears, resulting in the image shown in Figure 3.17b. Large vortices remaining in this forced plume are reminiscent of the inner vortices appearing on the lower surface of the unforced plume. These large vortices in the forced plume become gradually smaller in size with increasing forcing amplitude. Eventually the plume becomes completely relaminarized when $U_{SJ} \approx 0.3 \text{ m/s}$, as shown in Figure 3.17c.

With increased forcing amplitude, instability begins to grow from the relaminarized plume. This instability is shown in Figure 3.17d when $U_{SJ} \approx 0.9 \text{ m/s}$. This value is close to the centerline value of the pipe flow, measured at 0.9 m/s using the hot-wire. From this side-view there are structures resembling mushroom vortices pointing upstream on the upper surface of the plume. “Pointing” refers to the direction the pairs would self-propagate. With a very small increase in synthetic jetting amplitude, there is a sudden transition in these vortex structures to the structures seen on the upper surface of the plume in Figure 3.17e. Between these photographs forcing amplitude was increased by 6% (calculated from chamber pressure measurements) to make sure the transition did not occur while photographs were being taken. This transition point is so sensitive that the apparatus can be set for transition to occur intermittently with no controls being touched. After this second transition, the vortices appear to point downstream, and appear

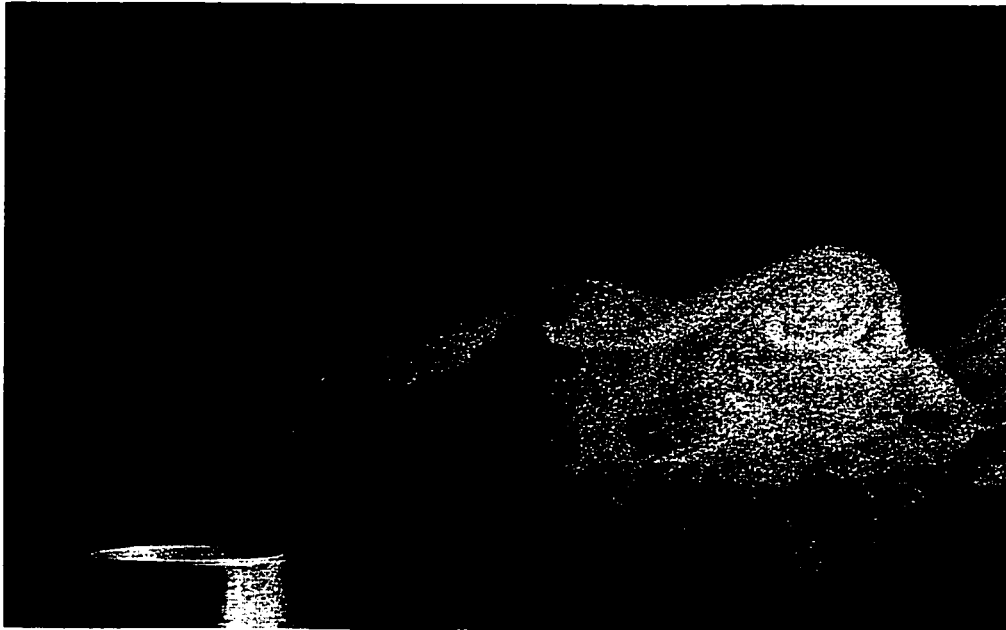
to more strongly consist of vorticity out of the page by the right-hand-rule. It also appears that after the transition these vortices contain more plume fluid than did the downstream-pointing vortices before transition. This is indicated by the denser smoke contained in the vortices, as compared to the rest of the plume. If true, this could represent an increase in the height of the plume mass-center, which is interesting given the small amount of additional forcing. As forcing amplitude is further increased, the vortices on the upper surface of the plume continue to lift off and form pinched-off lobes, as seen in Figure 3.17f where $U_{SJ} \approx 1.2$ m/s. In this Figure, the plume is clearly higher than in the unforced case, as well as showing an increased plume width, which suggests enhanced mixing between the plume and surrounding air. With even greater forcing amplitude the plume continues to rise, but becomes too turbulent to discern any structure within it.

While the two transformations discovered in the synthetic jet-forced laminar plume topology and vortex structure are clear and distinct, no corresponding behaviour in the turbulent plume has been observed, either through visual interpretation or measurements of the photographs. Although this vortex structure is fascinating, it was beyond the current project scope. No further work was done in understanding these preliminary observations made for the laminar plume.



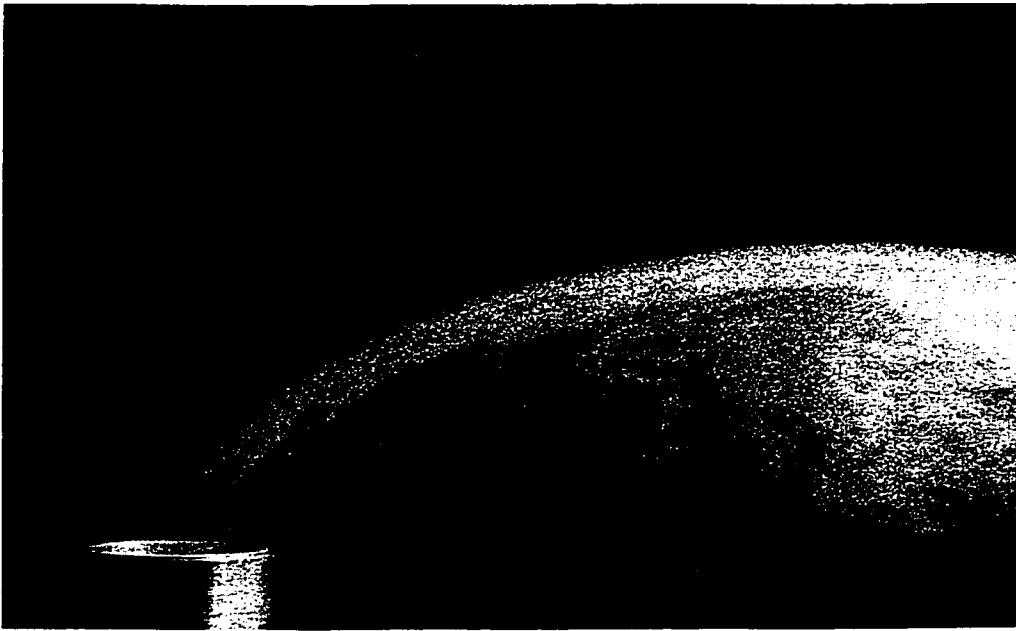
(a) Reference Photograph of Laminar Plume: No forcing, $U_\infty \approx 0.5 \text{ m/s}$, $W_p \approx 0.45 \text{ m/s}$.

Figure 3.17: Change in Structure of Laminar Plume Under Synthetic Jet Forcing



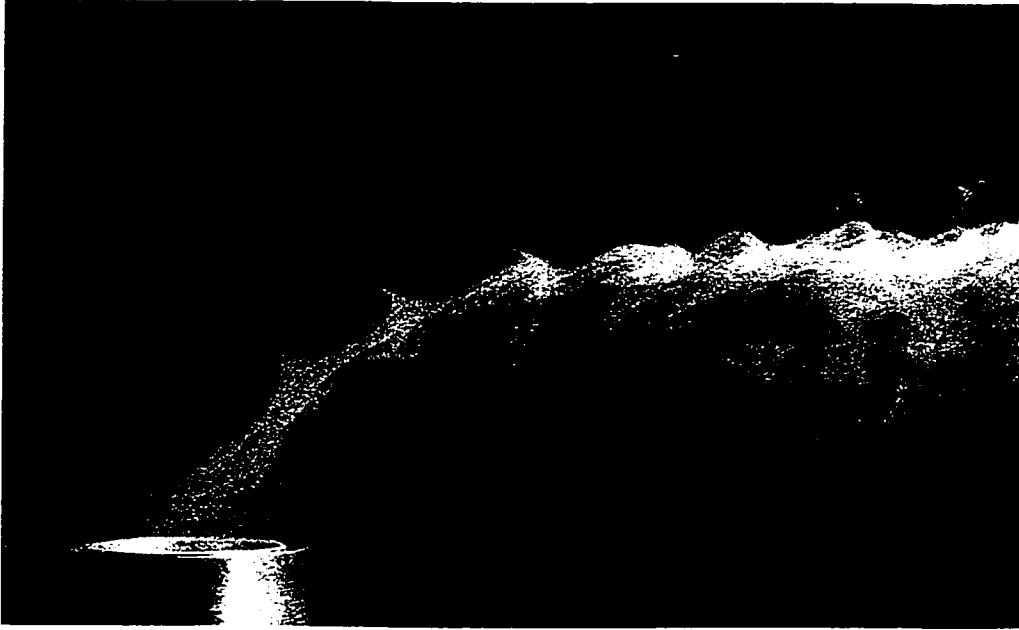
(b) Photograph of Laminar Plume Forced with 40 Hz Synthetic Jet: Just after the first transition the outer structure disappears, although the inner structure appears to remain, $U_\infty \approx 0.5 \text{ m/s}$, $W_p \approx 0.45 \text{ m/s}$, $W_{SJ} \approx 0.1 \text{ m/s}$.

Figure 3.17: Change in Structure of Laminar Plume Under Synthetic Jet Forcing (cont.)



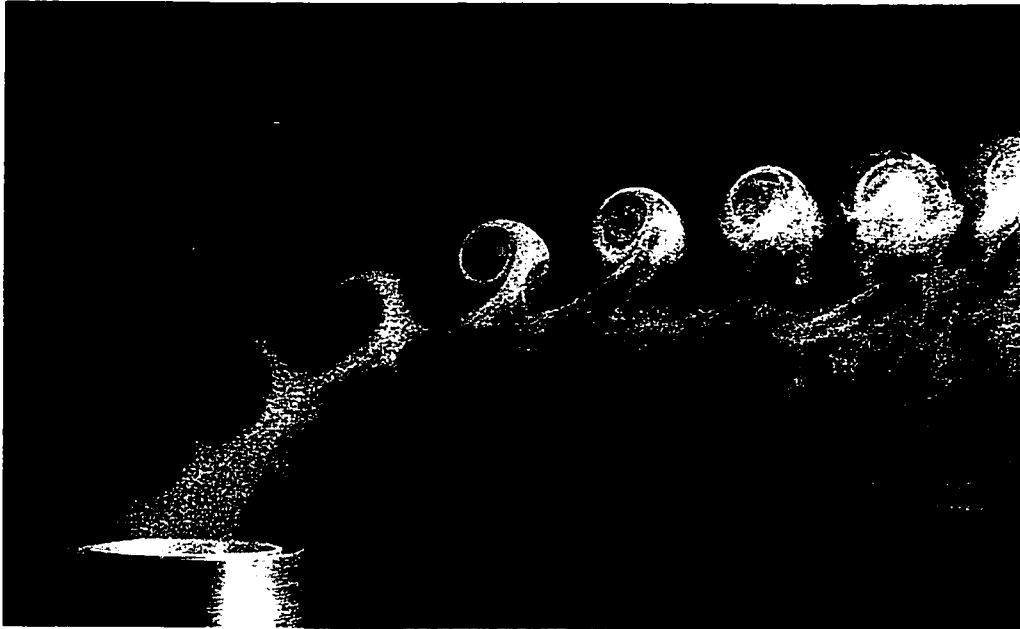
(c) Photograph of Laminar Plume Forced with 40 Hz Synthetic Jet: Plume relaminarizes, $U_\infty \approx 0.5 \text{ m/s}$, $W_p \approx 0.45 \text{ m/s}$, $W_{SJ} \approx 0.3 \text{ m/s}$.

Figure 3.17: Change in Structure of Laminar Plume Under Synthetic Jet Forcing (cont.)



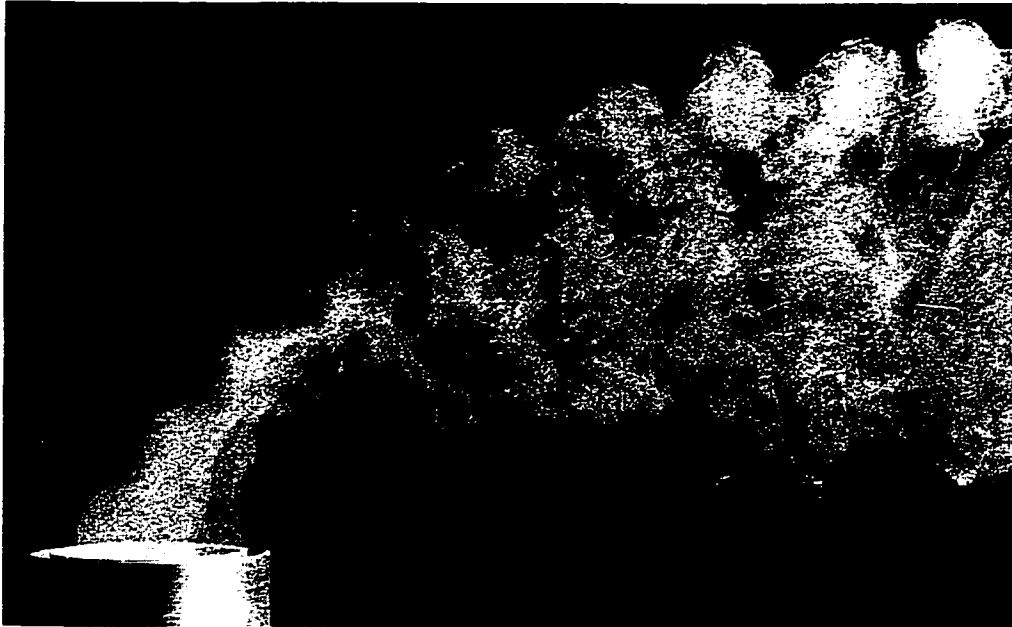
(d) Photograph of Laminar Plume Forced with 40 Hz Synthetic Jet: Upstream-pointing mushroom vortices emerge from upper surface, $U_{\infty} \approx 0.5 \text{ m/s}$, $W_p \approx 0.45 \text{ m/s}$, $W_{SJ} \approx 0.9 \text{ m/s}$.

Figure 3.17: Change in Structure of Laminar Plume Under Synthetic Jet Forcing (cont.)



(e) Photograph of Laminar Plume Forced with 40 Hz Synthetic Jet: After the second transition, vortices on the upper surface contain mainly one sign of vorticity and point downstream, $U_{\infty} \approx 0.5 \text{ m/s}$, $W_p \approx 0.45 \text{ m/s}$, $W_{SJ} \approx 0.9 \text{ m/s}$.

Figure 3.17: Change in Structure of Laminar Plume Under Synthetic Jet Forcing (cont.)



(f) Photograph of Laminar Plume Forced with 40 Hz Synthetic Jet: Plume is lifting off and becoming more turbulent with increased forcing amplitude, $U_\infty \approx 0.5 \text{ m/s}$, $W_p \approx 0.45 \text{ m/s}$, $W_{SJ} \approx 1.2 \text{ m/s}$.

Figure 3.17: Change in Structure of Laminar Plume Under Synthetic Jet Forcing (cont.)

3.5 Plume Forced with Steady Annular Blowing

As a comparison with synthetic jet forcing, data was also taken plume of the plume forced with only upwards-directed steady annular blowing from the slit around the plume at the stack exit. This annular slit is the same opening used to produce the synthetic jet for the experiments previously described. The method of applying this forcing is described in Section 2.3.2.2. Like synthetic jet amplitude, the steady blowing amplitude is represented by the mean centerline velocity 3mm (2 slit diameters) from the exit.

A photograph of case 16, forced with steady blowing, is shown in Figure 3.18, and can be compared to the photograph of case 1, forced with a 40 Hz synthetic jet, in Figure 3.19. Both have plume velocity ratios of 0.73, and a forcing velocity of 3.5 m/s. The most striking feature when comparing these two photographs is the lack of pulsation in the plume with steady blowing. This is expected given the lack of oscillatory forcing as with the synthetic jet. Another result of annular blowing is that less smoke is evacuated from the recirculation area in the immediate wake of the tip, when compared to synthetic jet forcing of similar amplitude. The jet shear layer caused by steady blowing does not entrain as much ambient air as the synthetic jet, which is composed entirely of entrained fluid. For the synthetic jet it is possible that this entrainment is clearing smoke from the recirculation area, and thus is more effective than the less-entraining steady blowing.

Plume height increases with steady annular blowing, but less so than with



Figure 3.18: Photograph of Plume Forced with Steady Annular Blowing:
 $R = 0.73, U_\infty = 4.0 \text{ m/s}, \frac{W_b}{U_\infty} \approx 0.88$

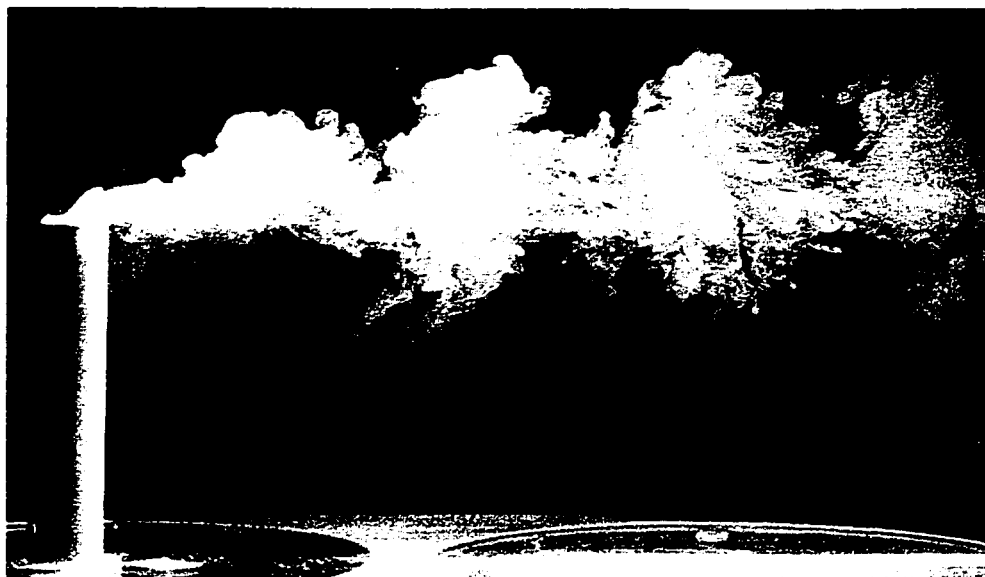


Figure 3.19: Photograph of Plume Forced with 40 Hz Annular Synthetic Jet:
 $R = 0.73, U_\infty = 4.0 \text{ m/s}, \frac{W_{SJ}}{U_\infty} \approx 0.88$

a synthetic jet of comparable amplitude. Figure 3.20 illustrates this with a plot of plume height versus both synthetic jet and steady blowing velocity (cases 1 and 16) normalized by cross-stream velocity. It can be seen that when the forcing velocity normalized by U_∞ is greater than one, the synthetic jet forcing increases the plume height by more than twice the amount of steady blowing. All of the steady blowing cases are shown in Figure 3.21 along with the reference unforced plume cases, in the same manner as Figure 3.7. The plume height data for steady blowing is consistent to some degree with the conjecture made in Section 3.4.1.2 regarding the independence of plume height to plume velocity at high forcing amplitudes. There is a suggestion that the curves for cases 16, 18, and 19 are beginning to converge at higher forcing amplitudes. However, a blowing velocity high enough to enable a conclusion to be made about this possible convergence couldn't be reached for all the cases. Case 20 in particular, with the highest plume velocity ratio, is not close in plume height to any other cases. This follows with the theory, however, as the greatest forcing amplitude should be required to overcome the effect of the relatively strongest plume. That amplitude has simply not yet been reached.

When Figure 3.21 is compared to Figure 3.7, it becomes clear that forcing the plume with steady annular blowing is less effective than synthetic jet forcing for all plume velocity ratios. This can also be seen in Figure 3.22, showing results of applying the momentum-weighted momentum velocity ratio defined in Equation 3.23. Unlike similar results for the synthetic jet cases

shown in Figure 3.13, the beginnings and ends of the curves for the various steady blowing cases are not contiguous. From looking at the steady blowing results of Figure 3.22, and comparing them with the synthetic jet results of Figure 3.13, it can be concluded that while steady annular blowing does have the general effect of increasing plume height for a given plume velocity ratio, it is a less effective forcing mechanism than synthetic jetting at similar forcing amplitudes. In the next section is a discussion of why.

3.6 Entrainment Due to Steady Blowing or Synthetic Jetting

From the introduction to the plume rise equations in Section 3.4.3, it becomes clear that entrainment of ambient air into the plume plays a large part in the dynamics of plume rise. Thus, it would not be surprising to find out that forcing the plume around its perimeter changes these entrainment characteristics. It turns out, however, that when considering suitable parameters and applying them accordingly, the plume forced by synthetic jets shows the same mean plume heights as the unforced plume, as Figure 3.13 on page 102 shows. What this suggests so far is that the gross entrainment characteristics, expressed as an entrainment coefficient β , of a synthetic jet-forced plume after it leaves the stack exit area, are comparable to those of an unforced plume of similar M_M . This does not appear to be true, however, when considering for comparison the performance of steady annular blowing in place of the synthetic jet (Section 3.5).

A possible reason for the smaller increase in plume height when applying

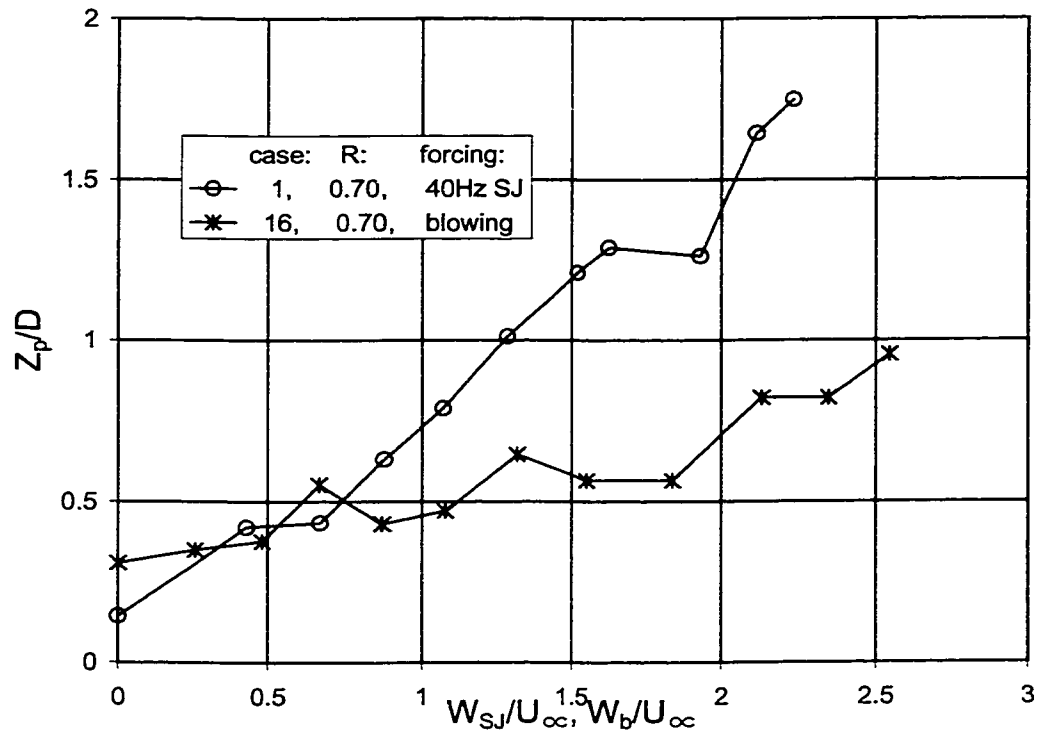


Figure 3.20: Comparison of Plume Heights Between Synthetic Jetting and Steady Annular Blowing For The Same Plume Velocity Ratio

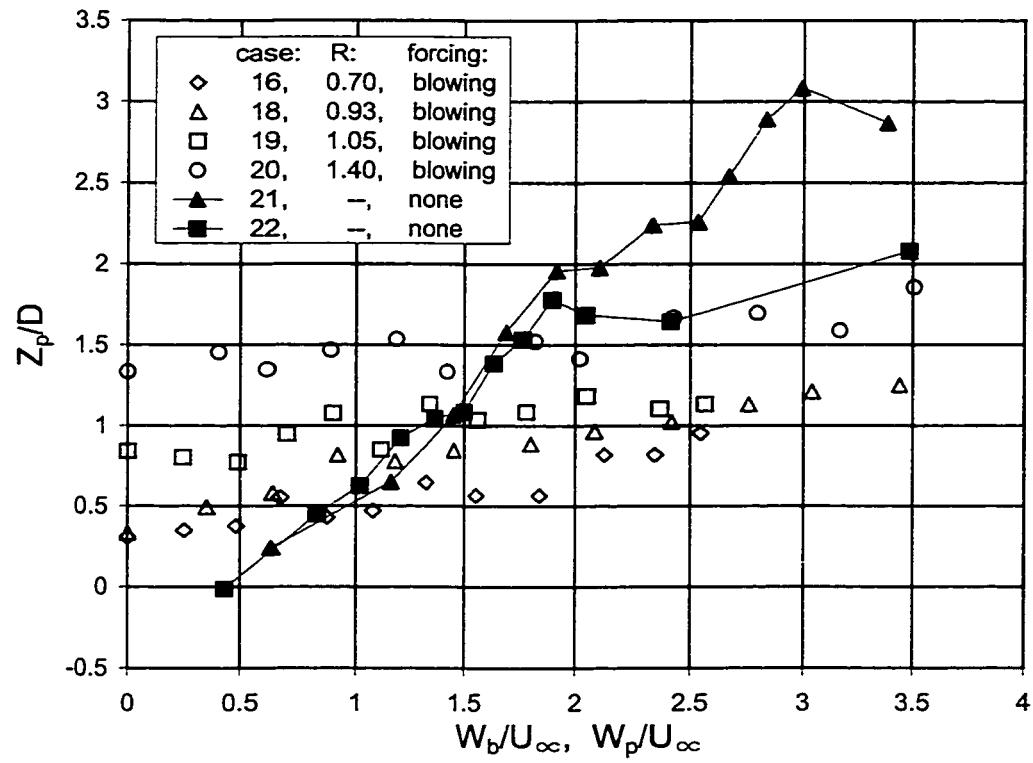


Figure 3.21: Plume Heights of Plumes Forced with Steady Annular Blowing and Reference Unforced Plumes

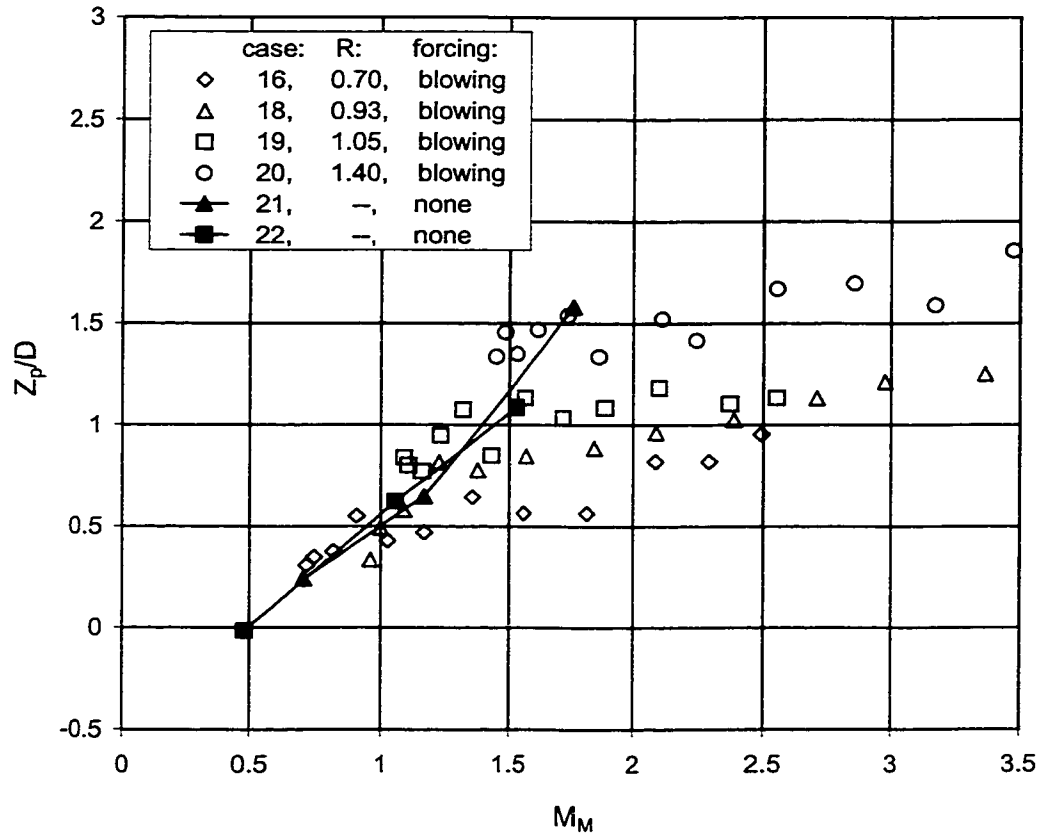


Figure 3.22: Plume Height With Steady Annular Blowing vs. Momentum Ratio Calculated Using Momentum-Weighted Area, M_M : Enlarged symbols represent data points of zero forcing amplitude for each case. Shown for reference are solid symbols representing unforced plumes.

steady blowing versus synthetic jetting may be motivated by taking a closer look at what happens right near the stack exit of the forced plume. The discussion to follow refers to entrainment caused by the forcing in the immediate vicinity of the orifice, and is a different concept than entrainment at the edges of the overall developed plume after it leaves the stack exit area, as previously discussed.

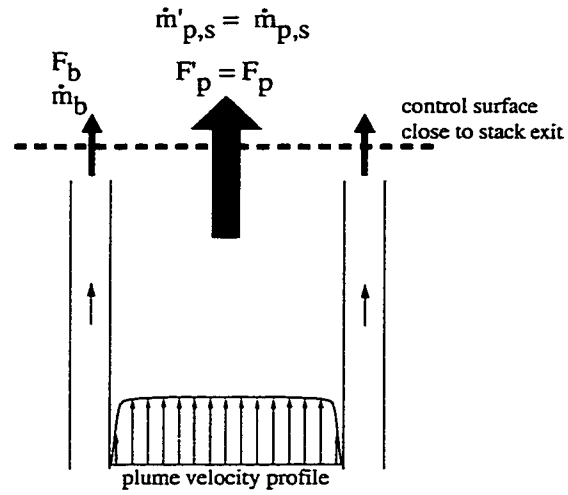
As explained in Section 1.2, the main difference between synthetic jetting and conventional jetting is the lack of a net mass flow through the synthetic jet orifice. This means that the synthetic jet is composed entirely of air entrained from the vicinity of the orifice. The consequences of this distinction are illustrated in Figure 3.23, showing an idealization of what occurs near the exit of the forced plume. Heuristically, it can be explained that synthetic jetting provides the same momentum addition but less mass addition than a steady blowing jet of similar velocity. Some analysis reveals that when leaving the stack exit area, a plume forced with steady blowing has a lower average velocity than a similar plume forced with a synthetic jet, assuming that the synthetic jet entrains at least some of its working fluid from the plume itself. This provides an explanation as to why steady blowing does not increase plume height as much as synthetic jetting of equal velocity. The rest of this section is devoted to explaining this idea in more detail.

As indicated in Figure 3.23, for both forcing cases a control surface is considered which is near, but not at, the stack exit plane. The steady blowing case is drawn with two discrete sources crossing the control surface: the

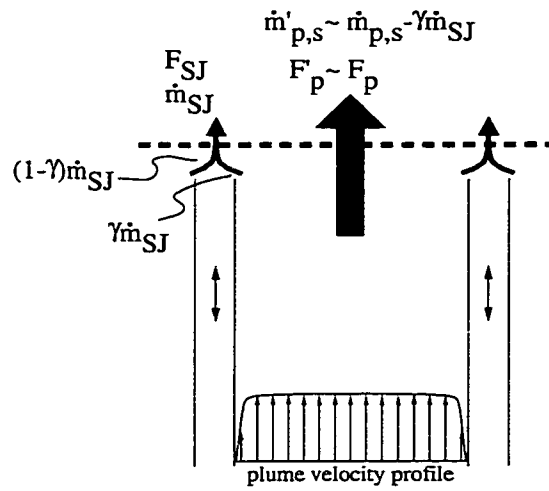
central plume flow and the annular blowing (\dot{m}_b). The synthetic jetting case is also drawn with two discrete sources: the plume and synthetic jet (\dot{m}_{SJ}) flows. The synthetic jet is shown as entraining its mass flux from both the edges of the plume ($\gamma\dot{m}_{SJ}$) as well as the surrounding ambient air $((1 - \gamma)\dot{m}_{SJ})$. The variable $\dot{m}_{p,s}$ is the mass flux of the unforced plume near the stack exit, and $\dot{m}'_{p,s}$ is the mass flux of the forced plume near the stack exit. Similarly, $F_{p,s}$ is the momentum flux of the unforced plume near the stack exit, and $F'_{p,s}$ is the momentum flux of the forced plume near the stack exit. The differentiation between the forced and unforced quantities using the “primed” symbol will be useful later on. It is assumed that the control surface is close enough to the exit so the plume and forcing can be thought of as discrete fluxes, yet far enough away that the synthetic jet has time to develop. If the plume forced with steady blowing is first considered, we make the assumption that the interaction between the plume and blowing has been negligible so close to the exit, so that $\dot{m}'_{p,s} = \dot{m}_{p,s}$. Now we may sum the mass flux over the control surface and write

$$\begin{aligned} \text{total mass flux} &= \dot{m}'_{p,s} + \dot{m}_b \\ &= \dot{m}_{p,s} + \dot{m}_b \end{aligned} \tag{3.27}$$

If a similar assumption is made for the momentum flux, we may also write



(a) Steady Annular Blowing



(b) Synthetic Jet Forcing

Figure 3.23: Idealization of Forced Flow Near Exit Plane

$F'_{p,s} = F_{p,s}$. So then for the summation of momentum flux we get

$$\begin{aligned} \text{total momentum flux} &= F'_{p,s} + F_b \\ &= F_{p,s} + F_b \end{aligned} \quad (3.28)$$

Now assuming that there is no external flow into the plume or steady blowing jet (ie: neglecting entrainment at the jet shear layer), we may define G_b , the average momentum flux per unit mass flux over the control surface, as

$$\begin{aligned} G_b &= \frac{\text{total momentum flux}}{\text{total mass flux}} \\ &= \frac{F_{p,s} + F_b}{\dot{m}_{p,s} + \dot{m}_b} \end{aligned} \quad (3.29)$$

(note: for a particle G is the particle velocity). The same procedure can be applied to the synthetic jetting case, with a few slight changes. As shown in Figure 3.23b, some amount of the synthetic jet mass flux must be entrained from the plume. The coefficient γ represents the fraction of \dot{m}_{SJ} that is taken from the plume. Consequently, the mass flow of the forced plume must be written as

$$\dot{m}'_p = \dot{m}_p - \gamma \dot{m}_{SJ} \quad (3.30)$$

so then to find the total mass flux of the synthetic jet-forced plume:

$$\begin{aligned} \text{total mass flux} &= \dot{m}'_p + \dot{m}_{SJ} \\ &= \dot{m}_p + (1 - \gamma) \dot{m}_{SJ} \end{aligned} \quad (3.31)$$

Likewise, a portion of the unforced plume's vertical momentum is transferred to the synthetic jet with the entrained flow. The approximation is made that the resultant change in plume momentum is negligible, giving:

$$F'_{p,s} \approx F_{p,s} \quad (3.32)$$

This results in the expression for momentum per unit mass in the case of synthetic jetting:

$$\begin{aligned} G_{SJ} &= \frac{\text{total momentum flux}}{\text{total mass flux}} \\ &= \frac{F_{p,s} + F_{SJ}}{\dot{m}_{p,s} + \dot{m}_{SJ}} \\ &= \frac{F_{p,s} + F_{SJ}}{\dot{m}_{p,s} + (1 - \gamma) \dot{m}_{SJ}} \end{aligned} \quad (3.33)$$

It can be seen that for $\gamma > 0$, $G_{SJ} > G_b$ by a factor of

$$\frac{G_{SJ}}{G_b} = \frac{\dot{m}_{p,s} + \dot{m}_b}{\dot{m}_{p,s} + (1 - \gamma) \dot{m}_{SJ}} \quad (3.34)$$

In words, Equation 3.34 shows that if the synthetic jet is entraining any mass from the plume at all, then the plume forced with a synthetic jet has a higher momentum per unit mass than if forced with a steady jet of similar mass flux. As an example, this ratio can be approximated for cases 4 and 18 assuming that $\gamma = 0.5$, or that half of the synthetic jet mass flux is taken from the plume. This results in $G_{SJ}/G_b \approx 1.29$ for a plume velocity of

$W_p=0.93$ m/s. This model provides an explanation for why steady blowing is not as effective in increasing plume height as synthetic jetting, in that synthetic jetting results in greater average momentum per unit mass over the total plume (average velocity) than does steady annular blowing. By using the same model, however, a decrease in plume height would be expected for the synthetic jet-forced plumes if the synthetic jets were to add any mass at all. The fact that this doesn't happen to any great extent suggests that either the synthetic jets are actually entraining their working fluid mostly from the plume, with very little from the surrounding air, or that there are other important factors not considered by this model.

3.7 Downwash Index

While measurements of mean plume height give a useful indication of overall plume behaviour, it is not necessarily the most important consideration. For the case of a plume in downwash, it is the lower edge of the plume that is the most important as far as ground concentration, as well as interaction with surrounding structures and facilities. Not surprisingly, the criteria for determining downwash vary between different studies. Using a qualitative scheme, Overcamp and Hoult (1971) rated experimental plumes as non-interacting, slightly interacting, and strongly interacting. In analyzing buoyant plumes from other studies, Overcamp (1983) inferred the absence of downwash if measurements of the plume center fit buoyant plume rise laws. In the early work of Sherlock and Stalker (1941), downwash was considered significant

when the lower plume edge fell more than one stack diameter below the stack tip. Snyder and Lawson (1991) defined downwash as when the time-averaged plume-gas concentration 1 diameter below the tip and 0.5 diameters downstream was 1% of the original stack concentration.

How these methods are similar is that they only consider an average indication of the plume's presence, and not transient peaks in concentration. These transient peaks are a result of organized structures extending downwards from the main plume. These structures contain concentrated plume material and ostensibly result from interaction of the plume with the stack wake. These structures are often seen in photographs of plumes with low-velocity ratio (Overcamp and Hoult, 1971; Hoult and Weil, 1972). In this thesis, these structures extending below the plume will be referred to as "puffs".

There are two main viewpoints that can be considered when evaluating downwash:

1. Average plume concentration near the ground.
2. Transient peak plume concentration near the ground.

Simply put, a passing amount of concentrated effluent may be as undesirable as having a continual amount of lower concentration (Hilderman, 2001). With this in mind, a qualitative grading system was devised to apply to the plume photographs taken for this study, with the intention of trying to capture the effect of low-level penetration of these puffs. This system is

presented in Table 3.3. Results using this system are shown in Figure 3.24, where grades for plumes forced by synthetic jets as well as steady blowing are shown and plotted against forcing velocity normalized by the cross-flow velocity. Because the downwash grade of -1.0 is the worst grade of the reference unforced plumes at a velocity ratio of 1.5, this is used as the cutoff for significant downwashing. This grade corresponds to a lower plume edge not more than 0.5 stack diameters below the tip. To collapse the data somewhat, the same data is plotted in Figure 3.25 against the modified momentum ratio M_M given in Equation 3.23. It can be seen by this curve that there is a drastic improvement in downwash given an initially small amplitude of forcing, but then this improvement plateaus at higher forcing amplitudes. Results for all of the forced cases extended outside of the zone of significant downwashing.

The downwash results in Figure 3.25 differ from results obtained in Sections 3.4 and 3.5, where the average plume height results are presented. The downwash data shows little difference in downwash between plumes forced with synthetic jetting and annular blowing, even though their mean plume height measurements do. Also, average plume height continually rises with increasing forcing, both steady and unsteady, instead of showing the plateau of the downwash data. What this suggests is that in terms of reducing downwash, forcing with either synthetic jets or annular blowing is most effective in alleviating severely downwashed cases. However, increased forcing, while raising the mean plume height, does not reduce downwash much more once a certain level is reached. This apparent limit suggests that neither of these

Table 3.3: Downwash Grading Criteria

Grade	Criteria
0.4	Lower edge of plume < 2.0 D above tip
0.3	Lower edge of plume < 1.5 D above tip
0.2	Lower edge of plume < 1.0 D above tip
0.1	Lower edge of plume < 0.5 D above tip
0	Lower edge of plume just at or above tip, no puffs
-0.02	Lower edge of plume just at or above tip, a few puffs
-0.04	Lower edge of plume just at or above tip, puffs
-0.06	Lower edge of plume just at or below tip, no puffs
-0.08	Lower edge of plume just at or below tip, puffs
-0.1	Lower edge of plume < 0.5 D below tip
-0.2	Lower edge of plume < 1.0 D below tip
-0.3	Lower edge of plume < 1.5 D below tip
-0.4	Lower edge of plume < 2.0 D below tip

forcing techniques would be very effective in improving downwash from very slightly downwashed plumes. Almost all plumes with indexes above the cut-off determined from the reference unforced plumes still have entrainment of plume gases into the immediate wake of the stack tip.

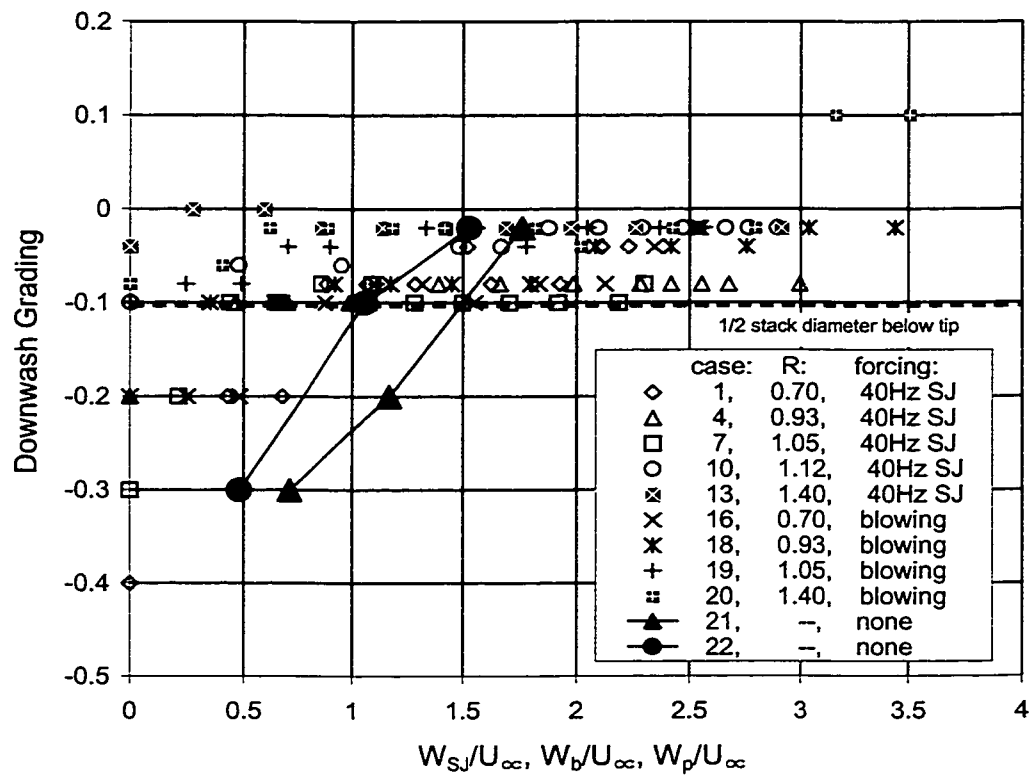


Figure 3.24: Downwash Grading versus Forcing Velocity Normalized by Freestream Velocity

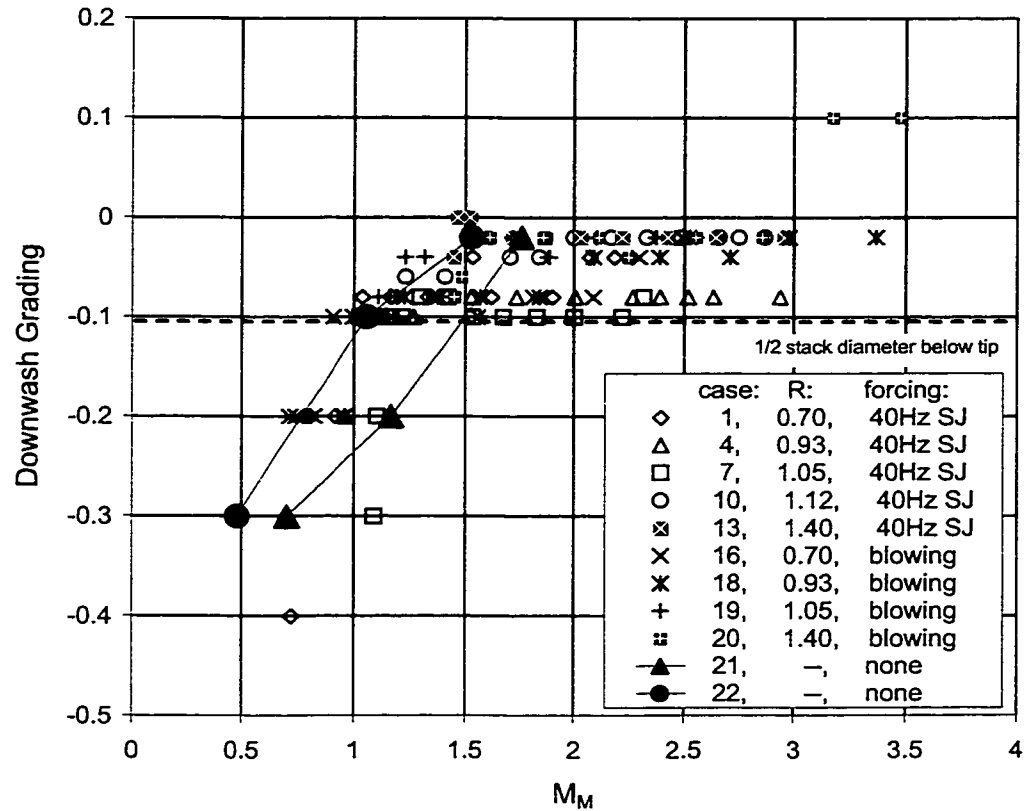


Figure 3.25: Downwash Grading vs. Momentum Ratio Calculated Using Momentum-Weighted Area, M_M : Enlarged symbols represent data points of zero forcing amplitude for each case. Shown for reference are solid symbols representing unforced plumes.

CHAPTER 4

CONCLUSIONS AND FUTURE WORK

4.1 Summary and Conclusions

An apparatus has been designed and built that allows the application of sinusoidal forcing to the edge of a turbulent or laminar plume in a crossflow. At higher forcing amplitude this creates a synthetic jet around the plume edge. It was found that with this forcing the severity of downwash in low-velocity plumes could be reduced, and this effect is expected to be scalable to a full-sized stack. A preliminary apparatus was first built and tested in order to both determine the optimal forcing configuration to reduce downwash, as well as to learn more about synthetic jetting properties that could influence the final apparatus design. In neither of these experiments was the planetary boundary layer taken into account. Photographic and hot-wire data gained from these experiments were used in designing the final apparatus and interpreting the results. It was determined that the most effective configuration is an upwards-pointing annular synthetic jet coaxial with the initial plume

flow. From photographs, plume height was measured 7.5 stack diameters downstream of the stack. This plume height was taken as an inverse indication of downwash. Another indicator of downwash comes from inspection of the lower plume edge and structures extending downwards from it containing concentrated plume gases, and is expressed as a downwash index. This index is meant to reflect the unfavourable result of a concentrated amount of passing efflux even though the averaged concentration may be low at that location. By analyzing results from the final apparatus as well as from the preliminary apparatus, the following conclusions were made:

Measurements from the preliminary apparatus show that developed synthetic jet velocity scaled by the perturbation velocity inside the jetting orifice is strongly frequency dependent and weakly amplitude dependent. Thus at any given frequency, the velocity of the developed jet is approximately linearly proportional to the amplitude of forcing. In the case of the final apparatus, synthetic jet velocity (W_{SJ} measured at the jet centerline 2 orifice diameters from the exit) is linearly proportional to forcing amplitude divided by the forcing frequency. This is the same scaling found for the oscillating velocity inside the slit (w'_{slit}), which results in a constant W_{SJ}/w'_{slit} ratio of 0.46 for any forcing amplitude and frequency.

In preliminary experiments, vertically-directed synthetic jets have the greatest beneficial influence on the downwashed smoke-wire streaklines passing over a finite cylinder in a cross-wind. While there is no plume actually present, this situation can be thought of as having a very weak plume. When

with the final apparatus similar forcing is applied to a downwashing plume in a crossflow, downwash is reduced and overall plume height increases. In the example of case 1 plume height increases by over 1.5 stack diameters with a forcing velocity to cross-wind velocity ratio of 2.2.

The change in mean plume height when a plume is forced with a synthetic jet depends only on mean synthetic jet amplitude (W_{SJ}), and is independent of forcing frequency. This is not necessarily the case when looking at instantaneous plume height. With a synthetic jet of high amplitude and low frequency, the instantaneous plume height becomes locked-in to the synthetic jet forcing and therefore depends on both synthetic jet amplitude *and* frequency. This was observed when using a synthetic jet of 40 Hz, the lowest frequency used in these experiments, with a resultant Strouhal number based on stack diameter and cross-wind velocity of 0.25.

When synthetic jet momentum is high compared to the plume momentum, mean plume height becomes independent of plume momentum and synthetic jet momentum dominates. This is shown with photographs as well as measured data:

- Photographs show that similar structures are visualized with both a plume forced at high synthetic jetting amplitude, as well as with only a synthetic jet in a similar configuration but without a plume flow. This suggests that the presence of the plume flow is of little or no consequence to the flow field. For the example of case 1 this occurs when the synthetic jet to plume momentum ratio is greater than approxi-

mately 1.3.

- When plume height data series are plotted against synthetic jet forcing velocity, these series all converge with each other at high forcing amplitude regardless of plume velocity ratio.

By applying this understanding, a simple model can be used which uses an equivalent plume based on combining the momentum fluxes of a forced plume and its forcing. A momentum velocity ratio was introduced with a correction factor that corrects for the non-uniform velocity profile occurring with real pipe flows. In the case of the forced plume this momentum velocity ratio is a convenient means to incorporate the momentum added to the plume by the forcing. Plume height was plotted against the momentum velocity ratio of this equivalent plume where the total combined area of the plume and forcing was considered. The synthetic jet-forced plume height data shows a reasonable collapse, but departs from the reference unforced plume data.

Through physical reasoning, it was determined that the correct area to use for calculating the equivalent momentum velocity ratio should satisfy the limits of no forcing, where only the plume area is appropriate to use, and very high forcing, where only the forcing area should be considered. This area A_M is expressed as a combination of the plume and forcing areas weighted linearly by their relative momentum fluxes. When the plume height data is plotted against M_M , the momentum velocity ratio of the equivalent plume using the momentum-weighted area term A_M , it was found that synthetic jet-forced

plume heights stayed reasonably collapsed, and were also comparable with those of unforced plumes. What this suggests is that after it leaves the stack exit area, the gross entrainment characteristics (expressed as an entrainment coefficient β) of a synthetic jet-forced plume are comparable to those of an unforced plume of similar M_M . This implies the possibility of successfully using traditional plume trajectory models for plumes forced in the current manner. One such model using a variable entrainment coefficient (Briggs, 1975) was tried, and it was found to reflect the trend of the forced as well as unforced data reasonably well without any fitting or adjustment of constants. None of the data showed any sign of Reynolds Number dependency, even though plume and cross-flow velocities varied by over 50%.

For comparison, steady annular blowing was used in place of the synthetic jet. It was found that steady blowing does not increase plume height as much as synthetic jetting for any given jet velocity. An argument was made as to why, based on a simplified model of the plume and forcing flows near the stack exit. The essential point of this argument is that a conventional steady annular jet adds mass as well as momentum into the plume. Additional entrainment from the shear layer of the steady blowing jet is not considered. The assumption is made that fluid from this steady blowing jet becomes well-mixed with the plume fluid. With vertical momentum flux as an invariant, the combined momenta of both the plume and the steady jet is redistributed among the combined mass of the plume and the steady jet. A synthetic jet on the other hand, being composed entirely of entrained fluid, obtains at least

some of its working fluid from the plume itself, and the rest from ambient air. Thus, less mass (only that entrained from the ambient air) is added to the total resulting plume mass for the same additional amount of momentum. This results in higher average vertical momentum per unit mass, which is the average vertical velocity. It is conjectured that this is why plumes rise more when forced with synthetic jetting than when forced with steady blowing.

Downwash as indicated by a downwash index was evaluated for forced as well as unforced plumes. The application of this system differs from plume height measurements in that instead of the overall height of the plume, it is the low-level penetration of the lower plume edge as well as concentrated “puffs” extending downward from this edge at any instant that are regarded as measures of downwash. This instantaneous view-point of the plume as opposed to an averaged viewpoint is meant to reflect the undesirability of a short-lived exposure to high-concentration efflux even though an averaged measurement might show a low concentration. Strongly downwashed plumes show significant improvement when either steady blowing or synthetic jet forcing is applied. The amount of improvement appears to be the same for both steady blowing and synthetic jetting, and independent of synthetic jetting frequency. As opposed to mean plume height, however, downwash reduction does not continue to improve with increased forcing amplitude, but instead shows a plateau. This apparent limit to downwash reduction suggests that while synthetic jetting is effective in increasing plume height, neither of these forcing techniques would be very effective in improving downwash from

very slightly downwashed plumes, as indicated by the downwash index.

As a contrast to the data taken for plumes with turbulent pipe flows, preliminary photos were also taken of a plume from a laminar pipe flow. The plume velocity ratio was about 0.9, and the plume was forced by a 60 Hz synthetic jet, giving a Strouhal number of $St = 0.3$ based on cross-stream velocity and stack diameter. Side-view photographs of the plume show two distinct transitions occurring in the naturally occurring plume structure as synthetic jet amplitude is increased from zero. After the first transition while increasing forcing amplitude, the plume relaminarizes before the next transition takes place. Corresponding transitions in the turbulent plume have not been observed, either through visual interpretation or measurement of the photographs.

Photographs of the laminar plume forced with a strong synthetic jet ($W_{SJ}/W_p \approx 2.7$) show that the vertical plume depth at a fixed location downstream increases as the plume lifts-off with increasing forcing, over a 40% increase from the unforced plume. This increased plume depth suggests that there is greater mixing of the plume with ambient air.

As synthetic jet forcing amplitude increases, the pressure head (P_h) required to drive the plume flow at the same flow rate decreases. During experimental runs this led to the plume velocity increasing with increasing forcing amplitude, and the voltage to the fan driving the plume had to be adjusted to keep a constant plume velocity. This effect is likely due to the suction known to exist at the synthetic jet exit plane (Smith and Glezer, 1998). P_h is the

differential pressure measured between a point just upstream of the plume-flow contraction and the static pressure inside the tunnel. It was found that P_h , normalized by a dynamic pressure term derived from the plume velocity, depends on the ratio of synthetic jet velocity to plume velocity. In the present experiments this normalized P_h was reduced by more than 30%.

Apart from the final synthetic jet forcing configuration, several other configurations were tested using the preliminary experiment and found to be less likely to reduce downwash. Forcing a synthetic jet into the wake of an infinite cylinder in a cross-wind reduces the wake size, but this occurs due to increased suction pressure on the lee side of the cylinder drawing in normally separated streamlines. This same suction draws streamlines down from over the tip of the finite cylinder, thereby actually increasing downwash. Jetting up-wind and cross-wind was also tried with little success.

It is important to note that the method used to produce the synthetic jets in the final apparatus is not the same that would be proposed for use on a full-sized stack. The long thin annulus was simply a convenient way to create the required jetting while keeping a clean aerodynamic profile for research purposes. In practice the actuators would be self-contained and simply added to the tips of existing stacks. Determination of the required forcing amplitude and frequency of a synthetic jet actuator applicable to a full-sized stack can be guided by results presented in this study.

Because increasing plume height as well as decreasing downwash as indicated by the downwash index is independent of forcing frequency, within

the ranges covered in this study, the choice of operating frequency can be based on other factors. It would be advantageous to operate at a low forcing frequency (f) for two reasons. First, synthetic jet velocity was found to be proportional to $1/f$ for a fixed forcing pressure amplitude, resulting in a higher jet velocity with lower frequency. Secondly, a low-frequency actuator may have benefits in terms of noise pollution if it is able to operate in the infrasonic range.

A sample calculation can be performed assuming a stack of 1 m diameter with a 0.1 m wide annular orifice around the circumference of the exit, and 1 to 5 m/s plume flow in a cross-wind of 2 to 10 m/s. The worst case scenario is with the 1 m/s plume flow and 10 m/s cross-wind, giving a plume velocity ratio of 0.1 which is in a strongly downwashing flow regime. In Section 3.4.4.3 it was determined that downwash should cease when M_M is equal to or greater than 1.5. Solving the equations developed in that section, W_{SJ} should be 15 m/s or greater in order for downwash not to occur. Assuming that the ratio of $W_{SJ}/w'_{slit} = 0.46$ holds for a scaled-up stack, this synthetic jetting velocity W_{SJ} can be related to the operational jetting frequency through the synthetic jet strouhal number (St_{SJ}), based on slit diameter d_a and w'_{slit} , the RMS average of the oscillating velocity inside the slit. The lowest St_{SJ} used in the final experiments was approximately 0.004, with a 40 Hz synthetic jet at 7 m/s. Solving for frequency with this Strouhal number and the scaled-up stack parameters gives a jetting frequency of around 1.2 Hz.

4.2 Future Work

The following are suggested for future work on this project:

- Use the smoke wire in conjunction with plume smoke in order to see if it better shows the interaction of the synthetic jet with the plume near the stack exit
- Use along with image correlation velocimetry (ICV) to determine the flow-field within and around the forced and unforced plume.
- More accurately quantify synthetic jet momentum flux by taking more spatially detailed velocity measurements near the orifice.
- Devise a system to make time-averaged as well as instantaneous plume concentration measurements.
- Implement a system to measure average plume trajectory. This would allow a comparison of the model with measured data at more than one location.
- Experiment with changing the apparatus chamber volume to try and obtain more synthetic jetting amplitude at higher frequencies.
- Incorporate a planetary boundary layer into the wind tunnel test section.
- Try and model the entrainment expected with steady annular blowing.

- Take velocity profiles of the forced plume to calculate actual momentum flux. This will test the assumption that the momentum of the plume and its forcing can simply be added.
- Calculating mass flux from velocity profiles of the forced plume may enable an approximation of how much fluid the synthetic jet is entraining the ambient surroundings.
- Full-scale tests to see if effect of the synthetic jet forcing can be scaled up.

BIBLIOGRAPHY

- Amitay, M., Honohan, A., Trautman, M., and Glezer, A. (1997). Modification of the aerodynamic characteristics of bluff bodies using fluidic actuators. In *28th AIAA fluid dynamics conference, Snowmass Village, CO*, AIAA 97-2004.
- Amitay, M., Smith, B., and Glezer, A. (1998). Aerodynamic flow control using synthetic jet technology. In *36th Aerospace sciences meeting and exhibit, Reno, Nevada*, AIAA 98-0208.
- Briggs, G. (1969). *Plume Rise*. U.S. Atomic Energy Commision.
- Briggs, G. (1975). Plume rise predictions. In *Lectures on Air Pollution and Environmental Impact Analyses*, pages 59–111. American Meteorological Society.
- Briggs, G. (1984). Plume rise and buoyancy effects. In Randerson, D., editor, *Atmospheric Science and Power Production*, pages 327–366. U.S. Department of Energy.
- Bryant, R., Fox, R., Lachowicz, J., and Chen, F. (1999). Piezoelectric syn-

- thetic jets for aircraft control surfaces. *SPIE conference on industrial and commercial applications of smart structures, Newport Beach, California*, 3674:220–227.
- Chapple, D. (1998). The role of turbulence in pulsation induced orifice plate flow metering error. Master's thesis, University of Alberta.
- Coe, D., Allen, M., Smith, B., and Glezer, A. (1995). Addressable micromachined jet arrays. In *Proceedings of the 1995 8th International Conference on Solid-State Sensors and Actuators, and Eurosensors IX. Stockholm, Sweden*, volume 2, pages 329–332.
- Corke, T., Koga, D., Drubka, R., and Nagib, H. (1977). A new technique for introducing controlled sheets of smoke streaklines in wind tunnels. *ICIASF 1977 Record, IEEE Publication*, pages 74–80.
- Coward, A. (2000). Personal communications.
- Crow, S. and Champagne, F. (1971). Orderly structure in jet turbulence. *Journal of Fluid Mechanics*, 48(3):547–591.
- Doebelin, E. (1972). *Measurement Systems*. Charles E. Merrill Publishing Co.
- Duke, R., Shrader, B., and Mo, J. (1993). Effects of a rear stagnation jet on the wake behind a cylinder. *AIAA journal*, 31(9):1727–1729.

- Fan, L. (1967). Turbulent buoyant jets into stratified or flowing ambient fluids. Technical Report KH-R-15, W.M. Keck Laboratory of Hydraulics and Water Resources.
- Fox, R. and McDonald, A. (1992). *Introduction to Fluid Mechanics*. John Wiley & Sons Inc., New York, 4th edition.
- Freund, J. and Moin, P. (2000). Jet mixing enhancement by high-amplitude fluidic action. *AIAA Journal*, 38(10):1863–1870.
- Hilderman, T. (2001). Measurement of high schmidt number concentration fluctuations in shear flow. Graduate Seminar, Mechanical Engineering Department, University of Alberta.
- Hinze, J. (1975). *Turbulence*. McGraw-Hill Book Company, New York, 2nd edition.
- Hoult, D. and Weil, J. (1972). Turbulent plume in a laminar cross flow. *Atmospheric Environment*, 6:513–531.
- Hsiao, F., Shyu, J., Liu, C., and Shyu, R. (1988). Experimental study of an acoustically excited flow over a circular cylinder. *3rd International symposium on transport phenomena in thermal control, Taiwan*.
- Hsiao, F., Liu, C., and Shyu, J. (1990). Control of wall-separated flow by internal acoustic excitation. *AIAA Journal*, 28(8):1440–1446.

- Ingard, U. and Labate, S. (1950). Acoustic circulation effects and the nonlinear impedance of orifices. *J. Acoust. Soc. Amer.*, 22(211).
- Johnston, C. (1994). Downwash of stack gas plumes. Master's thesis, University of Alberta.
- Johnston, C. and Wilson, D. (1997). A vortex pair model for plume downwash into stack wakes. *Atmospheric Environment*, 31(1):13–20.
- Karassik, I., Krutzsch, W., Fraser, W., and Messina, J., editors (1976). *Pump Handbook*. McGraw-Hill Book Company, New York.
- Lebedeva, I. (1980). Experimental study of acoustic streaming in the vicinity of orifices. *Soviet Physics Acoustics*, 26(4):331–333.
- Mednikov, E. and Novitskii, B. (1975). Experimental study of intense acoustic streaming. *Soviet Physics Acoustics*, 21(2):152–154.
- Mo, J. and Duke, M. (1993). Numerical investigation of a cylinder wake flow with a rear stagnation jet. *AIAA journal*, 32(5):1095–1098.
- Morton, B., Taylor, G., and Turner, J. (1956). Turbulent gravitational convection from maintained and instantaneous sources. In *Proceedings of the Royal Society*, volume 234 of A, pages 1–23.
- Moussa, Z., Trischka, J., and Eskinazi, S. (1977). The near field in the mixing of a round jet with a cross-stream. *Journal of Fluid Mechanics*, 80(1):49–80.

- Overcamp, T. (1983). Guidelines for stack downwash in plume modelling experiments. In *76th annual meeting of the air pollution control association*, volume 83-36.3.
- Overcamp, T. and Hoult, D. (1971). Precipitation in the wake of cooling towers. *Atmospheric Environment*, 5:751–765.
- Panton, R. (1996). *Incompressible Flow*. John Wiley & Sons, 2nd edition.
- Rizzetta, D., Visbal, M., and Stanek, S. (1999). Numerical investigation of synthetic-jet flowfields. *AIAA Journal*, 37(8):919–927.
- Schlichting, H. (1979). *Boundary-Layer Theory*. McGraw Hill, 7th edition.
- Scorer, R. (1958). *Natural Aerodynamics*. Pergamon Press.
- Seifert, A., Bachar, T., Koss, D., Shepshelovich, M., and Wygnanski, I. (1993). Oscillatory blowing: a tool to delay boundary-layer separation. *AIAA Journal*, 31(11):2052–2060.
- Sherlock, R. and Stalker, E. (1941). A study of flow phenomena in the wake of smokestacks. In *Engineering Research Bulletin No. 29*. University of Michigan, Ann Arbor, Michigan.
- Sigurdson, L. (1995). The structure and control of a turbulent reattaching flow. *Journal of Fluid Mechanics*, 298:139–165.
- Siller, H. and Fernholz, H. (2000). Trailing-edge separation control on an airfoil in low-speed flow. *Z. Angew. Math. Mech.*, 80:S89–S92.

- Smith, B. and Glezer, A. (1997). Vectoring and small-scale motions effected in free shear flows using synthetic jet actuators. In *35th Aerospace sciences meeting and exhibit, Reno, NV*, AIAA 97-0213.
- Smith, B. and Glezer, A. (1998). The formation and evolution of synthetic jets. *Physics of Fluids*, 10(9):2281–2297.
- Smith, D., Amitay, M., Kibens, V., Parekh, D., and Glezer, A. (1998). Modification of lifting body aerodynamics using synthetic jet actuators. In *36th Aerospace sciences meeting and exhibit, Reno, NV*, AIAA 98-0209.
- Snyder, W. and Lawson, R. (1991). Fluid modeling simulation of stack-tip downwash for neutrally buoyant plumes. *Atmospheric Environment*, 25A(12):2837–2850.
- Tatom, F. (1986). Prediction of stack plume downwash. *Journal of Fluids Engineering*, 108:379–382.
- Vadot, L. (1967). *Étude de la Diffusion des Panaches de Fumée dans l'Atmosphère*. Centre Interprofessionnel Technique d'Études de la Pollution Atmosphérique, Paris.
- White, F. (1999). *Fluid Mechanics*. McGraw-Hill Inc., New York, 4th edition.
- Wiltse, J. and Glezer, A. (1993). Manipulation of free shear flows using piezoelectric actuators. *Journal of Fluid Mechanics*, 249:261–285.

APPENDIX A

LABVIEW® PROGRAMS

This appendix contains information about the most important LabVIEW® programs (or “vi’s” for “virtual instruments”) used in these experiments. These vi’s are:

- *towerII-3.vi*—the main control panel for the whole experiment
- *average waveform.vi*—for estimating phase-average of time-series
- *integrate waveform.vi*—for de-rectifying and integrating hot-wire velocity measurement
- *popup-tow-6c.vi*—configuration panel for data acquisition and sensors

Significant portions of some of these vi’s have been contributed by Chapple (1998). A description of each of these vi’s is given along with Figures showing the vi control panel. Data shown on these vi control panels are with the hot-wire placed inside the synthetic jetting orifice. The LabVIEW® graphical programming language “G” was used to write these vi’s.

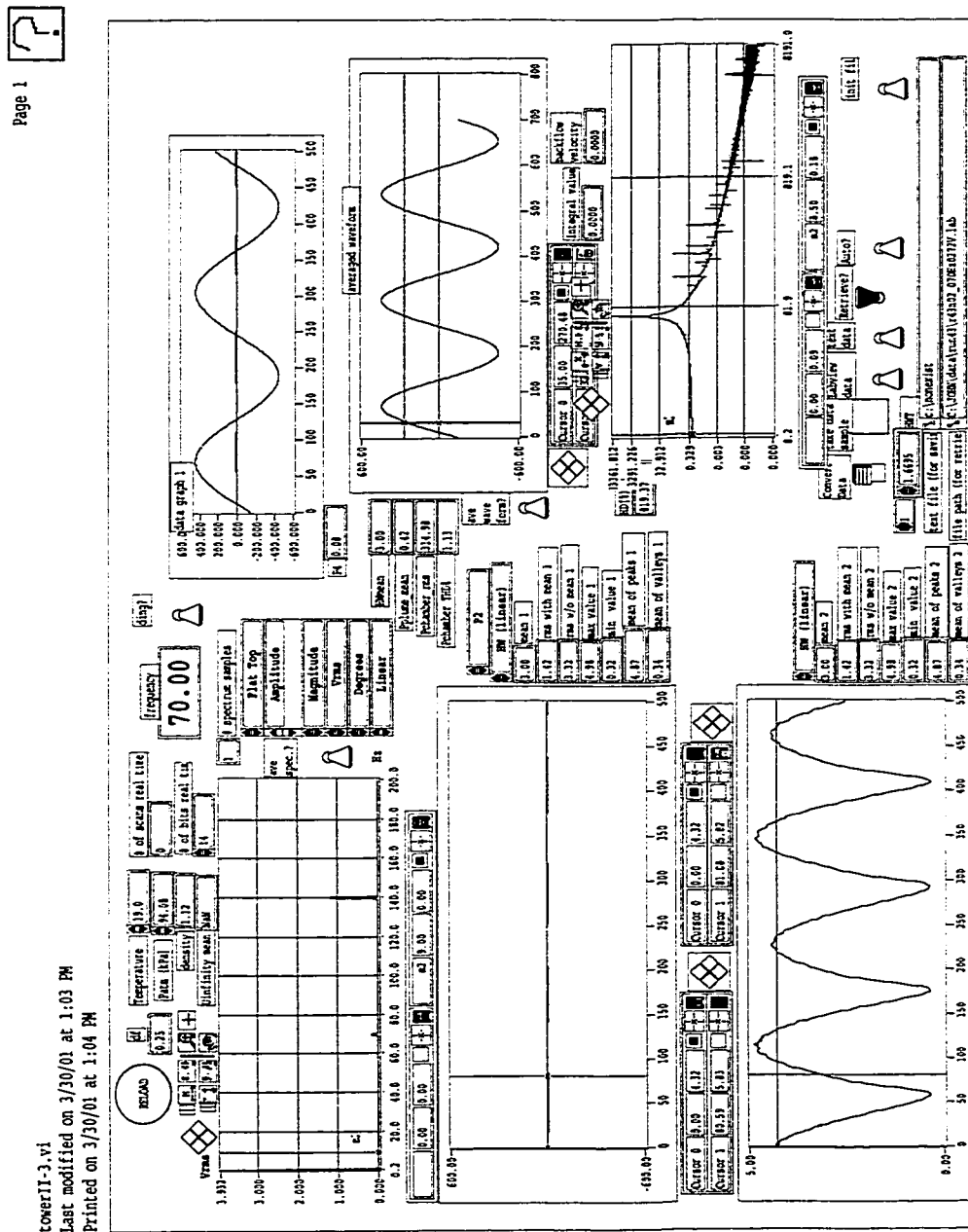
A.1 Description of *towerII-3.vi*

This vi is the main controller program used to monitor, record, and retrieve sensor data. Figure A.1 shows the control panel for this vi. Data is recorded from 6 data channels at a rate of around 16 Mhz. Typically 4 seconds of continuous data are acquired and analysed at a time, before refreshing the screen. If the “take a data sample” button is pushed, the program records data from the next 4 second sample to the hard drive. Depending on the positions of the “LabVIEW data” and “text data” toggle switches, different information is saved. If the “LabVIEW data” toggle is turned on, the entire raw data stream as well as instrument calibrations and ambient room conditions are saved to a data file. This data can later be retrieved using the same program by engaging the “Retrieve?” toggle, and the same 4 second data sample will be replayed continuously allowing further analysis. If the “text data” toggle is turned on, then the values of specific variables are written to a text file. This data generally includes the main experimental operating parameters such as cross-wind velocity, chamber pressure, forcing frequency, and plume flow pressure, as well as statistics on two other selected data channels. This text file is formatted for the data to be easily read into spreadsheet programs. If both toggles are turned on then both of these records are made.

There are 3 data graphs in the vi screen. In the top-right corner “data graph 1” shows traces of all the channels, while the other two graphs in the lower-left corner only show data traces and statistics for selected channels.

In the higher of these two graphs, two channels may be selected to be traced on the same graph.

In the upper-left is a chart showing the spectrum of one of the selected channels. Settings for the spectral analysis are set by controls to the right of this chart. In the lower-right is a spectrum of only the chamber pressure measurement. The chart on the mid-right shows the result of using *integrate waveform.vi* to estimate the phase-average of a signal. This vi is discussed in a following section.



A.2 Description of *average waveform.vi*

Using this vi, time-series data containing many periods of oscillation can be used to approximate a phase-averaged time-series. This is useful when the data acquisition is not coupled to the phase of the oscillating reading, as in the case of these experiments. This vi is particularly useful when trying to interpret low-velocity measurements of the periodic forcing applied to the plume. At low velocity random noise makes it difficult to interpret the time-series data. Approximating a phase-average reduces this noise.

This vi works by calculating the number of data points taken within a period of oscillation. This is a decimal number, which is rounded to the nearest integer to approximate the number of data points lying within a period. The unrounded value then multiplied by incrementing integers and rounded to the nearest whole number. These whole numbers becomes the indices that mark the beginning of each period. One period's worth of data points are read after each of these whole numbers and this is averaged for every "period", resulting in a phase-average approximation over this period. Aside from numerical machine error, the error from using this method comes from both the rounding of the beginning of each period to a discrete data point, as well as in rounding the period length to a discrete data point and in specifying the frequency to use for calculating the period. The chamber pressure signal is used as a reference signal to more accurately determine the correct frequency. This is done by comparing the data from a period

of the pressure signal to a phase-average of the series. The frequency is adjusted until these series overlay, and signal attenuation from the averaging is checked for by comparing peak values of the original signal to the phase-averaged signal. The control panel of this vi is shown in Figure A.2.

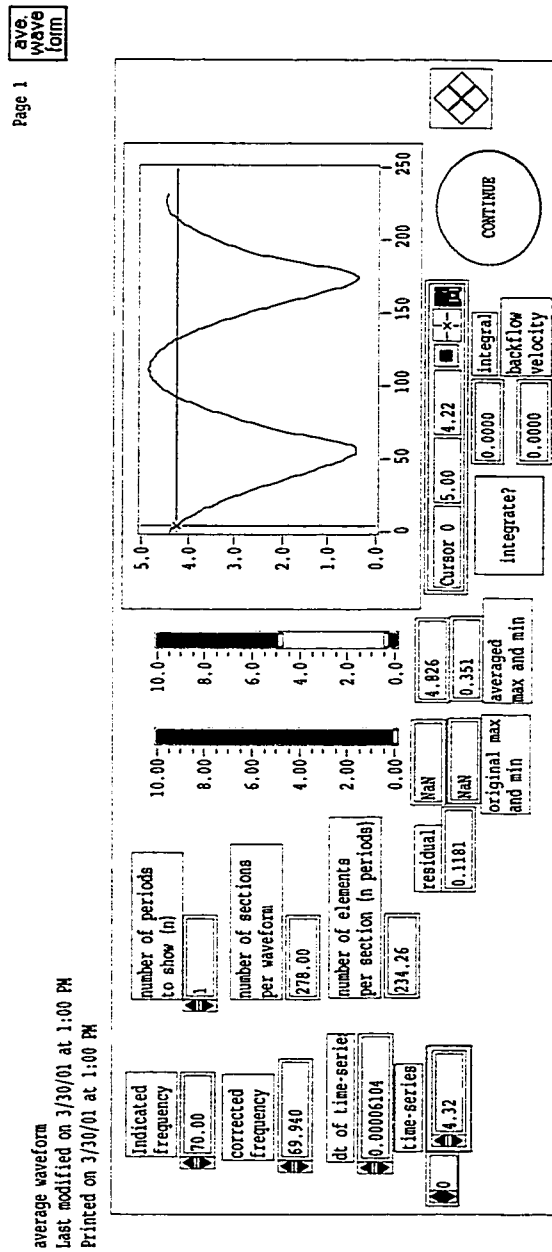


Figure A.2: Control Panel of Program to Approximate Phase-Average: *average waveform.vi*

A.3 Description of *integrate waveform.vi*

This is the vi used to de-rectify and integrate hot-wire data taken from the reversing flow of the synthetic jet near the jetting orifice. Figure A.3 shows the control panel for this vi. The control panel of this vi displays three charts. The top-left one is the original rectified trace. A data point is chosen to “begin” the trace at the start of the ejection phase, chosen as the data point corresponding to the minimum value before the largest maximum. The lower-left trace shows this same data shifted to start with this value. Next, two data points are chosen which are close to the minimum between the two local maximas representing the peaks of the suction and ejection phases. The curve is then “spliced” at these two values, and the values corresponding to the section phase are made negative. Values within this spliced region are replaced with a linear line segment continuous with the beginning and end of the splice. A linear line segment is used because this is the theoretical curvature of a zero-averaged sinusoid at its crossing points. Using this de-rectified and spliced waveform the integral is calculated for the ejection phase as well as over the entire period.

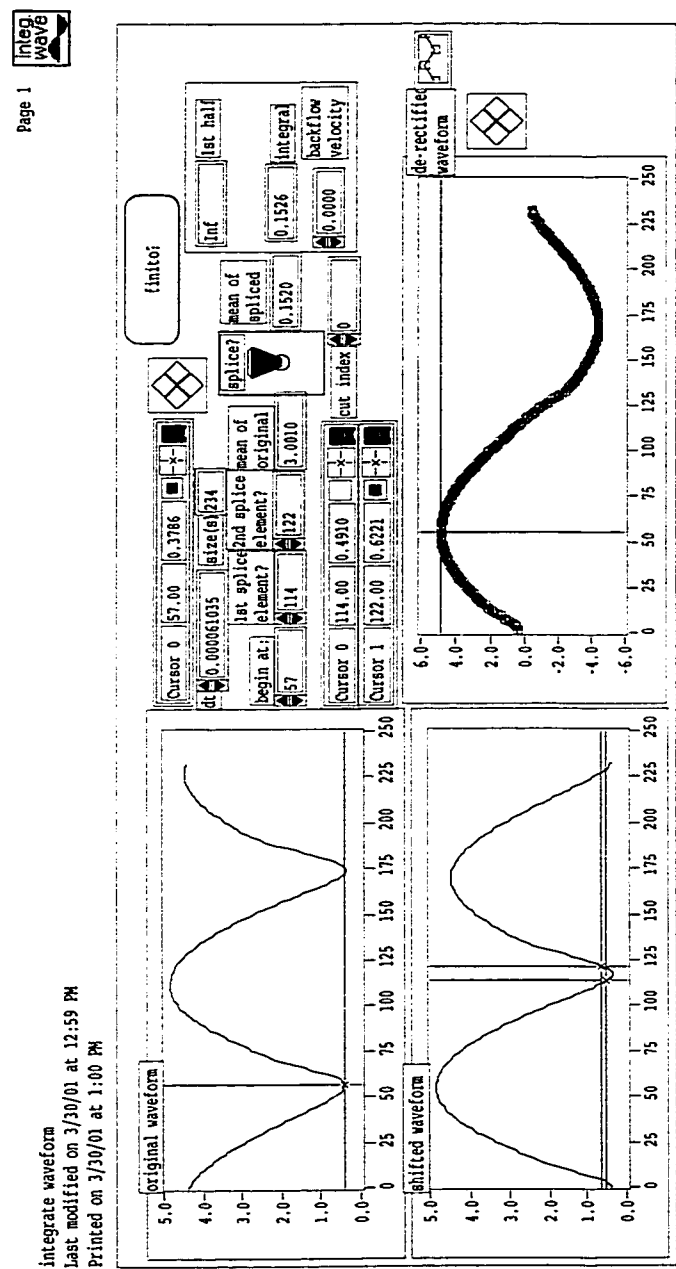


Figure A.3: Hot-Wire De-Rectification and Integration Program Control Panel *integrate waveform.vi*

A.4 Description of *popup-tow-6c.vi*

This vi is used to enter sensor calibrations as well as operational parameters for the data acquisition board measurement channels. The instrument calibration data shown in the control panel for this vi in Figure A.4 is saved along with raw instrument data readings whenever a data sample is taken with the “LabVIEW data” toggle engaged.

BOARD CONFIGURATION

Labels II		Calibration (Pa/V)		Channels II		Input Limits		Coupling & Input Config	
						Low (-10V)	High (10V)	(DI or RSE)	(DC)
0	Pulsator	1.00		0	14	-10.00	10.00	ref. single-ended	DC
1	P2	194.53		1	7	-10.00	10.00	ref. single-ended	DC
2	P3	30.75		2	13	0.00	5.00	ref. single-ended	DC
3	Plan	460.73		3	5	0.00	10.00	ref. single-ended	DC
4	HRT	1.00		4	1	0.00	5.00	differential	DC
5	Pilot	11.74		5	2	0.00	5.00	differential	DC

scan rate (16384secs/sec)

16384.00

8 seconds to record data

2.00

SPECTRO Source

Rotary Encoder

SPECTRA OUT

Traverse Clock

CONTINUE

device (1)

Pilot/Secra Zero Voltage

1.40

Digital Lines		Line Direction Map	
0	read	0	0
1	write	1	1
2	write	1	1
3	read	0	0
4	read	0	0
5	read	0	0
6	read	0	0
7	read	0	0

outputs off

direction

up limit

on limit

moving

end switch

110

Figure A.4: Data Aquisition and Sensor Configuration Panel of *popup-tow-6c.vi*

APPENDIX B

SAMPLE PHOTOGRAPHS

This appendix contains examples of images used to make plume measurements. These images are computer scans of contact sheets made from photographic negatives. “Strips” of 11 or 12 consecutive images are shown, where each strip represents a photographic data run corresponding to a particular case number. In general, cross-wind velocity is fixed while either the unforced plume flow is increased, or forcing amplitude is increased while the plume flow is kept constant.

Photographs from three cases are shown in this appendix. Figure B.1 shows photographs of case 21, a reference case where the plume is unforced and increases in magnitude with every consecutive photograph. A sample set of measurements for this case is given in Figure 3.1 on page 75. Figures B.2 and B.3 show photographs of cases 1 and 16, respectively. Case 1 is with a constant plume velocity ratio of 0.70 and increasing synthetic jetting velocity in every consecutive photograph, starting from zero amplitude.

Case 16 has the same plume and cross-wind settings, giving the same plume velocity ratio, but uses steady blowing instead of synthetic jetting. Plume height measurements from both of these cases are compared to each other in Figure 3.20 on page 122.

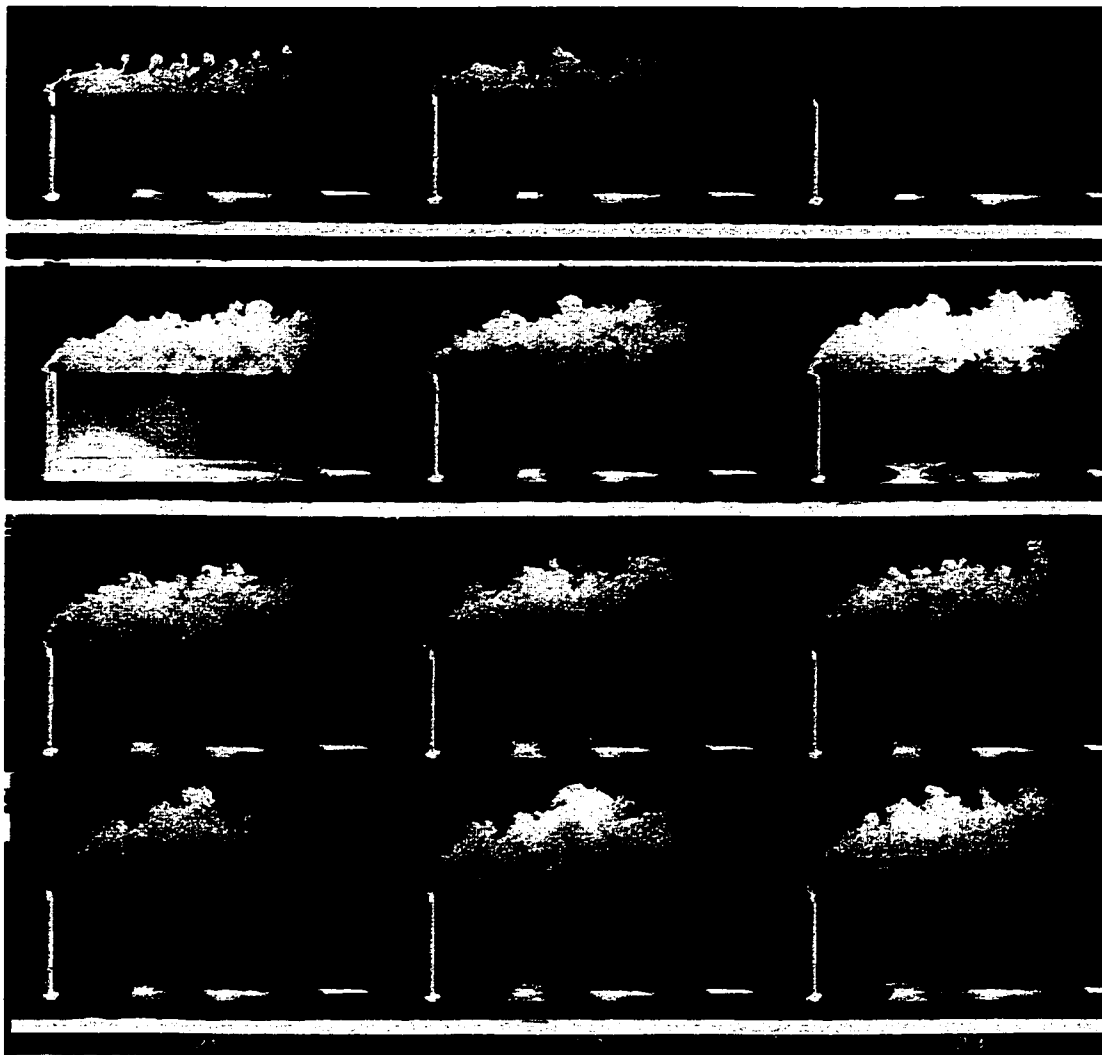


Figure B.1: Photographs from Case 21: $U_{\infty} = 2.5$ m/s, plume velocity ratio increased from 0.6 to 3.4

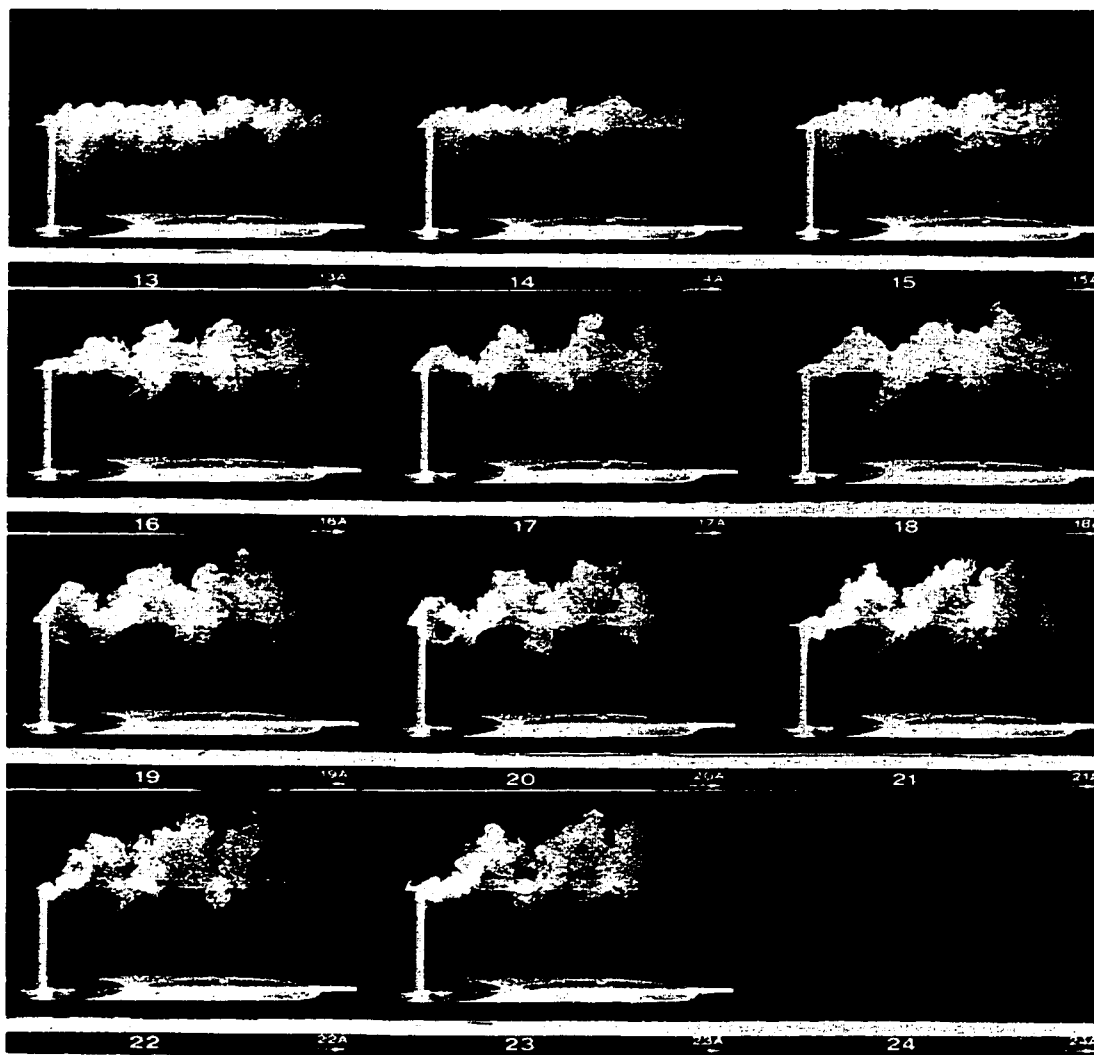


Figure B.2: Photographs from Case 1: pume velocity ratio fixed at 0.70, synthetic jet velocity increased from zero to 8.9 m/s

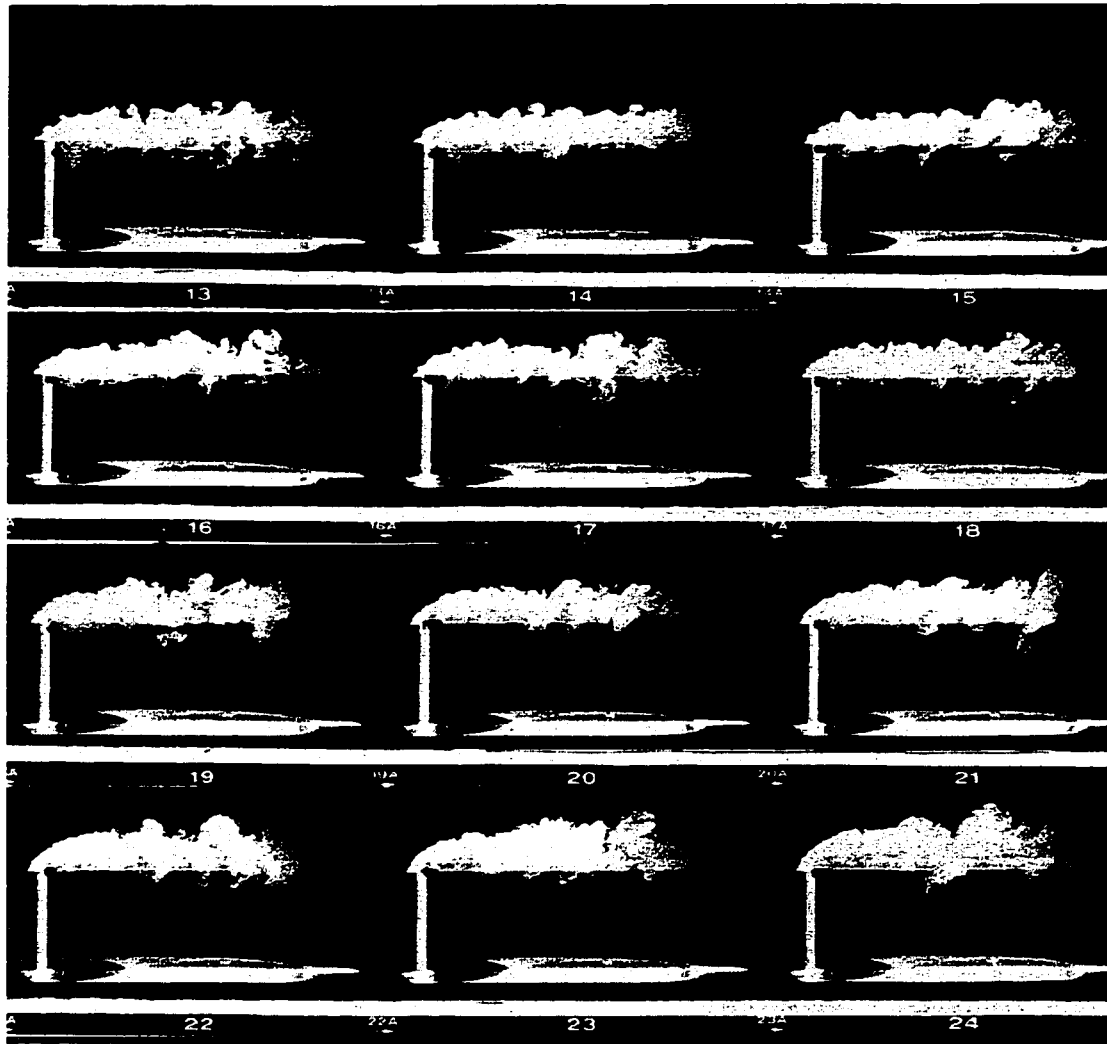


Figure B.3: Photographs from Case 16: plume velocity ratio fixed at 0.70, steady blowing velocity increased from zero to 10 m/s